

TARGETING SOLUBLE EPOXIDE HYDROLASE TO TREAT
CHOROIDAL NEOVASCULARIZATION

Bomina Park

Submitted to the faculty of the University Graduate School
in partial fulfillment of the requirements
for the degree
Doctor of Philosophy
in the Department of Pharmacology and Toxicology,
Indiana University

May 2022

Accepted by the Graduate Faculty of Indiana University, in partial fulfillment of the requirements for the degree of Doctor of Philosophy.

Doctoral Committee

Timothy W. Corson, Ph.D., Chair

Ashay D. Bhatwadekar, Ph.D.

January 25, 2022

Travis J. Jerde, Ph.D.

Tao Lu, Ph.D.

Richard M. Nass, Ph.D.

© 2022

Bomina Park

DEDICATION

To my parents who nurtured my childish curiosity, taught me to do every task in life to the best of my abilities, and emphasized to me that success is about the differences I make in other people's lives.

ACKNOWLEDGEMENT

No matter how strenuous the challenges of my Ph.D. journey were, I have taken them as opportunities to build on my intellectual curiosity, cogency, perseverance, and optimism. Importantly, these were qualities that transcended from mentors, friends, and family who inspired me to see what is possible and motivated me to act on that inspiration.

First, I would like to thank my undergraduate research mentors, Dr. Robert Holman and Dr. Kenneth Rodnick, with whom I had my first research experience. Their guidance fed my inquisitive mindset, and this research experience served as the cornerstone of my desire to pursue a Ph.D. and a career in science.

I am extremely grateful to my Ph.D. thesis advisor, Dr. Timothy W. Corson. I owe much of my growth as a scientist to his invaluable advice. He has supported me immensely in taking multidisciplinary approaches to make scientific discoveries, and he has cultivated my ability to clearly reason and make convincing arguments based on evidence. Most importantly, he championed my academic growth and success. I am forever thankful for his extensive support in helping me to realize my professional goals and motivating me to achieve those goals. His commitment to science and teaching inspired me to realize the power of a positive impact one can have on others.

Additionally, I would like to thank my colleagues from Corson lab - Dr. Sheik Pran Babu Sardar Pasha, Kamakshi Sishtla, and Dr. Trupti Shetty, who selflessly shared their knowledge with me and encouraged me to grow.

I would like to thank my thesis committee members - Dr. Ashay D. Bhatwadekar, who provided his expertise in retinopathy and ophthalmic research. Dr. Travis Jerde who

provided his expertise in signal transduction and inflammation, Dr. Tao Lu who provided her expertise in drug discovery research and pharmacology, and Dr. Richard Nass who provided his expertise in nondegenerative diseases and toxicology. Together they guided me through the process of proposing, writing, and revising my dissertation and offered their constructive feedback on my writing and research. I am thankful for their support and guidance in my growth as a scientist.

This work would not have been possible without the support I received from Pharmaceutical Research and Manufacturers of America (PhRMA) foundation predoctoral fellowship in Pharmacology/Toxicology, and Eli Lilly-Stark Neurosciences predoctoral fellowship in neurodegeneration research. These predoctoral fellowships allowed me to focus solely on research to achieve my career goals and bolstered my confidence as an independent scientist.

In the face of uncertainty, failure and criticism that are inherent to science, my friends and family offered support and encouragement, which gave me the determination to persevere. Lastly, I would like to thank my love, Nicholas Perry, for giving me the strength, courage, and hope to keep moving forward. I am so thankful for the happiness he has brought into my life.

Bomina Park

TARGETING SOLUBLE EPOXIDE HYDROLASE TO TREAT
CHOROIDAL NEOVASCULARIZATION

Neovascular or “wet” age-related macular degeneration (nvAMD) is a leading cause of blindness among older adults, affecting millions of people worldwide. Choroidal neovascularization (CNV) is a major pathological feature of nvAMD, in which abnormal new blood vessel growth from the choroid leads to irreversible loss of vision. Currently, the effort to treat nvAMD is hampered by resistance and refractory responses to the current standard of anti-angiogenic care, anti-vascular endothelial growth factor biologics. Thus, there is a critical need to develop novel therapeutic strategies.

Previously, we discovered an anti-angiogenic small molecule SH-11037, and identified soluble epoxide hydrolase (sEH) as a target of SH-11037 through a forward chemical genetics approach. sEH, encoded by the *EPHX2* gene, is a lipid-metabolizing enzyme that hydrolyzes epoxy fatty acids into corresponding diols. I hypothesized that sEH is a key mediator of CNV. Given that the kinetic mechanism of sEH inhibition by SH-11037 and the cellular role of sEH in CNV are poorly understood, the objectives of my thesis project were to elucidate drug-target interactions through enzyme kinetics, investigate sEH mediated mechanisms that regulate CNV, and preclinically validate sEH as a therapeutic target.

I discovered that SH-11037 is a mixed inhibitor of sEH with a binding affinity for both the enzyme and enzyme-substrate complex. I examined retinal spatial expression of sEH at both the protein and mRNA levels through immunohistochemistry and RNAscope

in situ hybridization and investigated the efficacy of adeno-associated virus (AAV) serotype 8 vector expressing shRNA against *Ephx2*, in the mouse laser-induced (L-) CNV model with features of nvAMD. My study revealed sEH protein and mRNA overexpression in the retinal pigment epithelium (RPE), vasculature and photoreceptors under the disease state. The delivery of AAV8-*Ephx2* shRNA, which has tropism towards RPE and photoreceptor cells, significantly reduced CNV. In addition, gene expression analysis showed normalized *Vegfc* and CNV-related inflammatory markers upon sEH knockdown. Thus, my study demonstrated sEH overexpression in disease-relevant cell types, highlighted a functional role of sEH in AMD pathophysiology, and provided a novel context to target these cell types for developing pharmacotherapies.

Timothy W. Corson, Ph.D., Chair

Ashay D. Bhatwadekar, Ph.D.

Travis J. Jerde, Ph.D.

Tao Lu, Ph.D.

Richard M. Nass, Ph.D.

TABLE OF CONTENTS

LIST OF TABLES	xii
LIST OF FIGURES	xiii
LIST OF ABBREVIATIONS.....	xv
CHAPTER 1. INTRODUCTION	1
1.1 Overview.....	1
1.2 Anatomy of the Retina	2
1.2.1 Retina	2
1.2.2 Choroid	5
1.2.3 Macula.....	5
1.2.4 Retinal Pigment Epithelium.....	5
1.2.5 Bruch’s Membrane.....	6
1.3 Age-related Macular Degeneration.....	6
1.3.1 Prevalence	6
1.3.2 Dry AMD	7
1.3.3 Neovascular AMD	8
1.4 Pathogenesis of Age-related Macular Degeneration.....	10
1.4.1 Aging.....	10
1.4.2 Sex differences.....	11
1.4.3 Genetics.....	12
1.4.4 Oxidative Stress	14
1.4.5 Hypoxia.....	16
1.4.6 Inflammation.....	16
1.4.7 Angiogenesis.....	18
1.5 Development of Choroidal Neovascularization.....	21
1.5.1 Initiation State.....	21
1.5.2 Inflammatory Active Stage	22
1.5.3 Involutional State	22
1.6 Therapy for Neovascular Age-related Macular Degeneration.....	23
1.6.1 Laser Photocoagulation.....	23
1.6.2 Photodynamic Therapy	23
1.6.3 Anti-VEGF.....	24
1.7 SH-11037, Anti-angiogenic Small Molecule and Soluble Epoxide Hydrolase.....	26
1.8 sEH inhibition and EpFAs in Angiogenesis and Inflammation.....	29
1.9 sEH in Other Ocular Diseases.....	33
1.9.1 Nonproliferative Diabetic Retinopathy.....	33
1.9.2 Diabetic Keratopathy	34
1.10 Summary and Dissertation Overview	36
CHAPTER 2. METHODS	39
2.1 Overview	39
2.2 Tissue-based sEH Activity Assay using trans-Stilbene Oxide	40

2.3 sEH Inhibitor Assay	41
2.4 sEH Enzyme Kinetics Assay	43
2.5 Human Retina	44
2.6 Animals	44
2.7 Mouse Model for L-CNV	45
2.8 Embedding and Cryosectioning.....	47
2.9 Immunofluorescence.....	47
2.10 RNAscope In Situ Hybridization	50
2.11 Generation of AAV8 Vectors	51
2.12 Intravitreal Injection.....	52
2.13 In vivo retinal imaging.....	52
2.14 Choroidal flatmounts and ex vivo CNV lesion quantification.....	53
2.15 Immunoblotting.....	54
2.16 Mouse eye RNA extraction and qPCR	55
2.17 Statistics	56
CHAPTER 3. MECHANISTIC ENZYMOLOGY OF sEH INHIBITION.....	57
3.1 Overview	58
3.2 Background and Rationale.....	58
3.3 Results.....	60
3.3.1 SH-11037 inhibits sEH activity in murine eye tissue homogenates	60
3.3.2 SH-11037 inhibits recombinant human sEH activity	61
3.3.3 SH-11037 is a mixed noncompetitive inhibitor of sEH.....	63
3.4 Discussion and Conclusions	69
CHAPTER 4. CELLULAR EXPRESSION OF sEH IN MURINE CHOROIDAL NEOVASCULARIZATION AND HUMAN NEOVASCULAR AGE-RELATED MACULAR DEGENERATION	72
4.1 Overview	72
4.2 Background and Rationale.....	73
4.3 Results.....	75
4.3.1 Immunolocalization of sEH in murine retinas	75
4.3.2 Immunolocalization of sEH in human retinas	79
4.3.3 RNAscope ISH evaluation of <i>EPHX2/Ephx2</i> mRNA expression	84
4.4 Discussion and Conclusions	88
CHAPTER 5. EFFICACY OF AAV8-shRNA TARGETING Ephx2 AGAINST MURINE CHOROIDAL NEOVASCULARIZATION	92
5.1 Overview.....	92
5.2 Background and Rationale.....	93
5.3 Results.....	97
5.3.1 In vivo transduction of AAV8- <i>Ephx2</i> shRNA.....	97
5.3.2 Localization of transduced cells.....	97
5.3.3 Suppression of L-CNV by AAV8- <i>Ephx2</i> shRNA	101
5.3.4 Inhibition of CNV-related inflammatory gene expression by AAV8- Ephx2 shRNA	105

5.4 Discussions and Conclusions.....	108
CHAPTER 6. DISCUSSION AND CONCLUSIONS	112
6.1 Overview.....	112
6.2 Research Aims and Findings	113
6.2.1 Background Review.....	113
6.2.2 Inhibitory activity of SH-11037 against sEH.....	115
6.2.3 Mechanistic basis of SH-11037 targeting sEH	118
6.2.4 Immunolocalization of sEH in RPE and photoreceptor cells in murine L-CNV and human nvAMD retinas.....	122
6.2.5 Cellular expression and localization of Ephx2 mRNA in murine L-CNV and human nvAMD retinas.....	124
6.2.6 Differential retinal distribution of sEH across species and disease models.....	126
6.2.7 Efficient and stable transduction of AAV serotype 8 mediated delivery of shRNA targeting <i>Ephx2</i> in photoreceptors and the RPE.....	127
6.2.8 AAV serotype 8 mediated delivery of shRNA targeting <i>Ephx2</i> inhibited CNV progression	129
6.2.9 AAV8 serotype 8 mediated delivery of shRNA targeting <i>Ephx2</i> suppressed expression levels of inflammatory molecules	132
6.3 Limitations	136
6.3.1 Use of synthetic substrate in sEH activity assay.....	138
6.3.2 Differences between human nvAMD etiology and murine L-CNV model.....	138
6.3.3 Lack of longitudinal monitoring of L-CNV.....	139
6.4 Future Directions	140
6.4.1 Drug development of sEH inhibitors	140
6.4.2 Functions of sEH in the RPE	142
6.4.3 Sex differential mechanisms of sEH regulation.....	143
6.5 Closing Remarks.....	146
REFERENCES	147
CURRICULUM VITAE	

LIST OF TABLES

Chapter 1

Table 1.1: Soluble epoxide hydrolase inhibitors tested in ocular disease animal models.....	35
---	----

Chapter 2

Table 2.1: Antibody and lectin information for the human and mouse retina immunofluorescence and immunoblotting (indicated in parentheses).	50
Table 2.2: Gene expression assays used in studies	57

Chapter 3

Table 3.1: Chemical structures and IC ₅₀ values of sEH inhibitors	64
--	----

Chapter 6

Table 6.1: The difference between inhibition constant and half-maximal inhibitory concentration.....	119
--	-----

LIST OF FIGURES

Chapter 1

Figure 1.1: Structure of retina.....	4
Figure 1.2: VEGF signaling in angiogenesis	20
Figure 1.3: The CYP-sEH pathway	28
Figure 1.4: Approaches to target validation in early drug discovery.....	38

Chapter 2

Figure 2.1: Reaction mechanism of trans-stilbene oxide with sEH.....	40
Figure 2.2: Reaction mechanism of PHOME with sEH	42
Figure 2.3: Laser-induced choroidal neovascularization and noninvasive retinal imaging methods.....	47

Chapter 3

Figure 3.1: Ex vivo treatment of eye tissue homogenates with SH-11037 or compound 7 inhibits cellular sEH activity.....	62
Figure 3.2: SH-11037 is an sEH inhibitor	63
Figure 3.3: Michaelis-Menten and Lineweaver Burk plots of SH-11037 inhibition of sEH.....	67
Figure 3.4: Michaelis-Menten and Lineweaver Burk plots of Compound 7 inhibition of sEH	68
Figure 3.5: Secondary plots for enzyme kinetic analyses.....	69
Figure 3.6: SH-11037 binds to sEH in an energetically favorable mode	71

Chapter 4

Figure 4.1: Upregulation and colocalization of sEH with rod photoreceptors in the eyes of mice undergoing choroidal neovascularization	77
Figure 4.2: Colocalization of sEH with apical and basal surface of RPE cells in murine retinas undergoing choroidal neovascularization	78
Figure 4.3: Immunolocalization of sEH with other retinal markers	79
Figure 4.4: Colocalization of sEH with photoreceptors and RPE in human retinas from neovascular AMD patients.....	82
Figure 4.5: Colocalization of sEH with photoreceptors in human retinas from additional human subjects.....	83
Figure 4.6: Colocalization of sEH with RPE in human retinas from additional human subjects.....	84
Figure 4.7: <i>EPHX2</i> mRNA is highly expressed in the retinal pigment epithelium (RPE) of AMD eyes.....	87
Figure 4.8: sEH mRNA expression is increased in the retinal pigment epithelium (RPE) of L-CNV eyes.....	89

Chapter 5

Figure 5.1: In vivo transduction of AAV8 in murine retina	100
Figure 5.2: Immunolocalization of mCherry with cone arrestin, rhodopsin and RPE65 in AAV8 injected murine eyes.....	101

Figure 5.3: AAV8-delivery of shRNA against sEH suppresses L-CNV	104
Figure 5.4: AAV8- <i>Ephx2</i> shRNA reduces sEH expression level.....	105
Figure 5.5: Inhibition of CNV-related inflammatory molecule expression by AAV-delivery of <i>Ephx2</i> shRNA.....	108

Chapter 6

Figure 6.1: Schematic summary of Chapter 3 research discovery of mixed noncompetitive inhibition of sEH enzymatic activity upon binding of sEH with SH-11037.....	122
Figure 6.2: Schematic summary of Chapter 4 and 5 studies.....	136
Figure 6.3: Synthetic and endogenous substrates of sEH hydrolase activity.	138
Figure 6.4: Sex differences in sEH protein expression in retina.....	146

LIST OF ABBREVIATIONS

AAV, Adeno-associated virus
AMD, Age-related macular degeneration
ANOVA, One-way analysis of variance
ARMS2, Age-related maculopathy susceptibility 2
BLamD, Basal laminar deposits
BLinD, Basal linear deposit
FGF, Fibroblast growth factor
BRB, Blood retinal barrier
BSA, Bovine serum albumin
CCL2, C-C motif chemokine ligand 2
CNV, Choroidal neovascularization
CMV, Cytomegalovirus
CFH, Complement factor H
COX, Cyclooxygenase
CYP, Cytochrome P450 epoxygenases
DHDP, Dihydroxydocosapentaenoic acids
DMSO, Dimethyl sulfoxide
DHA, Docosahexaenoic acid
EI, Enzyme inhibitor complex
EPA, Eicosapentaenoic acid
EIS, Enzyme inhibitor substrate
EDP, Epoxydocosapentaenoic acids
EEQ, Epoxyeicosatetraenoic acid
EET, Epoxyeicosatrienoic acids
ES, Enzyme substrate complex
ECM, Extracellular matrix
FA, Fluorescein angiography
FFPE, Formalin fixed paraffin embedded
GCL, Ganglion cell layer
GC, Genome copies
GST, Glutathione-S-transferases
AGE, Advanced glycation end products
HO-1, Heme oxygenase-1
HPLC, High-performance liquid chromatography
HREC, Human retinal endothelial cells
HTRA1, High temperature requirement A serine peptidase 1
HEK 293, Human embryonic kidney 293 cells
HREC, human retinal endothelial cells
I, Inhibitor
IC₅₀, Half-maximal inhibitory concentrations
ICAM1, Intercellular Adhesion Molecule 1
IF, Immunofluorescence
IHC, Immunohistochemistry
IL-1 β , Interleukin 1 beta

IL6, Interleukin 6
INL, Inner nuclear layer
IS, Inner segments
ISH, In situ hybridization
 K_i , Inhibition constant
 K_M , Michaelis–Menten
LARC, Laboratory Animal Resource Center
LamR, Laminin receptor
L-CNV, Laser-induced choroidal neovascularization
LPS, Lipopolysaccharide
LOX, Lipoxygenase
MPS, Macular photocoagulation studies
MMP, Matrix metalloproteases
MAC, Membrane-attack complex
mTOR, Mammalian target of rapamycin
nvAMD, Neovascular age-related macular degeneration
OCT, Optical coherence tomography
ONL, Outer nuclear layer
OS, Outer segments
OIR, Oxygen-induced retinopathy
P, Product
PBS, Phosphate buffered saline
PFA, Paraformaldehyde
PHOME, 3-phenyl-cyano(6-methoxy-2-naphthalenyl)methyl ester-2-oxiraneacetic acid
PIGF, Placental growth factor
PNA, Peanut agglutinin
PUFA, Polyunsaturated fatty acid
PVDF, Polyvinylidene difluoride
qPCR, Quantitative polymerase chain reaction
RIPA, Radioimmunoprecipitation assay buffer
ROS, Reactive oxygen species
RPE, Retinal pigment epithelium
S, Substrate
SD, Standard deviation
SEM, Standard error of the mean
shRNA, Short hairpin RNA
SNP, Single nucleotide polymorphism
siRNA, Small interfering RNA
sEH, Soluble epoxide hydrolase
TGF- β Transforming growth factor beta
TIMP, Tissue inhibitors of metalloproteinases
t-SO, Trans-stilbene oxide
TAP, Treatment of Age-Related Macular Degeneration with Photodynamic Therapy
TNF- α , Tumor necrosis factor- α
VEGF, Vascular endothelial growth factor
VEGFR, Vascular endothelial growth factor receptor

VCAM1, Vascular cell adhesion protein 1
 V_{\max} , Maximal velocity of the reaction
WGA, Wheat germ aggluti

CHAPTER 1. INTRODUCTION

1.1 Overview

The central region of the retina, known as the macula, is particularly crucial for our central vision. With aging and other contributors, this region of the retina gets progressively damaged, leading to permanent loss of vision. This is the neurodegenerative disease of the retina called age-related macular degeneration (AMD). Neovascular or 'wet' AMD (nvAMD) is a progressive form of the disease that is responsible for most of the blindness resulting from AMD. Neovascular AMD involves choroidal neovascularization (CNV), and it is a multifactorial disease for which the pathogenesis remains incompletely understood. Here, **Chapter 1** introduction reviews the tissue and layers of the retina that are involved in AMD pathophysiology, types of AMD including nvAMD, risk factors, pathogenesis, therapy, and the role of soluble epoxide hydrolase in AMD, CNV, disease-relevant physiological processes such as angiogenesis and inflammation, and other eye diseases.

1.2 Anatomy of the Retina

1.2.1 Retina

The retina is a light-sensitive layer of tissue comprised of distinct cellular layers of neurons that process visual information (Figure 1.1). The photoreceptor cell bodies reside in the outer nuclear layer (ONL), with their inner segments (IS), and outer segments (OS) extending to the retinal pigment epithelium (RPE) layer. The inner nuclear layer (INL) contains bipolar and horizontal cells. The bipolar cells accept synapses from the photoreceptor cells or horizontal cells, transmitting signals to the ganglion cells. The ganglion cells, the final output of neurons that transmit visual information to the brain, are found in the ganglion cell layer (GCL) (Wright, Chakarova et al. 2010, Veleri, Lazar et al. 2015). In addition, retinal glial cells known as Müller cells span across the entire retina radially, providing structural and metabolic support for retina and retinal neurons (Reichenbach and Bringmann 2013). The choroid provides the blood supply of photoreceptors and the RPE of the outer retina. The blood supply of the inner retina is provided by the retinal vasculature that consists of three vascular plexuses – the superficial plexus in the GCL, inner and deep plexuses in the plexiform layers (Figure 1.1) (Campbell, Zhang et al. 2017).

Visual processing refers to the ability to perceive, analyze, and interpret visual information and the process involves the ability to convert light energy into visual imagery (Ding and Alfonso 2016). As shown in Figure 1.1, vision begins with light entering the eye through the cornea, then some of this light passes through the pupil. The iris controls how much the light passes through the pupil. Then the light passes through the lens, which reflects light depending its shape to focus images on the retina, a process

known as accommodation (Kaplan 2007). When light reaches the retina, our visual cycle begins, allowing conversion of photon into an electrical signal. This is mediated by visual pigment molecules that are highly expressed in the outer segment of rod and cone photoreceptor cells. These pigment molecules are G protein-coupled receptors, consist of opsin (differentiating photoreceptor types) attached to a retinal/retinaldehyde, which is an aldehyde of vitamin A. There are 4 major types of opsins absorbing photons at different wavelengths, including rhodopsin of rod photoreceptor cells and 3 different opsins of cone photoreceptor cells. The functional differences are demonstrated in their sensitivity, where rods are much more sensitive than cones, therefore rods are well suited for low light vision and cones are better with light adaptation to remain photosensitive under the bright light (Kefalov 2012). The electrochemical reaction following the light interaction with the pigment molecule is consistent: There is a conformation change from 11-cis retinal form, to the trans retinal, leading to GPCR signal transduction cascades that closes the cyclic GMP-gated cation channels, and results in hyperpolarization of the photoreceptor cells. Thus, light energy is captured chemically, then transduced into electrical energy that the brain can comprehend (Wolf 2004, Mannu 2014).

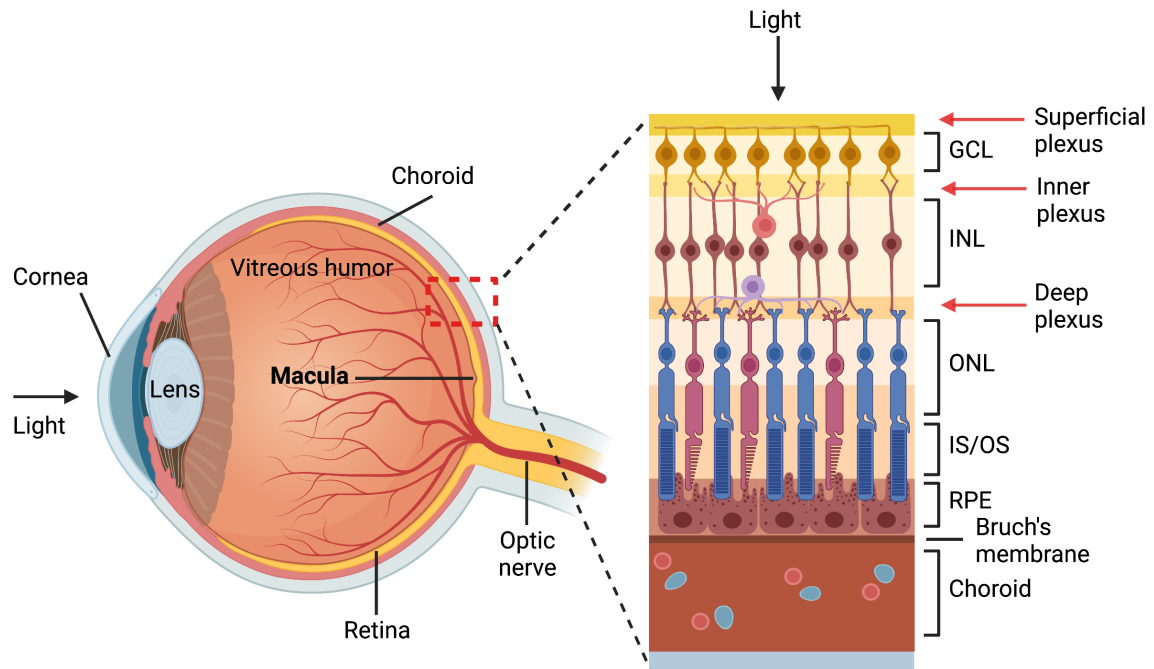


Figure 1.1: Structure of retina. Schematic cross-section through the human eye, indicating different cellular layers. The retinal vasculature that consists of three vascular plexuses – the superficial, inner, and deep plexuses – provides blood supply to the inner retina. The choroid provides blood supply to photoreceptors and RPE in the outer retina. GCL, ganglion cell layer; INL, inner nuclear layer; ONL, outer nuclear layer; IS/OS, photoreceptor inner segments/outer segments; RPE, retinal pigment epithelium

1.2.2 Choroid

The choroid is predominantly a vascular layer of tissue composed of choriocapillaris in its innermost layer. The choroid is responsible for the blood supply of photoreceptors and the RPE in the outer retina. Due to the high metabolic demand of photoreceptors, the choroid serves as the major blood supply in the eye, even more so than retinal vasculature and choroid is one of the most vascularized tissues in the body by weight (Nickla and Wallman 2010).

1.2.3 Macula

The macula is in the center of the retina, temporal to the optic nerve (Figure 1). It comprises only 4% of the retina. Still, it is responsible for central and color vision because the fovea, which lies within the center of the macula, contains the highest density of specialized neurons, light-sensitive cone photoreceptor cells. Therefore, damage in this region accounts for devastating loss of visual function (Hageman, Gehrs et al. 1995).

1.2.4 Retinal Pigment Epithelium

The retinal pigment epithelium (RPE) is a monolayer of pigmented cells between choroidal blood vessels and the avascular photoreceptor layer (Hageman, Gehrs et al. 1995). The RPE cells play a protective role in the retina by absorbing free radicals and preventing scattering of light (Parson 2009). RPE cells form the outer blood-retina barrier as tight junctions located between RPE cells allow them to regulate transport of molecules from choroid to the subretinal space, thereby playing an important role in immune privilege of the eye (Campbell and Humphries 2012). In addition, RPE cells are specialized in receptor mediated phagocytosis of damaged photoreceptor outer segments. Due to constant exposure to light and resulting photo-oxidation, photoreceptor outer

segments undergo constant shedding and phagocytosis of damaged tips (Hageman, Gehrs et al. 1995, Schraermeyer and Heimann 1999).

1.2.5 Bruch's Membrane

Bruch's membrane located beneath the RPE is an acellular, 5-layered extracellular matrix composed of– inner basement membrane of RPE, inner collagenous layer, elastin layer, outer collagenous layer, and outer basement membrane of choriocapillaris (Chen, Miyamura et al. 2003). Together, RPE and the Bruch's membrane complex serve as a barrier that regulates cellular migration, transport of molecules, and neovascularization from choroid into the subretinal space.

1.3 Age-related Macular Degeneration

1.3.1 Prevalence

Age-related macular degeneration (AMD) is a neurodegenerative disease of the retina, and it is the leading cause of blindness in patients 65 years of age or older in industrialized nations (Fine, Berger et al. 2000). AMD affects approximately 11 million people in the US and 170 million people globally. Due to increasing aging population, the prevalence of AMD is predicted to double by the year 2050 in the US, and the global prevalence is predicted to increase to 288 million by 2040 (Pascolini and Mariotti 2012, Wong, Su et al. 2014). AMD is a complex multifactorial disease associated with demographic, environmental, and genetic risk factors. The risk is further increased by other demographic factors, including female gender (see below) and Caucasian race. As well, environmental factors such as sunlight exposure and cigarette smoking are

associated with the development of AMD, among which cigarette smoking is the second most consistent risk factor after age (Heesterbeek, Lorés-Motta et al. 2020).

The chorio-retina toxicity induced by cigarette smoke has been shown to be mediated by oxidative damage to the RPE, vascular damage and inflammation, together contributing to AMD pathogenesis (Velilla, García-Medina et al. 2013). In addition, a genome-wide association study of AMD revealed genes associated with AMD, which are presented in The Retina International Disease Database (2010). Currently, genetic variation in complement factor H (CFH) and ARMS2/HTRA1 (Age-related Maculopathy Susceptibility 2/High Temperature Requirement A Serine Peptidase 1) genes are considered as major contributors to increasing the risk of AMD development (Sergejeva, Botov et al. 2016) as discussed further in the next sub chapters.

1.3.2 Dry AMD

Dry AMD or atrophic AMD is characterized by drusen, which are extracellular deposits that accumulate between retinal pigment epithelium (RPE) and Bruch's membrane. Several classification schemes are developed based on the number and size of drusen, degree of RPE changes, and geographic atrophy (Hageman, Gehrs et al. 1995, Yonekawa, Miller et al. 2015). Drusen, derived from the German word for nodes or geode, are extracellular deposits that accumulate beneath the RPE basal lamina and into the inner layer of Bruch's membrane (Williams, Craig et al. 2009). In the advanced stage of dry AMD, geographic atrophy develops, which is characterized by a change in pigmentation and loss of RPE-Bruch's membrane in the areas of drusen or independent of drusen (Yonekawa, Miller et al. 2015). Approximately 10-15% of all AMD patients

progress to the neovascular (nv) AMD, but occasionally there are nvAMD patients without prior dry AMD condition.

Although not all dry AMD cases progress to nvAMD, it can be considered as a risk factor or a preceding state for nvAMD. Any stage of dry AMD can turn into nvAMD (Miller, D'Anieri et al. 2021). The mechanistic basis of this disease progression is multifactorial, and it is not fully understood. The recurring theme is that the RPE is at the core of AMD pathogenesis, in which the crosstalk of RPE with the immune and vascular systems of the retina drives development of CNV (Ambati and Fowler 2012). The RPE dysfunction is a precursor state in later stage AMD including both geographic atrophy and CNV of nvAMD. This potential of the RPE to drive various pathways of AMD pathogenesis is strongly supported by RNA transcriptome analyses of human AMD donor eyes in which a number of RPE specific genes were differentially regulated under the AMD disease state (Newman, Gallo et al. 2012). It is important to note that significant inter-individual variations are displayed in RPE transcript expression of human AMD samples. This supports the theory that different categorical AMD phenotypes are responses driven by heterogenic AMD relevant stimuli or stress (Ambati and Fowler 2012). There are number of pathways in AMD pathology, including inflammation, complement factors, age-related anatomical changes, and stressors that all contribute to progression of the disease which are discussed in following sections.

1.3.3 Neovascular AMD

Neovascular AMD (nvAMD) accounts for only 10% of AMD cases, but it accounts for 90% of the blindness resulting from AMD (Morris, Imrie et al. 2007). Neovascular AMD is characterized by choroidal neovascularization (CNV) in which

proliferating choroidal blood vessels project through Bruch's membrane and the retinal pigment epithelium (RPE) layer (Bird 2010). These new blood vessels are leaky and prone to rupture, thereby causing vascular leakage and scarring of macula that lead to permanent vision loss. According to macular photocoagulation studies (MPS) and Treatment of Age-Related Macular Degeneration with Photodynamic Therapy (TAP) studies, nvAMD can be classified into subtypes based on the vascular leakage within the CNV lesion – classic and occult. The classic CNV is characterized by intense hyperfluorescence, and the source of vascular leakage can be readily defined. In contrast, occult CNV is characterized by irregular (type 1 occult) and/or multiple hyperfluorescent lesions (type 2 occult), presenting diffusive leakage (Tomi and Marin 2014).

Besides these classic nomenclatures, additional delineation of the subtypes of nvAMD were developed in a 2020 consensus meeting of an international team of experts in AMD and AMD imaging research as follows. Polypoidal choroidal vasculopathy is a variant of type 1 that is commonly seen in Asian persons. It is defined by a branching vascular network and nodular vascular agglomerations known as polyps. Polypoidal choroidal vasculopathy slowly invades sub-RPE space and may grow significantly until they affect vision. These polyps are especially prone to bleeding. There is also a type 3 macular neovascularization which involves down growth of retinal blood vessels towards the outer retina; therefore, the term choroidal neovascularization is not accurate for this. There can also be lesions those result from retina-choroidal anastomosis, which refers to a vascular communication between channels that are not connected by vessels. The detachment of RPE can occur in type 1 and 3, but not likely in type 2 although it is not known why similar RPE detachment does not occur in type 2 (Spaide, Jaffe et al. 2020).

1.4 Pathogenesis of Age-related Macular Degeneration

AMD is a complex multifactorial disease, and not all the causes of AMD are completely understood. The age-related structural changes in the eye, sex differences, hypoxia, oxidative stress, inflammation, and genetic predisposition are strongly related to the pathogenesis of AMD.

1.4.1 Aging

Aging and structural changes of Bruch's membrane and RPE are key contributors. Early-stage AMD is characterized by structural changes within Bruch's membrane, accumulation of waste products in RPE and formation of drusen between the RPE and Bruch's membrane (Ding, Patel, & Chan, 2009). Numerous early histological studies revealed morphological abnormalities in Bruch's membrane that are associated with aging and AMD (Guymer, Luthert, & Bird, 1999; Hogan & Alvarado, 1967; Sarks, 1976). These structural changes include increased collagen cross-linking (Ramrattan et al., 1994), calcification of the elastin layer (Spraul & Grossniklaus, 1997), accumulation of lipids (Sheraidah et al., 1993) and advanced glycation end products (AGEs) (Glenn et al., 2009). Such changes are a normal part of aging until they have detrimental effects on the functional aspect though some may view aging itself as a pathological condition. The collagen cross-linkage can cause Bruch's membrane thickening, resulting in decreased elasticity and altered membrane permeability (C. A. Curcio & Johnson, 2012; Ramrattan et al., 1994). The thickening of Bruch's membrane also contributes to retinal ischemia as will be discussed later. Calcification occurs in the connective tissue of Bruch's membrane as calcium readily builds up in the soft tissues (van der Schaft et al., 1992). Calcification of the elastin layer also reduces its elasticity, making the membrane brittle and

susceptible to breaks which means loss of barrier structure and function against neovascularization (Georgalas et al., 2009; Spraul & Grossniklaus, 1997).

Lipid accumulation in Bruch's membrane can be observed as forming a 'lipid wall' between the basal lamina of RPE and the inner collagenous layer of Bruch's membrane (Huang, Presley, Chimento, Curcio, & Johnson, 2007). In such a state, formation of the lipid wall can impede transport of macromolecules and fluid between RPE and choroid. Thus, alterations in the anatomical structure of Bruch's membrane result in functional defects. In addition, the lipid wall is considered to give rise to accumulation of lipoproteins known as basal linear deposit (BLinD) (Christine A. Curcio, Johnson, Rudolf, & Huang, 2011), which together with basal laminar deposits (BLamD) build up in the same compartment as drusen within the interface of RPE and choroid (Gregory S. Hageman, 2008).

1.4.2 Sex differences

According to the National Eye Institute, 65 percent of AMD cases were in women in 2010. The greater prevalence of AMD among older women could be explained by the longer life expectancy of women compared to men, given that AMD is an age-dependent disease (Aninye, Digre et al. 2021). However, studies adjusting for age as a factor still found higher AMD risk among women compared to men worldwide (Bourne, Steinmetz et al. 2021, Steinmetz, Bourne et al. 2021). As well, studies suggest there are factors other than age that contribute to sex differences observed in the AMD prevalence. Using data on the association between the late-stage AMD with BMI, systolic blood pressure and exercise, researchers found significant association for AMD risk only among women (Erke, Bertelsen et al. 2014). When it comes to the effects of estrogen on AMD, study

results are conflicting and inconclusive. A study by Snow et al. reported that postmenopausal estrogen therapy in the past was associated with significantly lower risk of developing AMD, suggesting a protective effect of exogenous estrogen against AMD in postmenopausal women (Snow, Cote et al. 2002). However, at least three other observational study results showed no significant association between estrogen treatment and AMD development (Klein, Klein et al. 2000, Abramov, Borik et al. 2004, Defay, Pinchinat et al. 2004). The sex difference is apparent in the prevalence of AMD development but investigating causes of sex differences in AMD pathogenesis requires future studies, along with considerations of biologic, environmental and socioeconomic factors (Pennington and DeAngelis 2016, Zetterberg 2016).

1.4.3 Genetics

There are numerous genes associated with AMD ("Retina international disease database: retinal and macular dystrophies," 2010; Sergejeva et al., 2016), among which genetic variation in complement factors and ARMS2/HTRA1 (Age-related Maculopathy Susceptibility 2/High Temperature Requirement A Serine Peptidase 1) are the most highly associated genes (Akagi-Kurashige et al., 2015; Francis, Hamon, Ott, Weleber, & Klein, 2009; Gold et al., 2006). The complement system refers to a group of more than 30 proteins that are activated as part of the innate immune response against pathogens or specific immune response activated by antigen-antibody complexes (Ding et al., 2009). As a result, cascades of complement system lead to pro-inflammatory responses, including production of membrane-attack complex (MAC), which initiates cell lysis (Walport, 2001). Several studies revealed enhanced expression of complement factors was localized in the drusen and RPE of AMD patients and those of L-CNV mice

(Johnson, Leitner, Staples, & Anderson, 2001; Nozaki et al., 2006). The complement factors also induce RPE secretion of VEGF and act as chemotactic attractants for macrophages to the choroid. Thus, the dysregulation of complement system is thought to play a role in AMD pathogenesis.

A single nucleotide polymorphism (SNP) in the gene coding for complement factor H (CFH) and other *CFH* variants have been reported to have strong associations with AMD (Ding et al., 2009; R. J. Klein et al., 2005). The *CFH* gene is therefore considered as a major susceptibility gene for dry AMD (Dewan et al., 2006). CFH is a negative regulatory protein of the complement system. It is thought that impaired inhibitory activity of CFH can result in dysregulated inflammation and damage to retinal cells, contributing to AMD pathogenesis. In addition, based on the detection of an AMD susceptibility locus from genome-wide linkage analysis of families with AMD, a focused SNP genotyping study revealed a highly significant association over two close-by genes – ARMS2 and HTRA1 (Jakobsdottir et al., 2005). Because there is strong linkage disequilibrium over the ARMS2/HTRA1 region, it is difficult to statistically identify differences between the two AMD risk gene candidates and genetic association studies alone do not give us enough information to determine which gene is more strongly associated with AMD (May, Su et al. 2021). While its function is not fully understood, ARMS2 expression was localized in mitochondria enriched inner segment ellipsoids of photoreceptors, suggesting that functional relevance of ARMS2 to AMD pathology may involve mitochondrial dysregulation (Ding et al., 2009; Fritsche et al., 2008). HTRA1 is a stress-inducible heat shock serine protease, and it is known to regulate TGF- β (transforming growth factor- β) signaling by binding to and cleaving TGF- β (Friedrich et

al., 2015; Zhang et al., 2011). The impaired TGF- β signaling due to structurally altered HTRA1 has been reported to result in microglial dysregulation (Friedrich et al., 2015). As well, HTRA1 is expressed in the RPE and vascular endothelium of retina and several studies reported that its expression is upregulated in drusen and CNV of AMD individuals carrying a specific HTRA1 SNP (Cameron et al., 2007; Chan et al., 2007).

Interestingly, HTRA1 targets cell surface receptors, ECM structural proteins and soluble secreted proteins that are involved in proteolytic degradation. Studies reported that overexpression of HTRA1 did not affect vasculature but compromised Bruch's membranes' elastin layer. While ARMS2-HTRA1 locus has been controversial in regards to being causal factors for AMD, evidence implicates HTRA1 as the causal element than ARMS2 particularly for the ECM fragment hypothesis of AMD in which ECM fragments from HTRA1 proteolysis produce pro-inflammatory peptide fragments that increase oxidative stress, which heightens chronic inflammation with monocyte infiltration and pro-angiogenic cytokines, and promote choroidal neovascularization by degrading Bruch's membrane (May, Su et al. 2021).

1.4.4 Oxidative Stress

Oxidative Stress caused by an imbalance between reactive oxygen species and antioxidant defense system has been implicated in pathogenesis of AMD (Jarrett & Boulton, 2012). ROS can be derived from intracellular metabolism and from photochemical reactions. The retina is susceptible to oxidative stress because of its exposure to high concentrations of oxygen, its exposure to light and high prevalence of photosensitive molecules generating additional sources of ROS formation. Due to the highly metabolic photoreceptor cells, retina is one of the highest oxygen consuming

tissues in the body. The choroid is the major source of blood supply for the retina. The high blood flow and oxygen tension of the choroid generate a large gradient of oxygen tension towards the photoreceptor layer of the retina, thus allowing efficient transport of oxygen from choroid to photoreceptor cells across the Bruch's membrane-RPE barriers. (Jarrett & Boulton, 2012; Nickla & Wallman, 2010) However, this creates an environment that is under oxygen concentration-dependent oxidative stress. In addition, several photosensitive molecules in photoreceptors and RPE can produce ROS in response to excessive light stimuli.

The polyunsaturated fatty acids that are abundant in the outer segments of photoreceptors can be subjected to lipid peroxidation, producing highly reactive lipid peroxy radicals and singlet oxygen species (Esterbauer, Schaur, & Zollner, 1991). These lipid-derived free radicals cause serious damage to the lipid bilayer of the photoreceptor cell membrane because they can further deprotonate nearby fatty acids, thus capable of both the initiation and propagation of oxidation (Jarrett & Boulton, 2012; Kohen & Nyska, 2002). Moreover, the oxidative-induced changes contribute to formation of the lipid-protein aggregate known as lipofuscin in the RPE (Jarrett & Boulton, 2012) and drusen formation between RPE and choroid. Also, RPE cells are constantly exposed to light stimuli and high oxygen tension. As described in **Chapter 1.1.4**, RPE cells are responsible for degradation and recycling of photoreceptor outer segments and are thereby under intense metabolic stress (Schraermeyer and Heimann 1999). With aging, the autophagic clearance by the RPE cells reduces, further amplifying the accumulation of cell debris (Keeling, Lotery, Tumbarello, & Ratnayaka, 2018; Kennedy, Rakoczy, & Constable, 1995). Since RPE is a monolayer of post-mitotic cells, there is considerable

proteolytic burden which conditions these cells to be more susceptible to damage (Kennedy et al., 1995).

1.4.5 Hypoxia

Hypoxia is implicated in the development of neovascular AMD. The features of early-stage AMD contribute to retinal hypoxia. As discussed in the above section, thickening of Bruch's membrane occurs as one ages. Bruch's membrane thickening and accumulation of cellular debris, particularly thick confluent deposits of drusen, increase the distance oxygen travels from choriocapillaris to the photoreceptors (Stefánsson, Geirsdóttir, & Sigurdsson, 2011). The diffusive oxygen flux from choriocapillaris to retina follows Fick's law, where F is the oxygen flux, D is the diffusion coefficient, dc/dx is the concentration gradient, with dc is the concentration change in oxygen and dx is the distance change (Stefánsson et al., 2011).

$$F = -D \, dc/dx$$

In the normal eye, oxygen diffuses from the choroid through Bruch's membrane and RPE, towards the avascular photoreceptor layer. According to Fick's law, increased distance from choroid to retina leads to a decrease in oxygen flux. As a result, there is a decrease in oxygen delivery from choroid in dry AMD, and the photoreceptors become hypoxic. It is well established that hypoxia-inducible factor is expressed in the CNV sites in nvAMD and is a major inducer of vascular endothelial growth factor (VEGF) mediated angiogenesis (see later).

1.4.6 Inflammation

The eye is considered an immunologically privileged site because of its unique physical barriers and microenvironment (R. Zhou & Caspi, 2010). This protects the retina

from daily inflammatory and oxidative insults by maintaining low-level activation of the retinal immune system (Mei & Heping, 2015). However, with aging and persistent insults, para-inflammation can turn into chronic inflammation (Xu, Chen, & Forrester, 2009). Indeed, there is strong evidence that chronic inflammation plays a role in age-related degenerative diseases of immunologically privileged tissues, such as Alzheimer's disease and AMD (Anderson, Mullins, Hageman, & Johnson, 2002; Lathe, Sapronova, & Kotelevtsev, 2014; McGeer & McGeer, 2004).

Several studies revealed elevation of systemic inflammatory markers in AMD. The systemic levels of tumor necrosis factor- α (TNF- α) and interleukin-6 (IL-6) were associated with the incidence of AMD (R. Klein et al., 2014). As well, systemic levels of complement factors and inflammatory cytokines have been found to be elevated in AMD patients (B. Liu et al., 2011). Within the AMD eye, drusen contains several inflammation related proteins. For example, the isolated drusen component amyloid-beta induced activation of NF- κ B and NLRP3 inflammasome pathways in a mouse model in which an intravitreal injection of a drusen component, A β , recapitulated features of early AMD (R. T. Liu et al., 2013; R. T. Liu et al., 2014). The production of inflammatory mediators as a result of inflammatory insults (e.g., oxidative stress, lipofuscin and drusen formation) can promote endothelium activation, resulting in increased adhesion molecules and vascular permeability. In response to inflammatory stimuli, microglia and macrophages migrate to the inflamed subretinal space while expressing pro-angiogenic factors such as vascular endothelial growth factor (VEGF) (Xu et al., 2009). The macrophages also secrete matrix metalloproteases (MMP) that degrade Bruch's membrane through which

proliferating choroidal blood vessels may invade into the subretinal space, thus promoting choroidal neovascularization (Campa et al., 2010).

1.4.7 Angiogenesis

Angiogenesis is the formation of new capillaries from pre-existing blood vessels. The process requires coordinated actions between pro-angiogenic and anti-angiogenic factors, leading to endothelial cell migration, proliferation, survival, and vascular maturation. The endothelial cells that line the ocular blood vessels are resistant to neovascular stimuli under the normal condition, therefore a quiescent state is maintained where negligible endothelial cell proliferation occurs due to a balance between pro-angiogenic and anti-angiogenic factors. However, this tightly regulated process can be disrupted under pathological conditions such as oxidative stress, hypoxia, and inflammation, which shift the balance towards neovascularization. Although angiogenesis is a physiological process that is integral to normal growth and development, pathological ocular angiogenesis can be harmful when it damages normal anatomic features – particularly in the retina and choroid – as it may result in significant impairment of visual function (Bressler 2009, Cabral, Mello et al. 2017).

Among many proangiogenic factors, the VEGF signaling pathway is most well characterized for its critical role in angiogenesis. Vascular endothelial growth factor (VEGF) is a family of secreted glycoproteins including VEGF-A, VEGF-B, VEGF-C, VEGF-D, VEGF-E (virally encoded), and placental growth factor (PlGF). The VEGF receptors (VEGFR) are transmembrane tyrosine kinase receptors and there are VEGFR-1, VEGFR-2, and VEGFR-3. Mainly, VEGF-A binds to both VEGFR-1 and 2 that is predominantly involved in regulation of angiogenesis. VEGF-B and PlGF bind to

VEGFR-1, and VEGF-C and D bind to VEGF-R3 which is widely known for its regulation of lymphangiogenesis, though it has an angiogenic role in early development (Adams and Alitalo 2007). In contrast to blood vessels that transport oxygenated blood, the primary function of lymphatic vessels are to absorb protein-rich fluids, lipids and macromolecules (Paduch 2016).

Considering angiogenesis and lymphangiogenesis occur concurrently, blood and lymphatic vessels may regulate each other (Nakao, Hafezi-Moghadam et al. 2012). VEGF-A and its receptors VEGFR-1 and VEGFR-2 that are predominantly expressed by endothelial cells are considered as the dominant regulators of angiogenesis during homeostasis and disease. VEGFR-2 is the main receptor of VEGF-A that promotes endothelial cell migration and vascular permeability (Apte, Chen et al. 2019). As shown in Figure 1.2, VEGF binds to its receptor and the receptor, then the activated receptors signal downstream pathways that are implicated in regulation of proliferation, survival, migration, and permeability of vascular endothelial cells mediating angiogenesis (Apte, Chen et al. 2019). Thus, the role that angiogenesis plays in late AMD is key to understanding why anti-VEGF therapy became critical in nvAMD treatment.

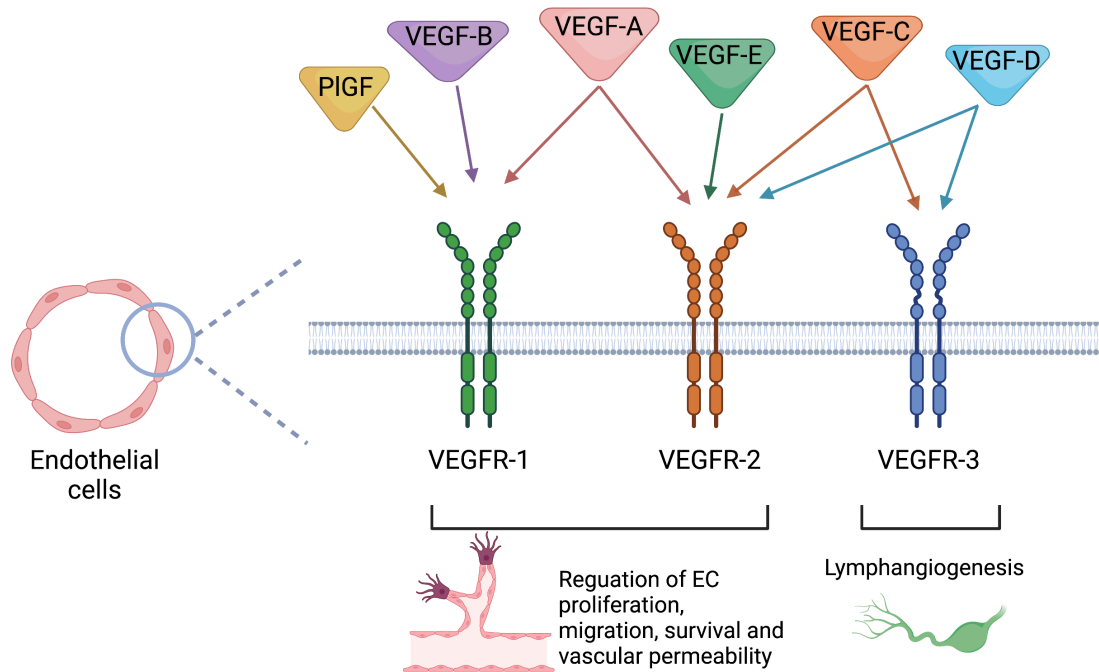


Figure 1.2: VEGF signaling in angiogenesis. The vascular endothelial growth factor family includes VEGF-A, VEGF-B, VEGF-C, VEGF-D, VEGF-E and placental growth factor (PIGF). VEGF signal transduction is carried out through the VEGFR tyrosine kinase receptor family. VEGF-A binds to VEGFR-1/2 with VEGFR-2 being the dominant signaling receptor regulating angiogenesis. VEGF-B and PIGF bind to VEGFR-1, and VEGF-C and VEGF-D bind to VEGFR-3 that is implicated in lymphangiogenesis.

1.5 Development of Choroidal Neovascularization

Choroidal neovascularization (CNV) is a major pathological feature of nvAMD, in which abnormal new blood vessels grow from the choroid into the retinal pigment epithelium (RPE) and neuroretina (Bird 2010). Leakage of these new blood vessels causes hemorrhage, retinal pathology, and eventual fibrotic scarring, with rapid, permanent vision loss (Ehrlich, Harris et al. 2008). In addition to being a specific feature of nvAMD, CNV can also be considered as a complication that results from pathological stimuli in numerous chorioretina disorders, posterior uveitis, and severe myopia (Green and Wilson 1986). The term CNV may suggest that it is just a vascular pathological condition, but CNV is properly defined as an abnormal tissue invasion of endothelial and inflammatory cells where there is a dynamic contribution of angiogenesis, inflammation, proteolysis and remodeling of the ECM (Campa, Costagliola et al. 2010, Kumar, Nakashizuka et al. 2017). The development of CNV can be divided into three stages: 1) Initiation, 2) Inflammatory Active, and 3) Involutional stages. (Grossniklaus and Green 2004, Campa, Costagliola et al. 2010)

1.5.1 Initiation Stage

In the **initiation stage**, RPE and photoreceptor cells produce VEGF, which plays a major role in inciting angiogenesis (Kvanta, Algvere et al. 1996, Lopez, Sippy et al. 1996). The production of VEGF by RPE, in particular, is conducted in a polarized manner in which basal secretion towards Bruch's membrane is greater than apical secretion towards photoreceptors (Blaauwgeers, Holtkamp et al. 1999). Furthermore, there are other growth factors and molecules produced by RPE that serve as a chemoattractant, recruiting macrophages, promoting endothelial cell differentiation, and

vascular permeability (Campa, Costagliola et al. 2010). All these processes stimulate pathological changes in Bruch's membrane, allowing the neovascular tissue invasion of endothelial cells, pericytes, fibrocytes and inflammatory cells into the subretinal space (Jensen, Jakobsen et al. 2020).

1.5.2 Inflammatory Active Stage

The following **inflammatory active stage** is distinguished by the progressive neovascular enlargement. This stage of active CNV progression is predominantly driven by inflammatory cells and abnormal production of cytokines through autocrine/paracrine mechanisms. The production of matrix metalloproteinases (MMPs) by the vascular endothelium and macrophages further facilitate CNV; invasion through Bruch's membrane is enhanced by degrading extracellular matrix (Steen, Sejersen et al. 1998). The RPE continues to play an important role during this stage. Basic fibroblast growth factor (FGF-2), that stimulates pathologic angiogenesis, TGF- β , and angiostatic proteins like pigment endothelial-derived factor (PEDF) are secreted by RPE (Campa, Costagliola et al. 2010). As an example, ECM fragments of complement components between Bruch's membrane and RPE may induce VEGF expression and exert chemotactic activity to recruit inflammatory cells that assist migration of choroidal capillaries (Bressler 2009). Thus, the disruption in homeostasis of angiogenesis, inflammation and proteolysis signaling mediate the progressive growth and maturation of CNV at this stage.

1.5.3 Involutional Stage

The **involutional stage** is distinguished by scarring and fibrosis. During this process, the balance shifts toward antiangiogenic and anti-proteolytic activities. Tissue inhibitors of metalloproteinases (TIMP) and TGF produced by RPE directs the regression

of neovascularization (Grossniklaus and Green 2004). Simultaneously, angiogenesis may continue until a state of normoxia is reached. Overall, maturation of blood vessels and formation of scar tissue leading to rapid vision loss, are the hallmarks of this late stage of CNV (Campa, Costagliola et al. 2010).

1.6 Therapy for Neovascular Age-related Macular Degeneration

1.6.1 Laser photocoagulation

Laser photocoagulation was the first treatment used to suppress the progression of nvAMD. It is a destructive form of therapy that results in occlusion of leaky blood vessels, as the light energy absorbed by ocular pigments gets converted into heat energy, raising the temperature and causing denaturation of the tissue in the region subjected to laser (Eong, Sanjay et al. 2006, Jian, Panpan et al. 2013). Laser photocoagulation therefore remains as the choice of therapy for patients with choroidal neovascularization outside the fovea to reduce the risk of visual loss from the treatment (Virgili and Bini 2007).

1.6.2 Photodynamic therapy

Photodynamic therapy with verteporfin (Visudyne, Novartis) was approved by the FDA in 2000 for treating CNV secondary to AMD. When irradiated with a 689 nm laser light, verteporfin releases singlet oxygen species that are highly reactive and able to denature choroidal neovascular endothelium. The non-thermal nature of this therapy was thought to prevent unwanted thrombosis of adjacent tissue; however, collateral damage to the surrounding tissue was still reported. Two large multicenter randomized clinical trials determined that photodynamic therapy with verteporfin halted significant loss of vision,

but it was not significantly effective in improving the visual acuity (Barak, Heroman et al. 2012).

1.6.3 Anti-VEGF

Anti-VEGF therapy revolutionized the treatment for neovascular eye diseases, including nvAMD. With the revelation that VEGF is a signaling protein that plays a key role in angiogenesis and vasculogenesis, targeting VEGF soon emerged as an effective therapeutic strategy against CNV. Pegaptanib sodium and Ranibizumab were the first intraocular anti-VEGF agents that were evaluated for the treatment of nvAMD in large, randomized, controlled clinical trials in which the efficacy of intraocular anti-VEGF pharmacotherapy was proven.

Pegaptanib sodium selectively inhibits VEGF-165, which is the most abundant VEGF isoform. Ranibizumab is a recombinant monoclonal antibody that binds to and inactivates all six isoforms of VEGF-A. Ranibizumab was designed specifically to treat nvAMD by altering the structure of a mouse monoclonal antibody, from which bevacizumab was derived. Bevacizumab is also a recombinant humanized monoclonal antibody that binds to and inhibits all isoforms of VEGF-A. It was originally approved by the FDA to treat colorectal, breast and lung cancer and designed to be delivered systemically, but soon, off-label use of intravitreal bevacizumab emerged as a strong alternative to ranibizumab because of the lower cost, comparable efficacy and grater duration of action (Bressler 2009, Campa, Costagliola et al. 2010, Barak, Heroman et al. 2012). Anti-VEGFs revolutionized the treatment and management of AMD, as they are not only effective in the inhibition of angiogenesis but also in arresting vascular

permeability, which accounts for the loss of visual acuity in patients with CNV (Campa, Costagliola et al. 2010, Barak, Heroman et al. 2012).

However, anti-VEGF agents present several limitations. Long-term use of anti-VEGF agents is associated with numerous systemic adverse effects including thromboembolic events and hypertension (Hayman, Leung et al. 2012). About 30% of patients were reported to be refractory to anti-VEGFs (Yang, Zhao et al. 2016), and there has been a concern regarding the long-term efficacy of current anti-VEGF agents with the reduction in bio-efficacy because of tachyphylaxis (Schaal, Kaplan et al. 2008). Novel anti-VEGF such as brolucizumab, which was recently approved for the treatment of nvAMD in the US, and conbercept that is moved to phase III clinical trials, have a greater affinity towards VEGF-A, enhanced chorio-retina penetration, and rapid systemic clearance (potentially reducing systemic side effects), therefore addressing some of the shortcomings of previous anti-VEGF agents (Tadayoni, Sararols et al. 2021, Zhou, Zheng et al. 2021).

Yet, the only current delivery route for anti-VEGF agents, due to their large molecular weight, is intravitreal injection which can be associated with intraocular complications, including infection (Cox, Elliott et al. 2021). Repeated intravitreal injections of anti-VEGF agents and thus frequent visits to clinics are required for maintenance, presenting a burden to clinicians, patients, and the healthcare system (Schmidt-Erfurth, Chong et al. 2014). As an example, in a recent survey study, patients at the Glick Eye Institute have expressed their preference towards visits more spaced out every three months while mode was 1 month. This and other factors, including physical discomfort that is inherent to the available drug delivery method for anti-VEGF, may

pose non-compliance issues (Jacobs, Palmer et al. 2021). Furthermore, CNV involved in nvAMD is a multifactorial process in which angiogenesis is not the only contributor. Thus, there is a critical need to elucidate other cellular components involved in pathophysiology and develop novel therapeutic strategies to combat CNV.

1.7 SH-11037, Anti-angiogenic small molecule and soluble epoxide hydrolase

To address the unmet needs in anti-angiogenic pharmacotherapy, Corson lab used a forward chemical genetics approach to identify a novel target involved in ocular angiogenesis. We previously reported the total synthesis of an antiangiogenic natural homoisoflavonoid, cremastranone, for the first time (Lee, Basavarajappa et al. 2014). Corson lab then completed a structure-activity relationship analysis of its derivatives and discovered a compound SH-11037 with greater potency and selectivity for endothelial cells, and efficacy in suppressing angiogenesis in the mouse laser induced choroidal neovascularization (L-CNV) model, a widely used model in which laser photocoagulation is used to rupture Bruch's membrane, resulting in angiogenesis from the choroid into the subretinal space (Basavarajappa, Lee et al. 2015, Sulaiman, Merrigan et al. 2016). Using SH-11037 based affinity reagents, we identified soluble epoxide hydrolase (sEH) as a cellular target of SH-11037 (Sulaiman, Park et al. 2018). Interestingly, sEH, encoded by the gene *EPHX2*, is a lipid-metabolizing enzyme that metabolizes bioactive epoxy fatty acids (EpFA).

Soluble Epoxide Hydrolase (sEH) is a 62 kDa enzyme with the N-terminal phosphatase activity and the C-terminal hydrolase function (Harris and Hammock 2013). sEH was first discovered through its activity on substrates such as epoxystearate.

Studying the differential hydrolysis of the epoxide lipid substrate, the epoxide hydrolase activity in the soluble fraction of multiple organs were detected, hence the enzyme was named soluble epoxide hydrolase (Gill and Hammock 1979).

sEH, with its hydrolase activity, metabolizes EpFAs like epoxyeicosatrienoic acids (EETs) from ω -6 arachidonic acid (AA), epoxydocosapentaenoic acids (EDPs) and epoxyeicosatetraenoic acid (EEQ) from ω -3 docosahexaenoic acid (DHA) and eicosapentaenoic acid (EPA) respectively. (Figure 3)(Park and Corson 2019). There is a growing awareness of the importance of bioactive lipid metabolism to ocular structure, function, and pathology.

Especially, the unique lipid profile of the retina gives an outsized role for DHA (22:6 ω -3) and DHA-derived PUFA metabolites in the eye. DHA is a major structural component of the membrane phospholipids in the retina (Querques, Forte et al. 2011), constituting 50–60% of the total fatty acids in the outer segments of photoreceptors (Stinson, Wiegand et al. 1991, Bush, Malnoe et al. 1994, Stillwell and Wassall 2003), in contrast to most tissues that contain only a small portion (~5%) of their fatty acids as DHA. In parallel with the arachidonic acid (AA, 20:4 ω -6) cascade, the metabolism of DHA involves three branches of oxylipin synthesis enzymes: cyclooxygenase (COX), lipoxygenase (LOX) and cytochrome P450 (CYP) epoxygenases, of which the CYPs are responsible for generating bioactive EpFAs (Morisseau, Inceoglu et al. 2010, Zhang, Panigrahy et al. 2013, Malamas, Chranioti et al. 2017). EpFAs like EETs and EDPs have garnered much attention in vascular disorders due to their vasodilatory and anti-inflammatory properties (Ye, Zhang et al. 2002, Zhang, Kodani et al. 2014, Capozzi, Hammer et al. 2016). EpFAs are physiologically unstable because they are rapidly

metabolized, mainly by soluble epoxide hydrolase (sEH) (Chacos, Capdevila et al. 1983) (Figure 1.3).

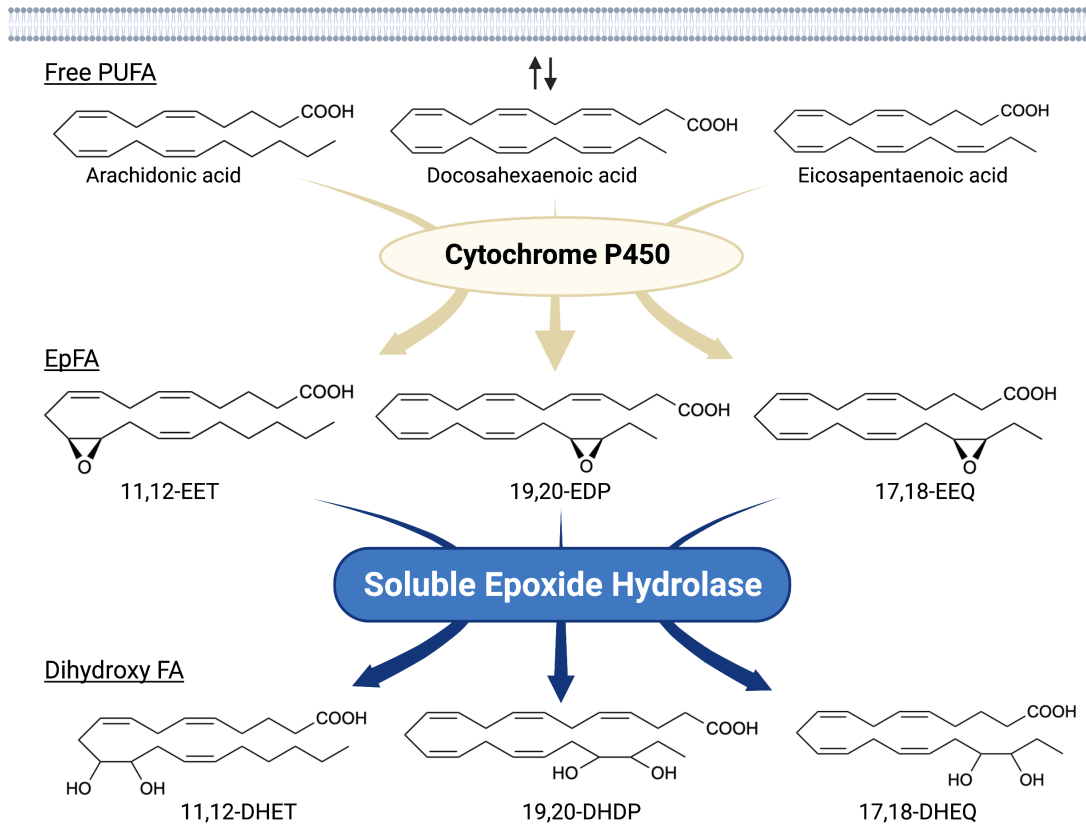


Figure 1.3: The CYP-sEH pathway. Arachidonic acid (AA), as well as docosahexaenoic acid (DHA) and eicosapentaenoic acid (EPA), are PUFAs metabolized by cytochrome P450 (CYP) to generate epoxy fatty acids (EpFAs) that have pro-resolving bioactivities. Inhibition of sEH preserves bioavailabilities of these EpFA. EET, epoxyeicosatrienoic acid; DHET, dihydroxyeicosatrienoic acid; EDP, epoxydocosapentaenoic acid; DHDP, dihydroxydocosapentaenoic acid; EEQ, epoxyeicosatetraenoic acid; DHEQ, dihydroxyeicosatetraenoic acid. Representative isomers are shown.

1.8 sEH inhibition and EpFAs in Angiogenesis and Inflammation

Genetic manipulation of CYP/sEH expression and small molecule mediated targeting of sEH has allowed investigation of the role of EpFAs in eye diseases, in particular diseases mediated by inflammation and angiogenesis. Through the metabolism of bioactive EpFAs and production of corresponding diols, sEH plays a role in the regulation of angiogenesis and inflammation relevant to the pathogenesis of numerous eye diseases.

Inhibition of sEH stabilizes EpFAs, enhancing their biological activities, which vary among EpFAs derived from ω -6 and ω -3 PUFAs. EETs and EDPs have vasodilatory (Oltman, Weintraub et al. 1998, Zhang, Oltman et al. 2001, Ye, Zhang et al. 2002) and analgesic effects, reducing inflammatory pain (Inceoglu, Jinks et al. 2008, Morisseau, Inceoglu et al. 2010, Wagner, Vito et al. 2014). But they have contradictory effects on angiogenesis: EETs usually have proangiogenic effects depending on the experimental context (Pozzi, Macias-Perez et al. 2005, Michaelis, Xia et al. 2008, Xu, Davis et al. 2013), whereas EDPs have antiangiogenic effects (Zhang, Panigrahy et al. 2013, Capozzi, McCollum et al. 2014, Hasegawa, Inafuku et al. 2017, Hu, Dziumbala et al. 2017). Moreover, sEH mediated metabolism of EpFAs produces lipid diols like dihydroxydocosapentaenoic acids (DHDP) (Figure 3). Thus, sEH inhibition can result in tissue-specific effects by modulating different classes of EpFAs depending on the abundance of individual PUFAs in the given tissue.

Targeting sEH with small molecule inhibitors effectively reduces ocular angiogenesis (Table 1.1). SH-11037 effectively blocked key angiogenic properties of human retinal endothelial cells (HRECs) — proliferation, migration, and tube formation

— without inducing cell death (Basavarajappa, Lee et al. 2015). As well, SH-11037 reduced angiogenesis in an ex vivo choroidal sprouting assay and inhibited developmental ocular angiogenesis in zebrafish larvae (Sulaiman, Merrigan et al. 2016). Local application of SH-11037 (1 μ M) into the eye via intravitreal injection significantly suppressed CNV lesions (Sulaiman, Merrigan et al. 2016) and was also effective in reducing retinal neovascularization in the oxygen-induced retinopathy (OIR) model (Basavarajappa, Lee et al. 2015), in which neonatal mouse pups are subjected to hyperoxia during their developmental retinal vascularization, causing ischemia-induced angiogenesis on return to normoxia (Scott and Fruttiger 2009, Kim, D’Amore et al. 2016). Structural, morphological and vascular examination of retina and electroretinography showed that up to 100 μ M intravitreal SH-11037 does not exert ocular toxicity (Sulaiman, Merrigan et al. 2016). Excitingly, SH-11037 also synergized with anti-VEGF therapy to reduce L-CNV (Sulaiman, Merrigan et al. 2016).

Intravitreal injection of other known sEH inhibitors *t*-AUCB (1–10 μ M) and “compound 7” (10–30 μ M) also suppressed L-CNV lesions (Sulaiman, Park et al. 2018) (Table 1.1). Moreover, intravitreal 10 μ M SH-11037 or *t*-AUCB treatment effectively increased the ratio of 19,20-EDP to 19,20-DHDP, indicating that local pharmacological inhibition of sEH can alter the lipid metabolism in the eye (Sulaiman, Park et al. 2018). These studies used 6–15 mice per treatment, plus vehicle-injected controls (Basavarajappa, Lee et al. 2015, Sulaiman, Merrigan et al. 2016, Sulaiman, Park et al. 2018), which should be sufficient to avoid any confounding effects of inflammation, which is a concern with this delivery route (Chiu, Chang et al. 2007). An inhibitory effect on ocular angiogenesis was also reported for other routes of administration of sEH

inhibitors. Oral administration of TPPU (1 mg/kg/day) not only reduced CNV lesions and vascular leakage but also its coadministration with i.p. injection of 17,18-EEQ or 19,20-EDP (50 µg/kg/day) potentiated anti-angiogenic effects on CNV (Hasegawa, Inafuku et al. 2017). In addition, normal neonatal mice that received i.p. injection of *t*-AUCB (2 mg/kg, twice/day) from 1-4 days had significantly reduced developmental retinal vascularization (Hu, Popp et al. 2014). Together, these studies support the therapeutic potential of sEH inhibitors for ocular neovascularization.

EDPs are anti-angiogenic *in vitro*: all the chemically stable EDP regioisomers inhibited VEGF-induced angiogenesis in a Matrigel plug assay (Zhang, Panigrahy et al. 2013). Of note, 19,20-EDP, which is the least efficient substrate for sEH, therefore most abundant isomer (Zhang, Kodani et al. 2014), had no effect on endothelial cell proliferation but strongly inhibited human umbilical vein endothelial cell tubular network formation and migration and weakly inhibited matrix metalloproteinase 2 (MMP-2) activity via a VEGF receptor 2 dependent manner (Zhang, Panigrahy et al. 2013), although the exact mechanism through which EDPs crosstalk with VEGF signaling remains to be clarified.

ω-3 EpFAs also have anti-inflammatory and anti-angiogenic effects in animal models of ocular angiogenesis. Dietary intake of ω-3 PUFAs but not ω-6 PUFAs reduces murine L-CNV (Yanai, Mulki et al. 2014). Dietary intake of ω-3 PUFAs in mice substantially enhanced levels of epoxide products - 17,18-epoxyeicosatetraenoic acid (EEQ) and 19,20-EDP in the serum lipid profile, however it did not increase levels of EDPs in the retinal lipid profile. Interestingly, dietary intake of 17,18-EEQ or 19,20-EDP also suppressed CNV, suggesting that the protective effect of ω-3 PUFAs against CNV

could be mediated by its downstream epoxy metabolites that are generated by CYP. In addition, dietary ω -3 PUFAs interfered with leukocyte invasion into the CNV lesions, while ω -6 PUFA did not (Yanai, Mulki et al. 2014). These effects were associated with anti-inflammatory properties of EpFAs. Specifically, they modulated leukocyte rolling velocity by changing the expression of adhesion molecules on the surfaces of leukocytes and in the CNV lesions (Hasegawa, Inafuku et al. 2017). In transgenic mice overexpressing CYP2C8 in endothelial cells, the dietary intake of ω -3 PUFAs, which increased production of 17,18-EEQ and 19,20-EDP in serum, reduced CNV lesions (Hasegawa, Inafuku et al. 2017). Likewise, dietary ω -3 PUFAs reduced CNV lesions in *Ephx2*^{-/-} mice. These mice also had increased plasma levels of 17,18-EEQ and 19,20-EDP, since sEH-dependent degradation of these epoxides into corresponding diols was blocked. In contrast, dietary ω -3 PUFAs did not confer inhibitory effects on CNV in mice overexpressing sEH.

In the developing mouse retina, sEH is highly expressed in Müller glia, and DHDP produced by sEH contributes to retinal angiogenesis (Hu, Popp et al. 2014). Müller glia spans the entire retina radially, providing structural and metabolic support for retinal neurons (Reichenbach and Bringmann 2013). The Müller cell-specific knockout of sEH or systemic deletion of sEH significantly impaired developmental retinal angiogenesis and altered the retinal lipid profile. The level of 19,20-DHDP was significantly reduced in the retina of *Ephx2*^{-/-} mice, and intravitreal injection of 19,20-DHDP rescued the impaired retinal angiogenesis in these mice. 19,20-DHDP was also found to be a signaling molecule, downregulating the endothelial Notch signaling pathway by inhibiting presenilin-1 dependent γ -secretase activity, which is required for

release of the Notch intracellular domain (Hu, Popp et al. 2014). Interestingly, the crosstalk between Notch and VEGF pathways in angiogenesis has been reported in numerous studies, where activation of Notch signaling modulates VEGF signaling (Hellström, Phng et al. 2007, Li and Harris 2009). Overall, there is a strong rationale to pursue sEH as a therapeutic target for CNV given that both inflammation and angiogenesis are underlying processes of the pathology.

1.9 sEH in Other Ocular Diseases

1.9.1 Nonproliferative Diabetic Retinopathy

sEH has also been implicated in nonproliferative diabetic retinopathy. This early phase of the disease is characterized by pericyte loss and increased vascular permeability, distinct from the late proliferative phase characterized by neovascularization (Hammes, Lin et al. 2002). A study (Hu, Dziumbo et al. 2017) reveals that increased retinal expression of sEH and corresponding production of 19,20-DHDP contribute to the progression of nonproliferative diabetic retinopathy in hyperglycemic *Ins2^{Akita}* mouse retinas and in the retinas and vitreous of human diabetic patients. Under normal conditions, retinal endothelial cells are connected by tight junction proteins and supported by pericytes. During the early phase of diabetic retinopathy, 19,20-DHDP alters the distribution of presenilin 1 in lipid rafts of the cell membrane, thereby preventing interaction between presenilin 1 and cadherins and disrupting endothelial cell to pericyte and endothelial cell-to-cell contacts. Treatment with sEH inhibitor *t*-AUCB (Table 1.1) in drinking water (2 mg/L) significantly reduced the retinal level of 19,20-DHDP and normalized vascular defects (reduced pericyte number, enhanced migration of vascular pericytes to the extravascular space, increased acellular capillaries and increased vascular

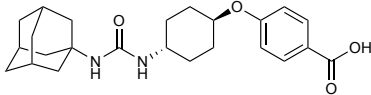
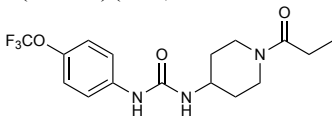
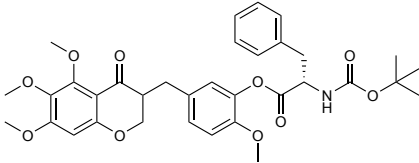
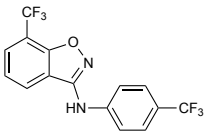
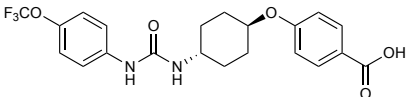
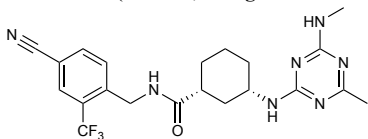
permeability) that were present in the eyes of diabetic mice. Overexpression of sEH (delivered by intravitreal adenovirus) in retinal Müller glia increased retinal 19,20-DHDP and induced retinopathy in non-diabetic mice, highlighting that sEH may play a causative role in progression of the disease (Hu, Dziumbala et al. 2017). This mechanism – disrupting endothelial cell junctions of the BRB by sEH-dependent production of 19,20-DHDP – is worth investigating further since defects in the BRB contribute to other eye diseases (Campochiaro, Soloway et al. 1999, Green 1999). Furthermore, a recent study reported that sEH inhibitor TPPU reduces fasting glucose level in rats (Minaz, Razdan et al. 2018).

1.9.2 Diabetic Keratopathy

Diabetic keratopathy is characterized by delayed corneal epithelial wound healing and epithelial erosion, resulting in a compromised defense system against corneal injury and infective agents (Kaji 2005). sEH is a potential therapeutic target for diabetic keratopathy, as tested in a mouse model where corneal erosions develop upon a single corneal debridement wound (Sun, Lee et al. 2018). The expression and enzymatic activity of sEH were increased in the corneal epithelial cells of streptozotocin-induced diabetic epithelial unwounded and wounded mice compared to control mice. *Ephx2*^{-/-} mice with streptozotocin-induced diabetes showed an increase in the rate of epithelial wound healing, decreased sensory nerve degeneration of corneas, and did not develop diabetes-associated dry eye symptoms. The loss of sEH also restored wound-induced STAT3 signaling and heme oxygenase-1 (HO-1) expression that were downregulated by hyperglycemic conditions. Similarly, sEH inhibition with subconjunctival 10 nM *t*-AUCB or clinical candidate inhibitor GSK2256294A (Table 1.1) promoted epithelial

wound healing and restored HO-1 expression in diabetic mouse corneas (Sun, Lee et al. 2018).

Table 1.1: Soluble epoxide hydrolase inhibitors tested in ocular disease animal models

sEH inhibitor (Reference)	Routes	Dose	Model	Reference
<i>t</i>-AUCB (UC1471) (Hwang, Tsai et al. 2007) 	Oral	2 mg/L	Mouse diabetic retinopathy, sEH in drinking water for 10 months	(Hu, Dziumbo et al. 2017)
	Intravitreal	1–10 μ M	Mouse L-CNV, single sEH injection	(Sulaiman, Park et al. 2018)
	Intraperitoneal	2 mg/kg	Mouse neonatal retinal angiogenesis, twice a day sEH injections for postnatal (P) days 1-4	(Hu, Popp et al. 2014)
	Subconjunctival	10 nM	Mouse diabetic keratopathy, single sEH delivery	(Sun, Lee et al. 2018)
TPPU (UC1770) (Rose, Morisseau et al. 2010) 	Intraperitoneal	0.3 mg/kg	Mouse OIR, daily sEH injections from P12-P16 Mouse L-CNV, daily sEH injections from day 0-6	(Gong, Fu et al. 2016)
	Oral	1 mg/kg	Mouse L-CNV, daily sEH delivery from 3 days before CNV induction to day 7	(Hasegawa, Inafuku et al. 2017)
SH-11037 (Basavarajappa, Lee et al. 2015) 	Intravitreal	0.1–100 μ M	Mouse ocular toxicity 1–10 μ M Mouse L-CNV, single sEH injection	(Sulaiman, Merrigan et al. 2016)
	Systemic (In larvae water)	1–10 μ M	Ocular angiogenesis in zebrafish larvae, sEH treatment 2-5 days post fertilization	
	Intravitreal	1 μ M	Mouse OIR, single sEH injection	(Basavarajappa, Lee et al. 2015)
“Compound 7” (Shen, Ding et al. 2009) 	Intravitreal	10–30 μ M	Mouse L-CNV, single sEH injection	(Sulaiman, Park et al. 2018)
<i>t</i>-TUCB (UC1728) (Hwang, Tsai et al. 2007) 	Subcutaneous	3 mg/kg	Rabbit LPS-induced uveitis, daily sEH injections	(McLellan, Aktas et al. 2016)
GSK2256294A (Podolin, Bolognese et al. 2013) 	Subconjunctival	10 nM	Mouse diabetic keratopathy, single sEH delivery	(Sun, Lee et al. 2018)

Abbreviations: L-CNV, laser-induced choroidal neovascularization; LPS, lipopolysaccharide; OIR, oxygen-induced retinopathy; P, postnatal; sEH, soluble epoxide hydrolase inhibitor

1.10 Summary and Dissertation Overview

Age-related macular degeneration (AMD) is a retinal neurodegenerative disease, and it is the leading cause of blindness in older adults. The advanced form of the disease, neovascular AMD (nvAMD), which accounts for 90% of the blindness resulting from AMD (Rein, Wittenborn et al. 2009), is distinguished by choroidal neovascularization (CNV), aberrant blood vessel growth from the choroid into the retinal pigment epithelium (RPE) and neuroretina. Despite its name, CNV is properly defined as an abnormal tissue invasion of endothelial and inflammatory cells where both angiogenesis and inflammation contribute.

Over the past decade, intravitreal anti-VEGF therapy has significantly advanced the treatment of neovascular eye diseases, including nvAMD. However, we have learned that targeting one pathway that is also involved in normal developmental and physiological processes poses limitations such as undesired adverse effects, tachyphylaxis and development of refractory nvAMD. Therefore, the development of novel therapeutic strategies is desired to address unmet needs in treatment. We previously used a forward chemical genetics approach using a lead anti-angiogenic small molecule and identified soluble epoxide hydrolase (sEH) as a target for inhibiting CNV. sEH, encoded by *EPHX2*, is a bifunctional enzyme with a C-terminal hydrolase function that is responsible for the hydrolysis of PUFA-derived EpFAs that have distinct bioactivities in pathological angiogenesis and inflammation (Park and Corson 2019). To this end, the hydrolase activity of soluble epoxide hydrolase (sEH) has been explored in the context of several eye diseases, although some conflicting results pose challenges for the synthesis of a common mechanism.

The objective of my thesis research is to determine sEH-mediated mechanisms that regulate CNV and preclinically validate sEH as a therapeutic target. Early in-depth target validation is critical in drug development to ensure that engagement of the target has a therapeutic benefit (Figure 1.4) (Hughes, Rees et al. 2011). Given that the kinetic mechanism of sEH inhibition by SH-11037 and the cellular role of sEH in CNV need to be further investigated, I proposed to elucidate drug-target interactions through enzyme kinetics, and I hypothesized that sEH is overexpressed by disease relevant retinal cells in CNV and targeting these cell types will suppress CNV.

In following Chapter 2, methods used in experiments are described in detail. Chapter 3 covers the kinetic mechanism of sEH inhibition by SH-11037, revealing crucial mechanism of action and drug-target interaction information. Chapter 4 establishes the relevance of sEH expression in retinal cell type involved in CNV development by defining the distribution of sEH expression in human nvAMD and murine L-CNV retinas. Chapter 5 addressed the hypothesis that sEH in the eye is required for CNV formation in vivo. Results from local sEH knockdown in the retina achieved through intraocular delivery of adeno associated virus mediated shRNA targeting *Ephx2* are presented. Chapter 6 provides discussion of the results and addresses study limitations and future directions of the studies.

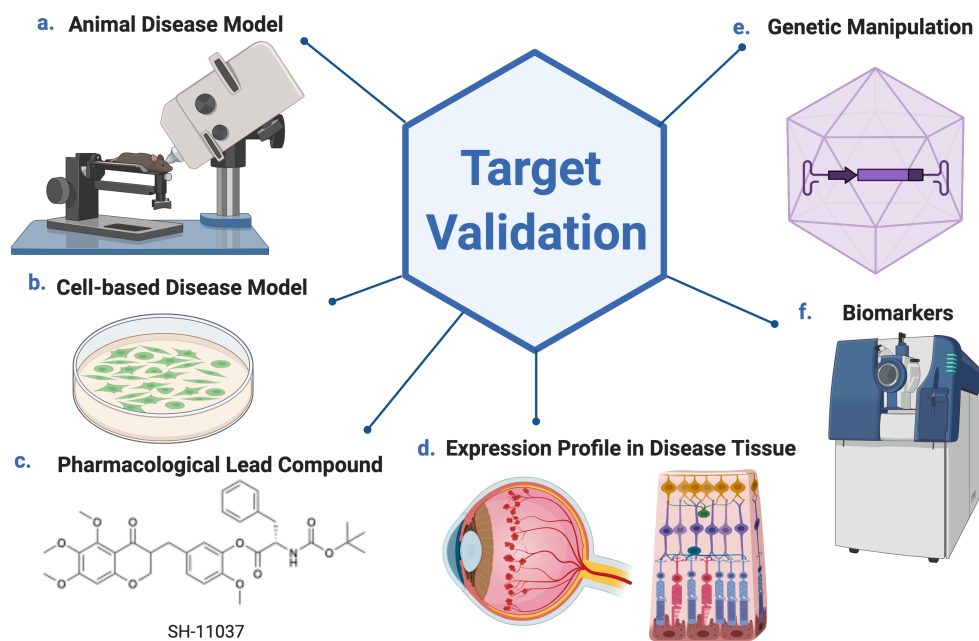


Figure 1.4: Approaches to target validation in early drug discovery.

CHAPTER 2. METHODS

2.1 Overview

In **Chapter 2**, each sub-chapter will describe research design and methods that align with the research aims. For the research objectives addressed in **Chapter 3**, methods of sEH inhibitor assay, enzyme kinetics experiments, and ex vivo sEH activity assay that were employed to answer the questions of drug-target interaction between SH-11037 and sEH, are described in detail. For the research objectives of defining spatial expression pattern and cellular expression of sEH in **Chapter 4**, the methods of immunofluorescence and RNAscope in situ hybridization are described and justified in detail. For the research objectives of determining the effect of ocular sEH knockdown *in vivo* in a murine choroidal neovascularization in **Chapter 5**, the relevant methods including AAV delivery, laser-induced choroidal neovascularization mouse model, non-invasive ophthalmic imaging, immunoblotting, and gene expression analysis are described in detail. Data analysis methods are also clarified, and the justifications of the research strategy chosen for each research objective are provided.

2.2 Tissue-based sEH Activity Assay using *trans*-Stilbene Oxide

The sEH activity in tissue homogenates of untouched control and L-CNV eyes was assayed using *trans*-stilbene oxide (*t*-SO) as substrate. The assay is based on the hydrolysis of *t*-SO that is tracked as a decrease in the absorbance at 230 nm (Figure 2.1) (Archelas, Zhao et al. 2016), and it presents a rapid and accurate procedure for quantifying sEH activity in tissue extracts (Hasegawa and Hammock 1982, Charles, Burgoyne et al. 2011). The assay was employed under room temperature conditions and the change in absorbance was detected at 27 °C in the plate reader (Biotek).

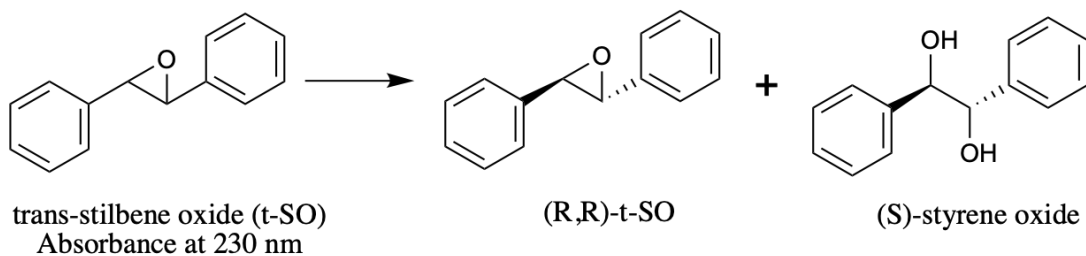


Figure 2.1: Reaction mechanism of *trans*-stilbene oxide with sEH. sEH dependent hydrolysis of the epoxide moiety of *t*-SO results in formation of (*R,R*)-*t*-SO and (*S*)-styrene oxide.

L-CNV was induced as described below in Chapter 2.6. After 3 days, enucleated eyes from both untreated and L-CNV mice were homogenized in 0.2 M sodium phosphate buffer, pH 7.4. To remove microsomal epoxide hydrolase and lenses, tissue extracts were centrifuged at 100,000×*g* for 30 minutes at 4°C. After protein estimation, 100 μL of tissue supernatants (100 μg/mL) and 98 μL of SH-11037 or 7 dissolved in DMSO/buffer (final 1% (v/v) DMSO) were added to a UV-transparent 96-well plate. After 5 minutes of incubation at room temperature, 2 μL of *t*-SO in ethanol (100 μM final

concentration) was added to assay wells to initiate the reaction. The absorbance was read at 230 nm for 20 minutes. sEH activity was determined as follows:

$$\text{sEH Activity} = [(A_0 - A_{20}) - (B_0 - B_{20})]/\text{mg of protein in a reaction}$$

Where A_0 and A_{20} are absorbance of test wells read at 230 nm at time 0 and 20 minutes respectively, and B_0 and B_{20} are absorbance of background wells read at 230 nm at time 0 and 20 minutes. This method was used in **Chapter 3**.

2.3 sEH Inhibitor Assay

In **Chapter 3**, small molecule inhibition of soluble epoxide hydrolase (sEH) enzymatic activity was evaluated to determine their half-maximal inhibitory concentrations. IC_{50} values were determined using the sEH inhibitor screening assay based on the synthetic, fluorogenic substrate PHOME (3-phenyl-cyano(6-methoxy-2-naphthalenyl)methyl ester-2-oxiraneacetic acid) (Cayman Chemical) following the manufacturer's instructions. The epoxide moiety of PHOME is hydrolyzed by epoxide hydrolase activity of sEH, leading to intramolecular cyclization and the release of cyanohydrin. The cyanohydrin rapidly decomposes into cyanide ion and the highly fluorescent 6-methoxy-2-naphthaldehyde that can be analyzed using an excitation wavelength of 330 nm and an emission wavelength of 465 nm (Figure 2.2) (Wolf, Morisseau et al. 2006). The assay was employed under room temperature conditions and the formation of fluorescent product was detected at 27 °C in the plate reader (Biotek, Winooski, VT).

Various concentrations of compounds were tested for their inhibitory activities: SH-11037 (synthesized as described (Basavarajappa, Lee et al. 2015)), t-AUCB (Cayman

Chemical), SH-11098 (synthesized as described) and compound 7. Benzisoxazole sEH inhibitor 7 was synthesized according to a published method, and characterization matched published parameters (Shen, Ding et al. 2009). Purity of all synthesized compounds was >95% by HPLC. All the small molecule synthesis was performed and provided to us by our collaborator Dr. Seung-Yong Seo of Gachon University.

Compounds were dissolved in DMSO (final DMSO concentration = 5% (v/v)). Activity was calculated according to:

$$\% \text{ Initial Activity} = [(F_{115} - F_{I0}) / (F_{T15} - F_{T0})] \times 100\%$$

Where F_I is the background corrected fluorescence signal obtained in the presence of an inhibitor and F_T is the background corrected fluorescence signal obtained for the total activity at times 0 and 15 minutes. IC₅₀ values were calculated using GraphPad Prism v.

7.0.

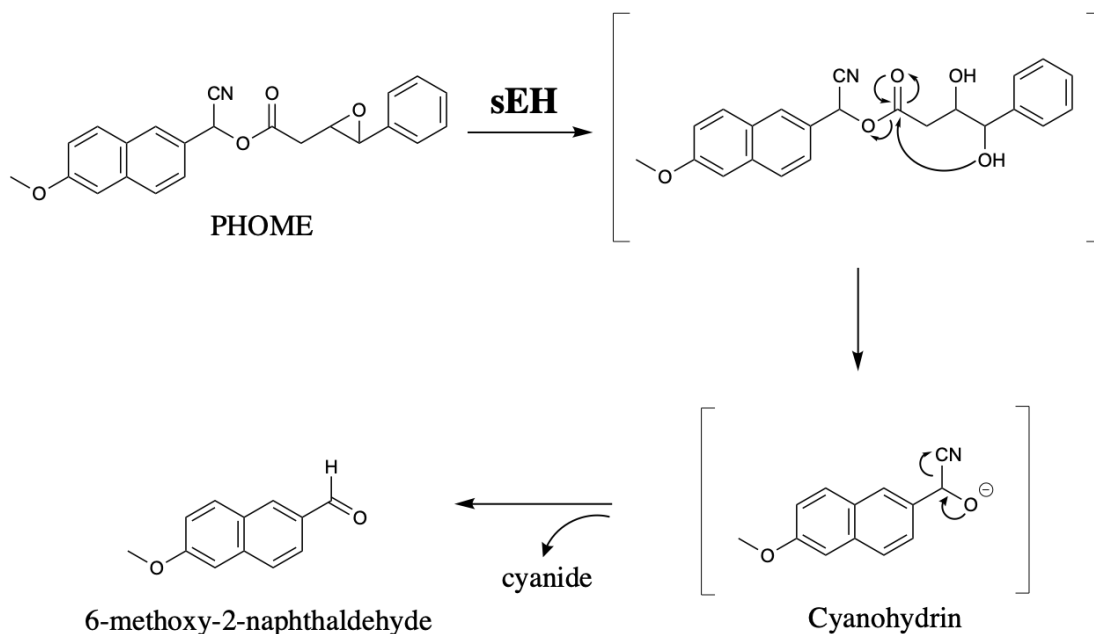


Figure 2.2: Reaction mechanism of PHOME with sEH. sEH hydrolyzes the epoxy moiety of PHOME, resulting in a highly fluorescent product. With this, inhibition potency can be readily and sensitively analyzed.

2.4 sEH Enzyme Kinetics Assay

In **Chapter 3**, enzyme kinetics studies were performed to elucidate the binding mechanisms of SH-11037 with sEH. Likewise, the assay was employed under room temperature conditions and the formation of fluorescent product was detected at 27 °C in the plate reader (Biotek, Winooski, VT). Various concentrations of SH-11037 or compound 7 were dissolved in DMSO (final DMSO concentration = 5% (v/v)) and human sEH (60 ng/mL final concentration; Cayman Chemical) in 25 mM bis-Tris-HCl buffer containing 0.1% (w/v) BSA were mixed in a 96 well plate. PHOME at indicated concentrations was added to the wells to initiate the reaction ($[S]_{\text{final}} = 30, 10, 3, 1$ and $0 \mu\text{M}$). The amount of substrate turned over by the epoxide hydrolase activity was measured by reading the fluorescent product with an excitation wavelength of 330 nm and an emission wavelength of 465 nm. The standard curve plotted from dilutions of the product, 6-methoxy-2-naphthaldehyde, was used to convert fluorescence reading (RFU/min) to sEH activity (nmol product formed/min). Initial velocities were calculated by linear regression by obtaining the slope of the line from time = 5 to 15 minutes for each substrate concentration. Results were analyzed using SigmaPlot 13.0 to determine Michaelis-Menten kinetic parameters and the inhibitory constant, K_i value.

Briefly, I conducted data analysis in the following three steps: 1) Measurement of reaction progress curves of product formation over time, to determine the rates from the linear portion of the reaction. 2) Construction of Michaelis-Menten plot of rate of reaction as a function of substrate concentration, and double-reciprocal (Lineweaver-Burk) plot of inverse initial velocity as a function of the inverse of the substrate concentration in SigmaPlot. 3) Using Exploratory Enzyme Kinetics option in SigmaPlot,

fitting an appropriate equation to the data of the secondary plot to determine enzyme kinetics parameters, I generated direct linear plots and a numeric report to elucidate the type of inhibition. To analyze the non-competitive mixed inhibition, the Lineweaver-Burk equation is written as following:

$$\frac{1}{V} = \frac{K_m}{V_{max}} \left(1 + \frac{[I]}{K_i} \right) \frac{1}{[S]} + \frac{1}{V_{max}} \left(1 + \frac{[I]}{K_i} \right)$$

Secondary plots can be derived from following equation:

$$Slope = \frac{K_m}{V_{max}} + \frac{K_m [I]}{V_{max} K_i}$$

2.5 Human Retina

For the **Chapter 4** research aim of defining the localization of sEH expression in human nvAMD retinas, formalin fixed paraffin embedded (FFPE) retinal sections were prepared from human donor eyes from nvAMD and control subjects with no documented ocular pathology that were obtained from the National Disease Research Interchange (NDRI; Philadelphia, PA) through our collaborator, Dr. Michael Boulton at the University of Alabama - Birmingham. All human sample tissues were deidentified with full ethical approval for research use.

2.6 Animals

All mouse experiments were approved by the Institutional Animal Care and Use Committee, Indiana University School of Medicine and followed the guidelines of the Association for Research in Vision and Ophthalmology (ARVO) Statement for the Use of Animals in Ophthalmic and Visual Research. Wild-type C57BL/6J male mice, 6-8 weeks of age, were purchased from Jackson Laboratory (Bar Harbor, ME). The mice were

housed under standard conditions in the Indiana University Laboratory Animal Resource Center (LARC) (Wenzel, O'Hare et al. 2015). Sample sizes for experiments were based on power analyses, and treatments were randomly assigned by cage and animals. The experimenter was masked to treatment during analyses.

2.7 Mouse Model for L-CNV

Laser-induced choroidal neovascularization is a widely used preclinical model of CNV in nvAMD. The model utilizes an argon laser to administer targeted injury to the RPE and Bruch's membrane, which results in blood vessel growth from the choroid into the subretinal space (Figure 2.3A). The image-guided laser system (Micron IV, Phoenix Labs) is established in our laboratory as a highly effective and reproducible tool for inducing CNV. Using the Micron IV, I also performed brightfield and fluorescence funduscopy, which provides wide view image of the retina, optical coherence tomography (OCT), which enabled me to take cross-section images of the retina and fluorescein angiography (FA) which allows visualization of the vascular network (Fig. 2.3B). This noninvasive *in vivo* retinal imaging method is detailed further in **Chapter 2.12**.

Mice were anesthetized by intraperitoneal injections of 90 mg/kg ketamine hydrochloride and 5 mg/kg xylazine mixture. Pupils of both eyes were dilated with topical drops of 1% tropicamide (Henry Schein Inc.) and 2.5% phenylephrine ophthalmic solution (Akorn, Lake Forest, IL). Corneas were kept lubricated with 2.5 % Gonak hypromellose ophthalmic solution (Akorn). The mouse was placed on the stage of a Micron IV Laser Injector (Phoenix Research Laboratories, Pleasanton, CA). By adjusting

the stage, the mouse was aligned to the camera and the iris and pupil were brought into focus. The Micron instrument was advanced forward while focusing on retinal features. Eyes were then subjected to 50 μm spot size, 70 ms, 250 mW pulses of the argon green ophthalmic laser coupled to the Micron IV ocular imager, resulting in 3 laser burns per eye approximately two-disc diameters from the optic disc (Figure 2.3AB). In **Chapter 3** sEH activity assay using *t*-SO as a substrate, and **Chapter 4** sEH expression analysis, mice received 10 laser burns. For this, eyes were enucleated on day 3 post laser and tissue samples were harvested for cryosectioning. In **Chapter 5** sEH knockdown study, mice received 3 laser burns on day 7 post intravitreal injection of AAV, then the eyes were enucleated 14 days after laser and tissue samples were harvested for cryosectioning, choroidal flatmounts, protein and RNA analysis described below.

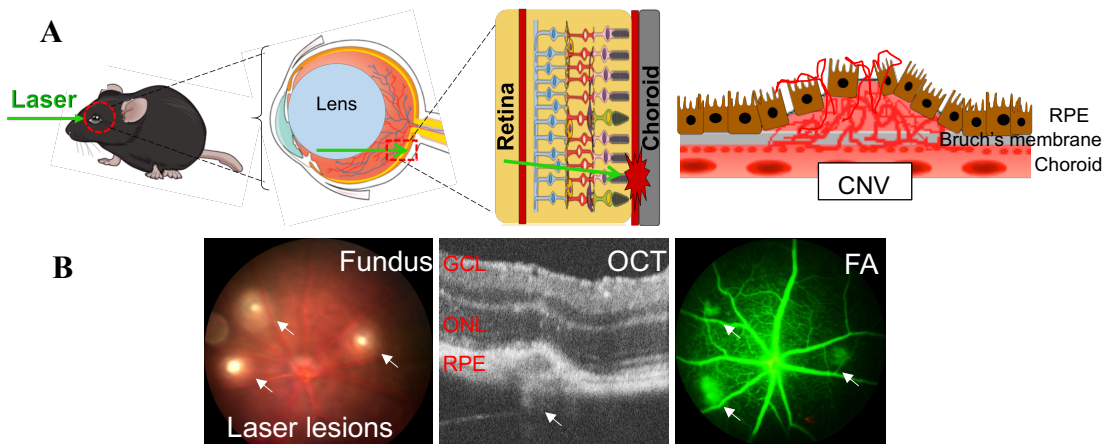


Figure 2.3: Laser-induced choroidal neovascularization and noninvasive retinal imaging methods. (A) Laser-induced choroidal neovascularization (L-CNV). (B) Noninvasive retinal image techniques – brightfield funduscopy, optical coherence tomography (OCT), fluorescein angiography (FA) from left to right. Three arrows in fundus and FA images indicate resulting laser lesions, and the arrow in the OCT image indicates a cross-section of a single lesion. GCL, ganglion cell layers; ONL, outer nuclear layer; RPE, retinal pigment epithelium.

2.8 Embedding and cryosectioning

Corneas of enucleated mouse eyes were punctured with a 29G needle and the whole eye was fixed in 4% formaldehyde in PBS at 4 °C overnight. Fixed whole eye was dissected to remove cornea and isolate posterior cup of chorioretinal tissue, which was rinsed in PBS and immersed in a sucrose gradient. Tissue was then transferred to a cryomold containing Optimum Cutting Temperature compound (Fisher Scientific, Hampton, NH) and stored at -80 °C until sectioning. Samples were sectioned using a cryostat (Leica Biosystems, Wetzlar, Germany) at -20 °C, with section thickness of 10 µm and mounted on SuperFrost Plus Slides (Fisher Scientific). This method was used in **Chapters 2 and 3**.

2.9 Immunofluorescence

For immunostaining of FFPE human eye sections, sections were deparaffinized, rehydrated and underwent heat-induced antigen retrieval in which tissue slides were immersed in citrate buffer (Thermo Scientific, Waltham, MA) and heated (>95°C) for 5 minutes. Sections were then washed with TBS and blocked in 10% DAKO diluent in 1% BSA in TBST for an hour at room temperature, then incubated overnight at 4 °C with primary antibodies or lectins: mouse anti-sEH, A5 (1:100; Santa Cruz, Dallas, TX), *Ricinus communis* agglutinin I (FITC-labeled, 1:400 for human; Vector Labs, Malvern, PA), PNA biotin conjugate, L6135 (1:250; Sigma, St. Louis, MO), WGA Alexa Fluor 647 conjugate, W32466 (1:250; Thermo Fisher, Waltham, MA), rabbit anti-RPE65, ab231782 (1:400; Abcam, Cambridge, United Kingdom). The specificity of PNA binding to cone matrix domains and that of WGA binding to rod matrix domains in human retinas

have been well characterized in the literature (Sameshima, Uehara et al. 1987, Tien, Rayborn et al. 1992). Sections were then incubated with the following secondary antibodies for an hour at room temperature: goat anti-mouse IgG (H+L) Alexa Fluor 555, Streptavidin DyLight 488, or goat anti-rabbit IgG (H+L) Alexa Fluor 480 (each at 1:400, Thermo Fisher). After a brief wash in TBS and dehydration with ethanol and xylene treatments, sections were mounted with Vectashield mounting medium plus DAPI (Vector Biolabs).

For the immunostaining of AAV-transduced fixed-frozen mouse retina, cryosections were prepared as described above. Sections were brought to room temperature and washed with PBS, then blocked in 2.5% BSA, 0.3% Triton-X 100 in PBS for 1 hour at room temperature. In **Chapter 4** elucidating localization of sEH in retina, the sections were incubated with the following primary antibodies overnight at 4 °C: mouse anti-sEH, A5 (1:400; Santa Cruz), *Ricinus communis* agglutinin I (rhodamine labeled, 1:250, Vector Labs); rabbit anti-RPE65, ab231782 (1:500; Abcam); mouse anti-rhodopsin, ab3424 (1:300; Abcam); rabbit anti-cone arrestin, AB15282 (1:500; Millipore, Burlington, MA); mouse-anti-calbindin, ab11426 (1:300, Abcam); rabbit anti-Brn3a, AB5945 (1:400; Millipore); and rabbit anti-vimentin PLA0199 (1:300; Sigma) diluted in 10% (v/v) DAKO diluent in TBST/1% (w/v) BSA (only PBS/1% (w/v) BSA for human) (Table 2.1). In **Chapter 5** elucidating localization of AAV induced retinal cells, the sections were incubated with the following primary antibodies overnight at 4 °C: rabbit anti-RPE65, ab231782 (1:500; Abcam), mouse anti-rhodopsin, ab3424 (1:300; Abcam) and rabbit anti-cone arrestin, ab15282 (1:500; Millipore). Subsequently, sections were incubated with the following secondary antibodies for 1 hour at room temperature: goat

anti-mouse IgG (H+L) Alexa Fluor 555 or goat anti-rabbit IgG (H+L) Alexa Fluor (Thermo Fischer) diluted 1:400 (1:500 for human) in 10% (v/v) DAKO diluent in TBST/1% (w/v) BSA (only PBS/1% (w/v) BSA for human) for an hour at room temperature. Sections were washed in PBS and mounted with Vectashield mounting medium-plus DAPI. Images were acquired using the 20x objective of a Zeiss LSM 700 laser scanning confocal microscope with ZEN imaging software.

Antigen/Lectin	Catalog #	Company	Dilution ratio (1:N)	
			Human retina	Mouse retina
sEH	A5	Santa Cruz	100	400, 1000 (IB)
RCA	RCA I	Vector labs	400	250
PNA	L6135	Sigma	250	N/A
WGA	W32466	Thermo Fischer	250	N/A
RPE65	ab231782	Abcam	400	500
Rhodopsin	ab3424	Abcam	N/A	300
Cone arrestin	AB15282	Millipore	N/A	500
Calbindin	ab11426	Abcam	N/A	500
Brn3a	AB5945	Millipore	N/A	400
Vimentin	PLA0199	Sigma	N/A	300
GS-IB4	I21411	Thermo Fischer	N/A	250
β -actin	AC-49	Sigma-Aldrich	N/A	5000 (IB)

Table 2.1: Antibody and lectin information for the human and mouse retina immunofluorescence and immunoblotting (indicated in parentheses).

2.10 RNAscope In Situ Hybridization

For the spatial expression examination, RNAscope ISH was performed on both murine L-CNV and human nvAMD retinas to provide important information regarding gene expression and identify the cell of origin, in addition to information where the protein localizes and address limitations of antibody and immunohistochemistry methods. RNAscope is a recently developed ISH technique with high sensitivity and low background. RNAscope utilizes a unique probe system to amplify the signal from rare RNAs. Additionally, the double Z probe enables a significant reduction in nonspecific signal amplification. The assay was performed on FFPE human retina sections and frozen mouse retina sections as directed by the manufacturer (ACD, Advanced Cell Diagnostics, Newark, CA).

Briefly, sections were treated with hydrogen peroxide, then antigen retrieval and protease digestion. After the pretreatment, RNAscope Multiplex Fluorescent Assay was performed to hybridize target-specific probes. RNAscope Hs-*EPHX2* (Cat No. 558681) was used to detect human *EPHX2* mRNA. RNAscope Mm-*Ephx2* (Cat No. 558701) and Mm-*ApoE* (Cat No. 313271) were used to detect mouse *Ephx2* mRNA and *ApoE* mRNA along with ACD universal negative control probe targeting the *DapB* gene (accession # EF191515) from the *Bacillus subtilis* strain SMY. After the hybridization, a three-step amplification process was performed followed by development of channel specific signal and binding of 570 Opal fluorophore, SKU FP1488001KT (1:500, Akoya Biosciences, Marlborough, MA) for *EPHX2/Ephx2* mRNA and 520 Opal fluorophore, SKU FP1487001KT (1:500, Akoya Biosciences) for *ApoE* mRNA. Sections were then counterstained with DAPI for nuclear identification and cover slipped using antifade

mountant, Fluoromount-G (SouthernBiotech, Birmingham, AL). Slides were imaged on a Zeiss LSM 700 laser scanning confocal microscope with ZEN imaging software. To allow quantitative and qualitative comparisons, standardized settings remained constant. Using a 20x objective, images providing coverage across retina, RPE and choroid were obtained. In addition, a higher magnification oil immersion objective was used to acquire cell layer specific detection of mRNA signals. This method was used in **Chapter 2**.

2.11 Generation of AAV8 Vectors

Adeno-associated virus serotype 8 (AAV8) vector is well known to transduce photoreceptor and RPE cells (Lee, Kim et al. 2018), and was therefore selected to target the CNV and disease relevant cells for delivering shRNA against *Ephx2*. Mouse *Ephx2* shRNA (5'-GCCATGGAATTGCTGTGTAAGTTCAAGAGACTTACACAGTAA TTCCATGGCTTTTTT-3') and non-targeting scrambled shRNA constructs were cloned into a pAV CMV-mCherry vector under the control of a U6 promoter, and these were packaged into AAV serotype 8 by Vigene Biosciences (Rockville, MD). Briefly, the transfer plasmid/s, the Rep/Cap and the Helper plasmid were co-transfected into HEK293 cells. After 70 hours, the cells were collected and lysed by a freeze and thaw cycle. The crude lysate was clarified by centrifugation and the viral particles were purified via ultracentrifugation in an iodixanol gradient to remove impurities and empty viral capsids for safe use in vivo. After collection from the gradient, the viral titer was then determined using quantitative PCR with primers to the inverted terminal repeats present in the viral genome, and viral particles were buffer exchanged into 1 x PBS, 0.01% Pluronic F-68 and stored at -80°C prior to use. This method was used in **Chapter 3**.

2.12 Intravitreal Injection

Pupils of both eyes were dilated with topical drops of 1% tropicamide (Henry Schein Inc., Melville, NY) and 2.5% phenylephrine ophthalmic solution (Akorn). Mice were anesthetized by intraperitoneal injections of 90 mg/kg ketamine hydrochloride and 5 mg/kg xylazine mixture. 0.5% tetracaine hydrochloride ophthalmic solution (Bausch & Lomb, Laval, QC, Canada) was applied for topical anesthesia. Anesthetized mice were positioned on a stereotaxic instrument with a head holder (World Precision Instruments, Sarasota, FL) and mice were held in position by inserting the ear and tooth bars. Mice were then placed on the platform of a Nikon stereomicroscope (SMZ745/SMZ745T). A small incision was made thorough the limbus using a 30-G insulin syringe needle. A Hamilton syringe with 33-G needle was inserted carefully into the vitreous body without damaging the lens. 4.9×10^6 GC or 1.9×10^7 GC of viral vectors or PBS vehicle control in a total volume of 0.5 μ L was intravitreally injected. This method was used in **Chapter 3**.

2.13 In vivo retinal imaging

Mice were anesthetized, pupils were dilated, and corneas were lubricated under the same condition as L-CNV described above. The Micron IV ocular imager was used for in vivo retinal imaging – bright-field fundus, OCT, fluorescent fundus, and fluorescein angiography (Figure 2.3B). Simultaneous bright-field live fundus images and OCT scans were acquired to assess retinal features and to visualize CNV lesion development in cross-sectional retinal layers. Several horizontal and vertical OCT scans per lesion were taken to calculate CNV lesion volume as previously described. Briefly,

using the OCT imaging system, both the horizontal and vertical plans of the each of laser-induced lesion are obtained. Then the radii a (width) and b (depth relative to the retina) measured from the horizontal OCT scan, and the radius c (length) measured from the vertical OCT scan were plugged into an ellipsoid volume equation to calculate the lesion volume (V) as following (Sulaiman, Quigley et al. 2015).

$$V = \frac{4}{3} \pi abc$$

Fluorescent fundus imaging of mCherry was performed to assess in vivo AAV transduction. Fluorescein angiography by i.p. injection of 100 μ L of 10% fluorescein sodium (Fisher Scientific) was performed to assess vascular leakage resulting from L-CNV. Images were acquired using the manufacturer's image acquisition software. This method was used in **Chapter 3**.

2.14 Choroidal flatmounts and ex vivo CNV lesion quantification

On day 14 post L-CNV induction, mice were euthanized by isoflurane overdose followed by cervical dislocation. The eyes were enucleated and fixed in 4% PFA in PBS for 1 h at 4°C. The anterior portion, including lens and the retina, were removed, then the posterior eyecups were dissected out and underwent further fixation in 4% PFA in PBS overnight. The fixed eyecups were washed in blocking buffer (0.3% Triton X-100, 5% bovine serum albumin [BSA] in PBS) for 2 h at 4°C. The eyecups were then stained for vasculature using Alexa Fluor 488 conjugated-GS-IB4 (Molecular Probes, Thermo Fisher Scientific) at 1:250 dilution in buffer containing 0.3% Triton X-100, 0.5% BSA in PBS, overnight at 4°C. The posterior eyecups were washed three times with PBS and mounted in VectaShield fluorescent mounting medium (Vector Labs) and cover slipped. Confocal

imaging and analysis of L-CNV lesion volume were performed as previously described (Sulaiman, Merrigan et al. 2016): Choroidal flatmount images were acquired using a Zeiss LSM 700 laser scanning confocal microscope with ZEN imaging software. Three z-stack images that are equal distance apart were acquired. The area measurements were performed using the freehand tool in ImageJ software. The areas were averaged and multiplied by height to obtain the lesion volume. This method was used in **Chapter 3**.

2.15 Immunoblotting

In **Chapter 2**, mice were sacrificed 3 days post L-CNV. In **Chapter 3**, mice were sacrificed 21 days post injection of 1.9×10^7 GC AAV8-*Ephx2* shRNA or AAV8-scrambled shRNA control, or PBS vehicle control. The eyes were enucleated, placed immediately in ice-cold 1X PBS, and dissected under a microscope to remove optic nerve and periocular tissue, followed by removal of cornea and lens to obtain the posterior cup of the chorioretina. The neuroretina and RPE/choroid tissues were gently separated and then snap frozen. Tissue lysates were prepared by homogenizing the tissue in RIPA buffer (Sigma-Aldrich, St. Louis, MO) with protease inhibitor cocktail (Roche, Basel, Switzerland), and then centrifuged at 12,000 rpm for 15 minutes at 4 °C. The supernatant was recovered, and the total protein concentration was determined using the Protein Assay Dye Reagent Concentrate (Bio-Rad). Immunoblotting was performed as following: Electrotransferred PVDF membranes were incubated with murine antibody against sEH (A-5, sc-166561, Santa Cruz, 1:1000) overnight at 4 °C. As a loading control, membranes were incubated with murine antibody against β -actin (AC-40, Sigma-Aldrich, 1:5000) for 1 hour at room temperature. Prior to immunoblotting for β -actin, Restore Western Blot

Stripping Buffer (Thermo Scientific) was used according to the manufacturer's protocol to strip the membrane. Secondary antibody was horseradish peroxidase (HRP)-conjugated goat-anti-mouse IgG (1:10,000, Jackson ImmunoResearch, West Grove, PA) for 1 hour at room temperature. Signals were detected using ECL immunoblotting detection reagents (Amersham, Amersham, United Kingdom) on a c600 imaging system (Azure biosystems, Dublin, CA). The bands were quantified by densitometry using ImageJ software.

2.16 Mouse eye RNA extraction and qPCR

Mice treated with AAV and L-CNV were sacrificed 21 days post injection. The eyes were enucleated, and the retina and choroid tissues were separated using the dissection procedure described above. The retina or choroid tissue was placed in 500 μ L of TRIzol reagent and homogenized by a tissue grinder and vortexing. Total RNA was isolated using the TRIzol reagent according to the manufacturer's instructions (Thermo Scientific). To clean up RNA, RNA Clean & Concentrator kit was used according to the manufacturer's protocol (Zymo Research, Irvine, CA). cDNA synthesis was carried out on 400 ng total RNA using the iScript cDNA synthesis kit (Bio-Rad) as per the manufacturer's protocol. qRT-PCR reactions were prepared using TaqMan Fast Advanced Master Mix, TaqMan gene specific probe (Thermo Fisher) and cDNA in nuclease free water. All TaqMan probe sets are listed in Table 2.2. A ViiA 7 Real-Time PCR system (Thermo Fisher) was used to perform qPCR under the following conditions: hold at 50 °C for 2 min, hold at 95 °C for 2 min, and 40 cycles of denature at 95 °C for 1 sec and anneal/extend at 60 °C for 20 sec.

Target	Primer
<i>Ccl2</i>	Mm00441242_m1
<i>Ephx2</i>	Mm01313813_m1
<i>Hprt</i>	Mm03024075_m1
<i>Icam1</i>	Mm00516023_m1
<i>Il1b</i>	Mm00434228_m1
<i>Il6</i>	Mm00446190_m1
<i>Tbp</i>	Mm01277042_m1
<i>Tnfa</i>	Mm00443258_m1
<i>VegfC</i>	Mm00437310_m1

Table 2.2: Gene expression assays used in studies

2.17 Statistics

For Chapter 3, the rate of enzymatic reaction was analyzed with the GraphPad Prism software using a linear regression model. Enzyme inhibition data were analyzed with the Exploratory Enzyme Kinetics option in SigmaPlot. With this, the direct linear plot, secondary plots, and a numeric report were created to determine Michaelis-Menten kinetics parameters and define the type of inhibition. In the *ex vivo* sEH activity assay, the data were analyzed with GraphPad Prism software using one-way analysis of variance (ANOVA) with Tukey's post hoc tests, and the results were presented as mean \pm SEM. Values of $p < 0.05$ were considered statistically significant. For Chapter 5, immunoblotting, OCT L-CNV lesion volume quantification, choroidal flatmount lesion volume quantification, and qPCR gene expression data were analyzed with the GraphPad Prism software using one-way ANOVA with Tukey's post-hoc tests. Likewise, $p < 0.05$ was considered statistically significant.

CHAPTER 3. MECHANISTIC ENZYMOLOGY OF sEH INHIBITION

3.1 Overview

In the forward chemical genetics approach of drug discovery, the process starts from identifying small molecules with the ability to generate a desired phenotype in a biological system and proceeds through rounds of structural changes and optimization to develop a lead compound with pharmacological properties. In the later step, a cellular target that interacts with the compound is identified. Our group previously has taken this approach to develop an anti-angiogenic small molecule SH-11037 and discovered sEH as its cellular target. However, quantitative measurement of how SH-11037 performs against sEH, and the precise mechanism of inhibition remained elusive. In the present chapter, I tested the hypothesis that SH-11037 binds to sEH and inhibits the enzymatic activity of sEH. Using an epoxide hydrolase spectrophotometric activity assay, I demonstrated that in vitro treatment of eye tissue homogenates with SH-11037 or a previously known sEH inhibitor inhibited sEH catalytic hydrolase function. Then, I assessed the inhibitory activity of SH-11037 in the recombinant sEH activity assay using a fluorogenic substrate and characterized IC_{50} values of SH-11037 and other known sEH inhibitors. Lastly, I discovered the mode of inhibition – mixed noncompetitive inhibition and K_i value of SH-11037 through enzyme kinetics studies, providing crucial information regarding drug potency and selectivity against its target.

3.2 Background and Rationale

Enzymes are physiological catalysts involved in all life processes, including metabolism, cellular signaling, cell growth and division. An enzyme inhibitor is any substance that reduces the velocity of an enzyme-catalyzed reaction. Enzymes are appealing drug targets because of their well-defined substrate-binding pockets that can be utilized as binding sites for enzyme inhibitors (Rufer 2021). Indeed, enzymes now make up roughly one-third or more of the drug targets in the portfolios of the pharmaceutical industry, and small-molecule enzyme inhibitors have demonstrated therapeutic and commercial success (Holdgate, Meek et al. 2018). In the process of drug discovery and development, it is essential to understand the reaction mechanisms of enzymes and the molecular mode of action of enzyme inhibitors. Thus, quantitatively measuring how the compound performs against its target and performing enzyme kinetics studies are indispensable components of ensuring the potency, efficacy and safety of novel drugs (Rufer 2021).

Corson lab previously utilized a forward chemical genetics approach to drug discovery, which involved identification of a small molecule cremastranone with the ability to suppress angiogenesis and proceeded through rounds of optimization to discover a compound SH-11037 with greater potency and selectivity for endothelial cells (Basavarajappa, Lee et al. 2015, Sulaiman, Merrigan et al. 2016) Then, using SH-11037 based affinity reagents, we identified sEH as a cellular target of SH-11037 (Sulaiman, Park et al. 2018). However, the knowledge regarding potency and selectivity of SH-11037 against sEH, and the precise drug-target interaction remained unknown. It was recognized that addressing these questions would provide the information required to

conceptualize the type of inhibitor and successfully optimize the lead compound in the future.

The objectives of studies presented in Chapter 3 are to measure the inhibitory activity of sEH inhibitors, including SH-11037 quantitatively, and investigate the molecular mode of action of enzyme inhibition by SH-11037 for the first time. I characterized half-maximal inhibitory concentration (IC_{50}) and inhibition constant (K_i), elucidating both the inhibitory activity and potency of SH-11037 against sEH. By combining classical concepts of enzymology with new data analysis methods, I identified kinetic parameters of sEH inhibition and revealed SH-11037 as a mixed noncompetitive inhibitor of sEH.

3.3 Results

3.3.1 SH-11037 inhibits sEH activity in murine eye tissue homogenates

To assess the inhibitory activity of SH-11037 in eye tissue, I collected tissue lysates from mice 3 days post-L-CNV and untreated control mice. To assess the cellular sEH activity in the tissue lysate, I used a spectrophotometric assay in which sEH dependent hydrolysis of the substrate *trans*-stilbene oxide (*t*-SO) can be measured as a change in absorbance at 230 nm. To test the inhibitory activity of SH-11037 on the cellular sEH activity, I incubated the isolated murine eye tissue lysates with SH-11037 and a known sEH inhibitor compound 7 (Shen, Ding et al. 2009) as a positive control. The change in *t*-SO absorbance was greater after laser induction compared to no laser, untreated control, indicating the upregulation of sEH activity under the disease state. Moreover, *t*-SO absorbance change was significantly reduced by SH-11037 or compound 7 treatment, indicating inhibitory activities of these compounds on cellular sEH activity *ex vivo* (Figure 3.1).

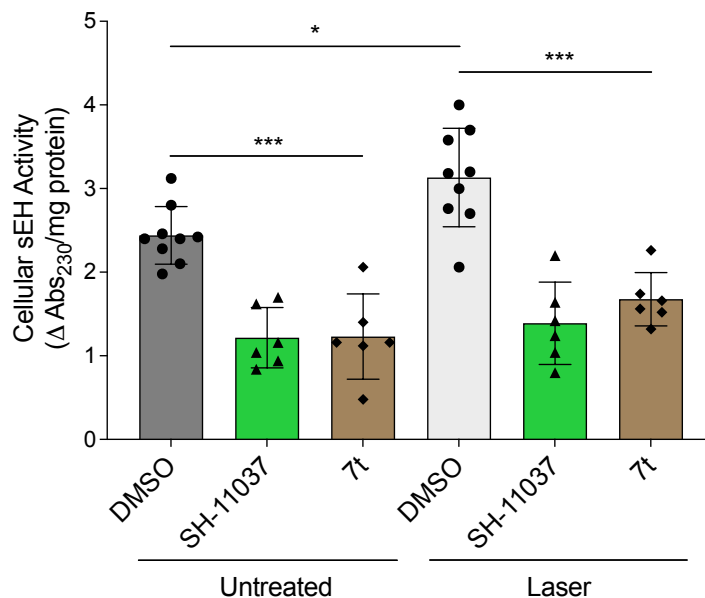


Figure 3.1: Ex vivo treatment of eye tissue homogenates with SH-11037 or compound 7 inhibits cellular sEH activity. sEH activity is up-regulated in L-CNV eye lysates (* $P < 0.05$) and normalized by 20 μM SH-11037 or 7 treatment (*** $P < 0.001$), as indicated in a trans-stilbene oxide enzymatic activity assay performed 3 days post-laser-treatment. Mean \pm SEM, ANOVA with Tukey's post hoc tests. Pooled data from three experiments, $n = 6-9$ eyes per condition per experiment.

3.3.2 SH-11037 inhibits recombinant human sEH activity

Upon determining the inhibition of the epoxide hydrolase activity in the tissue lysate with SH-11037 and a known sEH inhibitor compound 7, I aimed to assess quantitative metrics of inhibitory activity of SH-11037, IC_{50} values, to investigate the functional strength of SH-11037 against the purified target enzyme. I used recombinant human sEH and the fluorogenic substrate, PHOME (3-phenyl-cyano(6-methoxy-2-naphthalenyl)methyl ester-2-oxiraneacetic acid) (Cayman Chemical) in the enzyme activity assay, in which epoxide hydrolysis releases a fluorescent product, 6-methoxy-2-naphthaldehyde. With this, I tested whether the compound interferes with the epoxide hydrolase activity of recombinant human sEH, compared to known sEH inhibitors. Trans-4-(4-[3-adamantan-1-yl-ureido]-cyclohexyloxy)-benzoic acid (t-AUCB) is a urea

based specific inhibitor of the epoxide hydrolase activity of sEH, widely used in preclinical studies. Meanwhile, 7-(trifluoromethyl)-N-(4-(trifluoromethyl)phenyl)benzo[d]isoxazol-3-amine (compound 7), is a structurally distinct benzisoxazole inhibitor with excellent potency and pharmacokinetic properties (Hwang, Tsai et al. 2007, Shen, Ding et al. 2009, Park and Corson 2019).

To test whether these effects are specific to SH-11037, I included a negative control SH-11098, which is an inactive homoisoflavonoid analog of SH-11037 that showed no activity in angiogenesis assays in vitro and is distinguished from SH-11037 as it lacks the Boc-Phe group on the C3' position of the B-ring and one of the methoxy groups on the A ring (Basavarajappa, Lee et al. 2015). Additional known sEH inhibitors, compound 7 and *t*-AUCB were included as positive controls (Table 3.1). Interestingly, SH-11037 inhibited sEH enzymatic activity in a concentration-dependent manner with an IC_{50} value of 0.15 μ M (Figure 3.2), although not as potently as *t*-AUCB or compound 7. SH-11098, related compound used as a negative control had minimal inhibitory activity, suggesting that structural features of SH-11037 specifically interact with sEH.

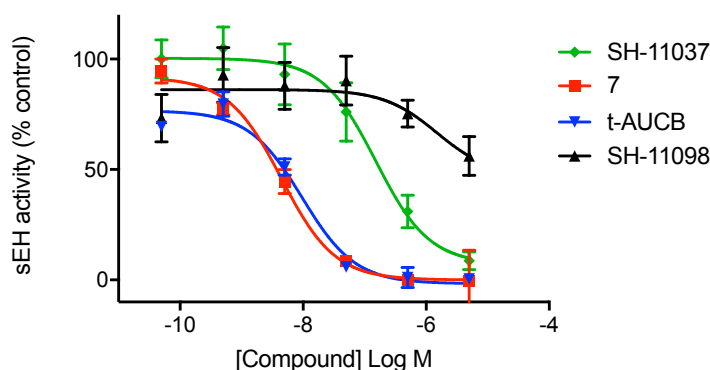


Figure 3.2: SH-11037 is an sEH inhibitor. SH-11037, but not its inactive analog SH-11098, significantly suppressed recombinant human sEH enzymatic activity, $IC_{50} = 0.15$ μ M (SH-11098 $IC_{50} > 10$ μ M). The specific sEH inhibitors *t*-AUCB and compound 7 were used as positive controls, $IC_{50} = 9.5$ nM for each. Mean \pm SEM from triplicate wells shown. Representative of $n=3$ independent experiments.

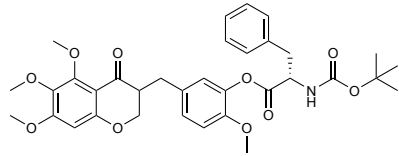
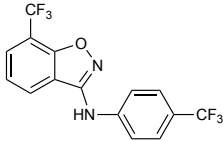
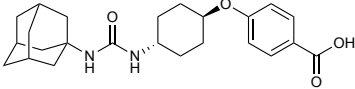
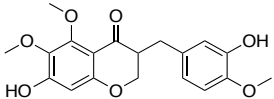
Compound	Structure	Human sEH IC ₅₀
SH-11037	(Basavarajappa, Lee et al. 2015) 	0.15 μM
Compound 7	(Shen, Ding et al. 2009) 	9.5 nM
<i>t</i> -AUCB	(Hwang, Tsai et al. 2007) 	9.5 nM
SH-11098	(Basavarajappa, Lee et al. 2015) 	> 10 μM

Table 3.1: Chemical structures and IC₅₀ values of sEH inhibitors

3.3.3 SH-11037 is a mixed noncompetitive inhibitor of sEH

Through recombinant sEH activity assay and obtaining IC₅₀ values, I was able to demonstrate concentration-response analyses. While useful, IC₅₀ values have limitations. IC₅₀ value is not reflective of inhibitor affinity because the value of IC₅₀ is affected by experimental conditions, particularly the substrate concentration. For example, the IC₅₀ value of a competitive enzyme inhibitor will increase with increasing substrate depletion, which can lead to underestimating its potency. IC₅₀ values also do not indicate an inhibitory mechanism. Therefore, IC₅₀ can only be considered as apparent potency under the experimental condition in a particular assay, in contrast to inhibition constant, K_i which is reflective of intrinsic potency (Holdgate, Meek et al. 2018, Rufer 2021). I recognized these shortcomings and sought out to apply detailed mechanistic enzyme

kinetics to effectively profile properties of SH-11037 and gain insight into the mode of inhibition that mediates drug efficacy.

Following the determination of the rate of reaction through linear regression of enzyme activity under different substrate concentrations with the range of inhibitor concentrations, I constructed a Michaelis-Menten plot of rate of reaction as a function of substrate concentration (Figure 3.3A), and double-reciprocal (Lineweaver-Burk) plot of initial inverse velocity as a function of the inverse of the substrate concentration (Figure 3.3B). Enzyme kinetics analysis showed that increasing concentrations of SH-11037 decreased V_{\max} and increased K_M , with $K_i = 1.73 \pm 0.45 \mu\text{M}$. Increased K_M with increasing concentrations of SH-11037 indicates that a higher concentration of substrate is required to attain enzymatic rate, which is a characteristic of competitive inhibition; however, there is also a decrease in V_{\max} in the presence of SH-11037, indicating SH-11037 binding to both the enzyme and enzyme-substrate complex with different affinities, though the increase in K_M indicates that SH-11037 has a greater affinity for the enzyme than to the enzyme-substrate complex (Figure 3.3A, B).

Given these complexities, I used the Exploratory Enzyme Kinetics option in SigmaPlot to obtain secondary plots to confirm if Michaelis-Menten kinetics are satisfied and to characterize the type of inhibition. In the Dixon plot, a noncompetitive inhibitor extrapolates straight lines converging on the axis at $-K_i$ at different concentrations of the substrate, whereas a competitive inhibitor gives lines intersecting at single point ($-K_i$ values) in the fourth quadrant at different substrate concentrations. For SH-11037, the lines did not converge on the axis, but intersected at a single point in the second quadrant. This indicated that sEH is a mixed-type inhibitor (Figure 3.3C). As well, the secondary

plots of K_{Mapp}/V_{maxapp} and $1/V_{maxapp}$ as a function of [SH-11037] fit the mixed inhibition model where two inhibition constants intercept at the inhibitor axis (Figure 3.5A, B). Compound 7 is also a mixed-type inhibitor (Figure 3.4 A-C, 3.5C and D) with a $K_i = 19.6 \pm 5.4$ nM (Figure 3.4C).

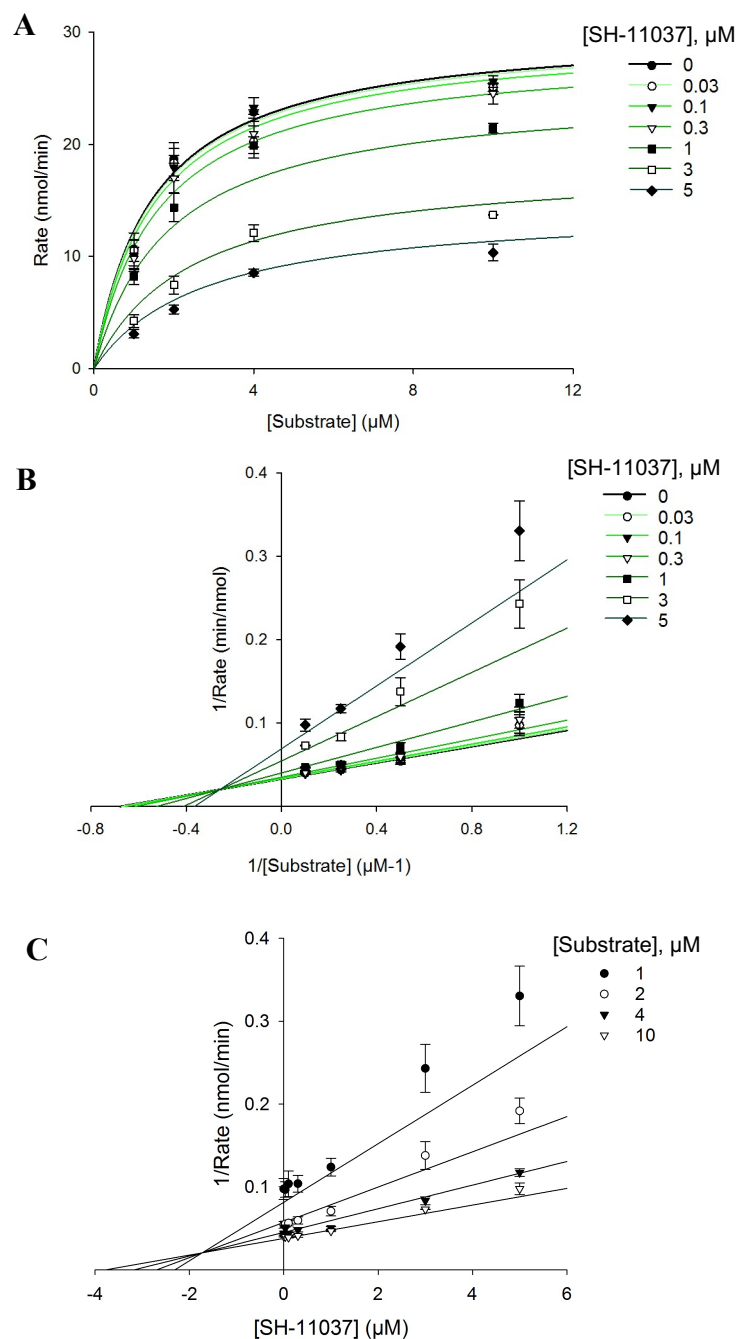


Figure 3.3: Michaelis-Menten and Lineweaver Burk plots of SH-11037 inhibition of sEH. (A) Michaelis–Menten kinetic response plot for sEH-mediated hydrolysis of fluorogenic substrate, PHOME, for varying SH-11037 concentrations. (B) Lineweaver–Burk plot of these data shows that increasing concentrations of SH-11037 decreased V_{\max} and increased K_M , revealing that SH-11037 is a mixed-type inhibitor of sEH (C) $K_i = 1.73 \pm 0.45 \mu\text{M}$ is illustrated on Dixon plot of reciprocal rate of reaction ($1/\text{Rate}$), against the inhibitor concentration, at different substrate concentrations. Representative results from at least two independent experiments. Mean \pm SEM from triplicate wells shown from $n = 3$ independent experiments.

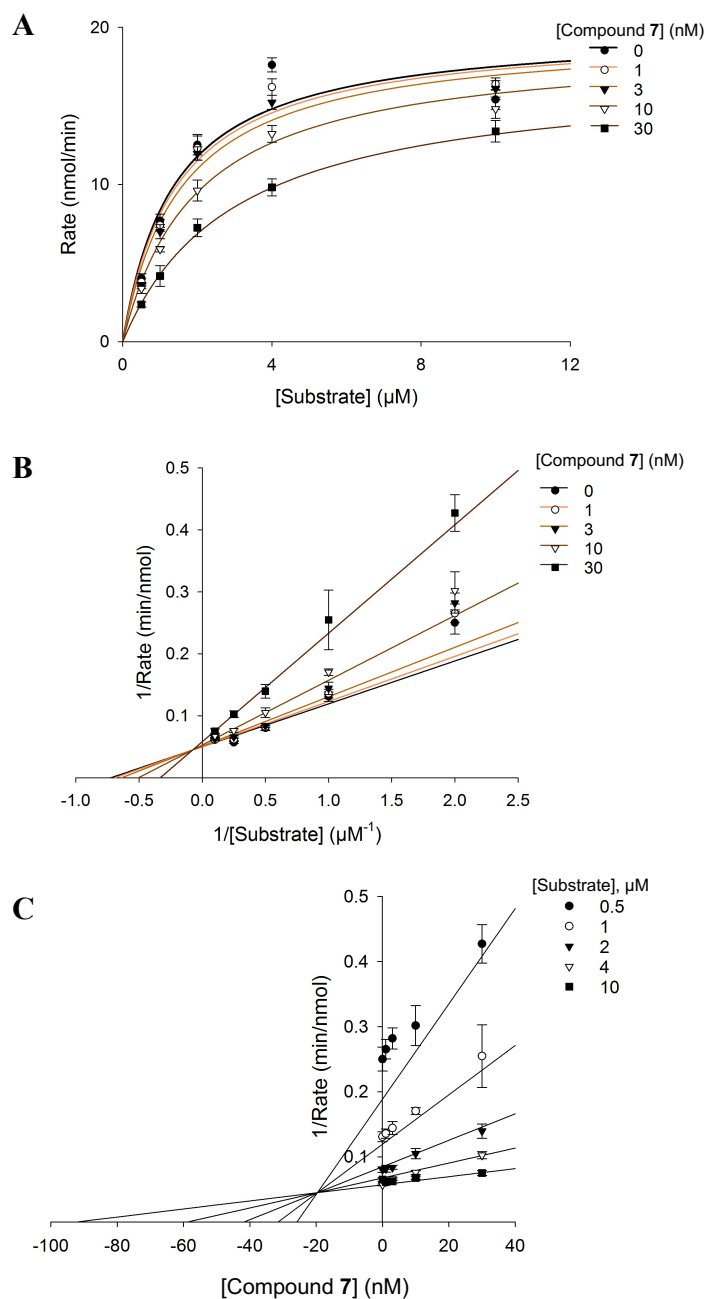


Figure 3.4: Michaelis-Menten and Lineweaver Burk plots of Compound 7 inhibition of sEH. (A) Michaelis–Menten kinetic response plot for sEH-mediated hydrolysis of fluorogenic substrate, PHOME, for varying **compound 7** concentrations. (B) Lineweaver–Burk plot of these data shows that increasing concentrations of **compound 7** decreased V_{\max} and increased K_M , revealing that **compound 7** is a mixed-type inhibitor of sEH. (C) $K_i = 19.6 \pm 5.4$ nM is illustrated on Dixon plot of reciprocal rate of reaction (1/Rate), against the inhibitor concentration, at different substrate concentrations. Representative results from at least two independent experiments. Mean \pm SEM from triplicate wells shown from $n = 3$ independent experiments.

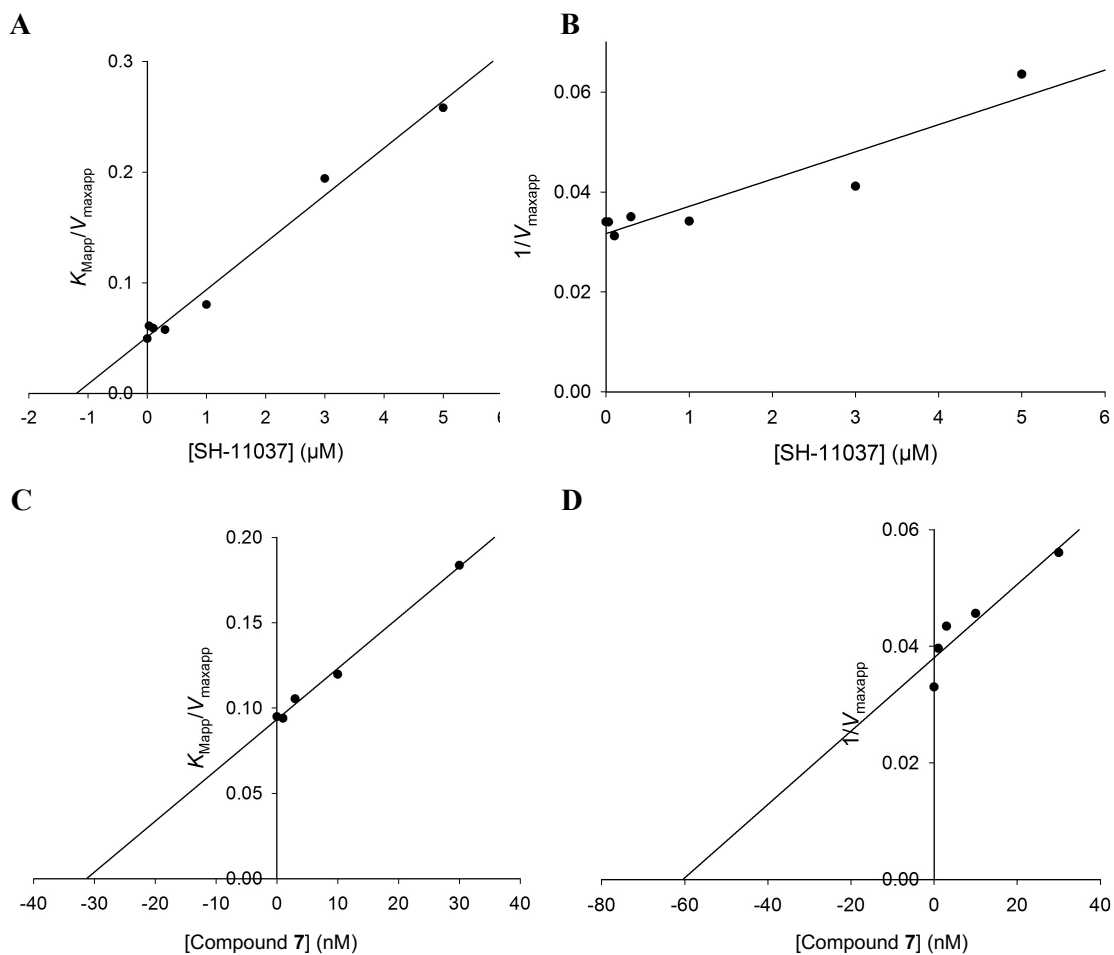


Figure 3.5: Secondary plots for enzyme kinetic analyses. The apparent K_M/V_{max} data fit the expected profiles for mixed-type inhibition by SH-11037 and compound 7. Secondary plots of (A) K_{Mapp}/V_{maxapp} and (B) $1/V_{maxapp}$ vs. [SH-11037] fit the curves expected for mixed-type inhibition. Secondary plots of (C) K_{Mapp}/V_{maxapp} and (D) $1/V_{maxapp}$ vs. [Compound 7] fit the curves for mixed-type inhibition.

3.4 Discussion and Conclusions

Here, I quantitatively assessed the inhibitory activity of SH-11037 against sEH and uncovered the mode of enzyme inhibition by SH-11037 for the first time. By doing so, I presented different methods of drug-target evaluation and provided knowledge for future optimization of this lead compound. The noncompetitive mixed inhibition mode by SH-11037 is interesting considering the reaction mechanism by sEH in epoxide hydrolysis. Mixed inhibition contains competitive and uncompetitive inhibition components, indicating binding to both the enzyme and enzyme substrate complex.

The catalytic mechanism of sEH proceeds as a nucleophilic attack onto the epoxide substrate by an Asp residue, which results in a tetrahedral intermediate, requiring activated water to release the diol and regenerate free enzyme (Borhan, Jones et al. 1995). Given that sEH has two substrates (in my assay, the fluorogenic substrate 3-phenyl-cyano(6-methoxy-2-naphthalenyl)methyl ester-2-oxiraneacetic acid [PHOME] and water), and involves a covalent intermediate, it is possible that SH-11037 may bind and stabilize an enzyme species late in the catalytic cycle that is still in conformational equilibrium with the free enzyme. SH-11037 binding in the active site of such an enzyme species may not compete with the substrates (Shen and Hammock 2012).

The binding affinity of SH-11037 is also supported by a docking study performed by our collaborator Dr. Samy Meroueh at Indiana University. Molecular docking of SH-11037 to sEH (Figure 3.5A) shows a binding mode in which the compound occupies nearly the entire active site of the enzyme. The homoisoflavonoid portion of SH-11037 occupies the site where the catalytic Asp335 and Tyr466 residues of sEH are located (Borhan, Jones et al. 1995). Both aromatic rings of the homoisoflavonoid are involved in

π - π interactions with sEH residues, including His524 and Trp336 (Figure 3.5B). The benzyl substituent of the peptide moiety of SH-11037 is ensconced into a hydrophobic cavity created by Trp473, Met503, Ile363, and Phe362. This supports the enzyme kinetics results that showed binding affinity of SH-11037 towards the enzyme complex in addition to the enzyme-substrate complex.

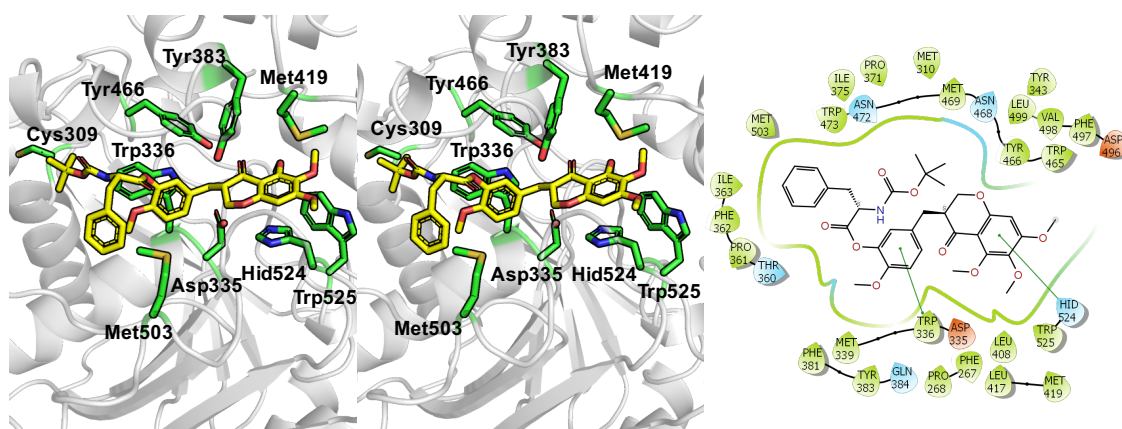


Figure 3.6: SH-11037 binds to sEH in an energetically favorable mode. (A) SH-11037 (yellow) docks in the substrate-binding cleft of sEH, as shown in this stereoview. Key residues are shown in green. (B) 2D interaction diagram for docked SH-11037. The protein “pocket” is displayed with a line around the ligand, colored with the color of the nearest protein residue. The π - π stacking interactions are shown as green lines. Figure adapted from (Sulaiman, Park et al. 2018)

The binding affinity of SH-11037 is also supported by a docking study performed by our collaborator Dr. Samy Meroueh at Indiana University. Molecular docking of SH-11037 to sEH (Figure 3.5A) shows a binding mode in which the compound occupies nearly the entire active site of the enzyme. The homoisoflavonoid portion of SH-11037 occupies the site where the catalytic Asp335 and Tyr466 residues of sEH are located (Borhan, Jones et al. 1995). Both aromatic rings of the homoisoflavonoid are involved in π - π interactions with sEH residues that include His524 and Trp336 (Figure 3.5B). The benzyl substituent of the peptide moiety of SH-11037 is ensconced into a hydrophobic

cavity created by Trp473, Met503, Ile363, and Phe362. This supports the enzyme kinetics results that showed the binding affinity of SH-11037 towards the enzyme complex in addition to the enzyme-substrate complex. Taken together, these findings indicate that SH-11037 represents a novel, distinct chemotype from known sEH inhibitors. With the confidence that an antiangiogenic small molecule, SH-11037, binds and inhibits sEH, I next went on to investigate the role of this druggable target protein in disease states mediated by angiogenesis.

CHAPTER 4. CELLULAR EXPRESSION OF sEH IN MURINE CHOROIDAL NEOVASCULARIZATION AND HUMAN NEOVASCULAR AGE-RELATED MACULAR DEGENERATION

4.1 Overview

Soluble epoxide hydrolase expression has been characterized in numerous tissues and dysregulation of sEH expression is a feature of multiple retinal diseases. Yet, mechanistic understanding of sEH at the cellular level in CNV of nvAMD is limited. Because the retina is a highly structured system with numerous cell types with distinct functions, understanding the spatial expression pattern of a potential therapeutic target is crucial. Given this knowledge gap about which retinal cells express sEH under the disease state, I aimed to define the localization and cellular origin of sEH through immunohistochemical and RNAscope in situ hybridization analysis in human nvAMD and murine laser induced CNV (L-CNV) retinas. Costaining of sEH with major retinal cell type markers revealed that sEH is overexpressed in CNV lesions, photoreceptors and RPE cells in areas with degenerative changes. By RNAscope, *EPHX2/Ephx2* mRNA encoding sEH was also highly expressed in the pathological conditions compared to controls. *EPHX2/Ephx2* mRNA was seen in the inner nuclear layer, outer nuclear layer and RPE of the normal and diseased human and mouse retina. My study revealed sEH protein and mRNA overexpression in the retinal pigment epithelium (RPE), vasculature and photoreceptors in retinas under the AMD relevant stimuli.

4.2 Background and Rationale

The retina is comprised of distinct cellular layers of neurons, cell types, and vasculature that cooperate to process visual information to the brain (Figure 1.1). In addition to this complexity of cell types, the retina is subject to a host of cell type specific disorders, including AMD. CNV in nvAMD involves pathological changes within photoreceptors, RPE, Bruch's membrane and the choroid, underlying visual impairment. Therefore, knowing the localization of the therapeutic target expression is critical for unraveling the mechanistic role of the druggable target in the CNV pathology, and developing optimal therapeutic strategies.

sEH is widely expressed in various tissues, with the highest levels of expression seen in liver, kidney, and brain in neuronal cell bodies and astrocytes (Sura, Sura et al. 2008, Norwood, Liao et al. 2010). In the developing mouse retina, sEH is immunolocalized notably to Müller glial cells (Hu, Popp et al. 2014) and in oxygen-induced retinopathy in neonatal mice, expression is seen in retinal ganglion cells, neovessels, and inner nuclear layer neurons in retina (Shao, Fu et al. 2014). Overexpression of sEH is implicated in the progression of nonproliferative diabetic retinopathy in hyperglycemic *Ins2^{Akita}* mouse retinas and in the retinas and vitreous of human diabetic patients (Hu, Dziumbila et al. 2017). We had previously demonstrated that sEH is overexpressed in tissue homogenates of L-CNV (Sulaiman, Park et al. 2018), but it is difficult to compare analysis from whole retina or choroid tissue homogenates to immunohistochemistry data from other studies with different disease models in highly structured organs such as the retina that is involved in cell type specific disorders.

Thus, there is a knowledge gap involving where the sEH is expressed in the retina under the disease state (CNV) involved in nvAMD. Additionally, given the differences in structure and gene expression between human and mouse retinas, there needs to be expression profiling study conducted in both human and mouse retinas to address any differential expression that may arise. Here, I tested the hypothesis that sEH is expressed in retinal cell types involved in the CNV pathology. I profiled sEH expression at the protein level in several major retinal cell types through immunohistochemistry, and further validated these results at the single-cell mRNA level through RNAscope in situ hybridization (ISH). As a result, my study revealed that sEH is highly expressed in the photoreceptor and RPE cells at the protein and mRNA level in CNV. These disease-relevant cell types overexpressing sEH suggest a functional role of sEH in AMD pathophysiology and provide a context to target these cell types for developing pharmacotherapies.

4.3 Results

4.3.1 Immunolocalization of sEH in murine retinas

I aimed to build on our previous findings that sEH is overexpressed in the vasculature of L-CNV lesions in mouse retinas and human nvAMD retinas (Sulaiman, Park et al. 2018). To define the localization of sEH upregulation in murine retinas undergoing CNV, I immunostained for sEH and other markers of retinal cell types in retina cross sections of untreated C57BL/6J adult mouse eyes or in eyes of mice that had undergone L-CNV, three days post-laser: RPE (RPE65), cone photoreceptor cells (cone arrestin), rod photoreceptor cells (rhodopsin), Müller glia (vimentin), horizontal cells (calbindin), and retinal ganglion cells (Brn3a). Interestingly, the pattern of sEH expression in adult murine retina undergoing CNV was different than what was reported in developing mouse retina, and other retinal disease models that identified Müller glial cells as a major cell type expressing sEH (Hu, Popp et al. 2014, Shao, Fu et al. 2014). Instead, there was a prominent colocalization with rod photoreceptors in the eyes of L-CNV mice compared to controls (Figure 4.1), and sEH partially colocalized with RPE65 (Figure 4.2), but not with markers of other retinal cell types, including retinal ganglion cells, horizontal cells, Müller glial cells, and cone photoreceptors (Figure 4.3A-D). Collectively, my findings demonstrated that upregulated sEH under CNV stimuli is highly expressed in rod photoreceptor cells and their outer segments and apical and basal regions of the RPE cells.

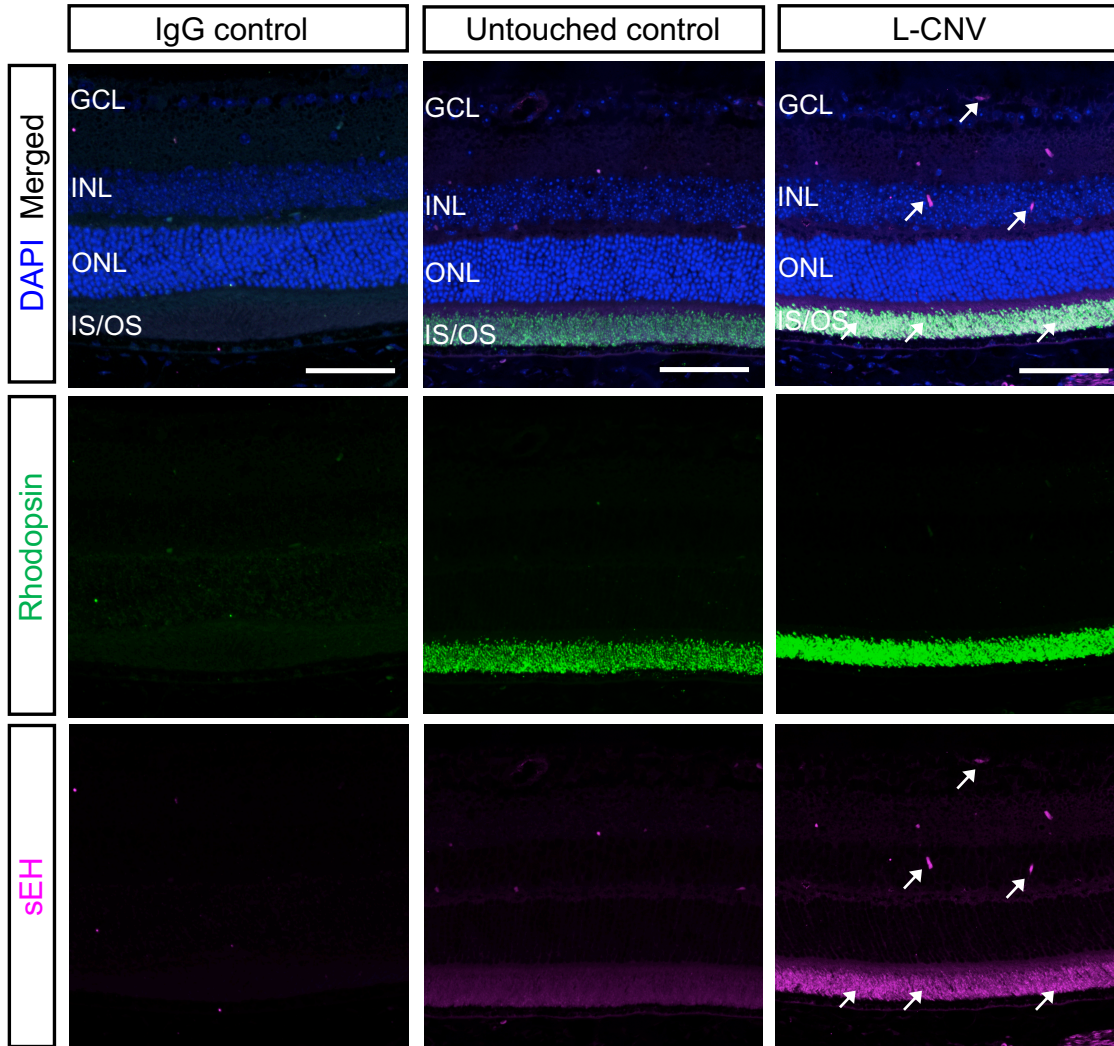


Figure 4.1: Upregulation and colocalization of sEH with rod photoreceptors in the eyes of mice undergoing choroidal neovascularization. Representative images of retinal sections from L-CNV (3 days post-laser-treatment) and control eyes stained with DAPI (blue), sEH (magenta), and rod photoreceptor cell marker rhodopsin (green). Scale bars = 50 μm . IgG is a negative control with preimmune primary antibodies. GCL, ganglion cell layer; INL, inner nuclear layer; ONL, outer nuclear layer; IS/OS, photoreceptor inner/outer segments. Representative images from $n = 3$ untouched eyes and $n = 3$ L-CNV eyes.

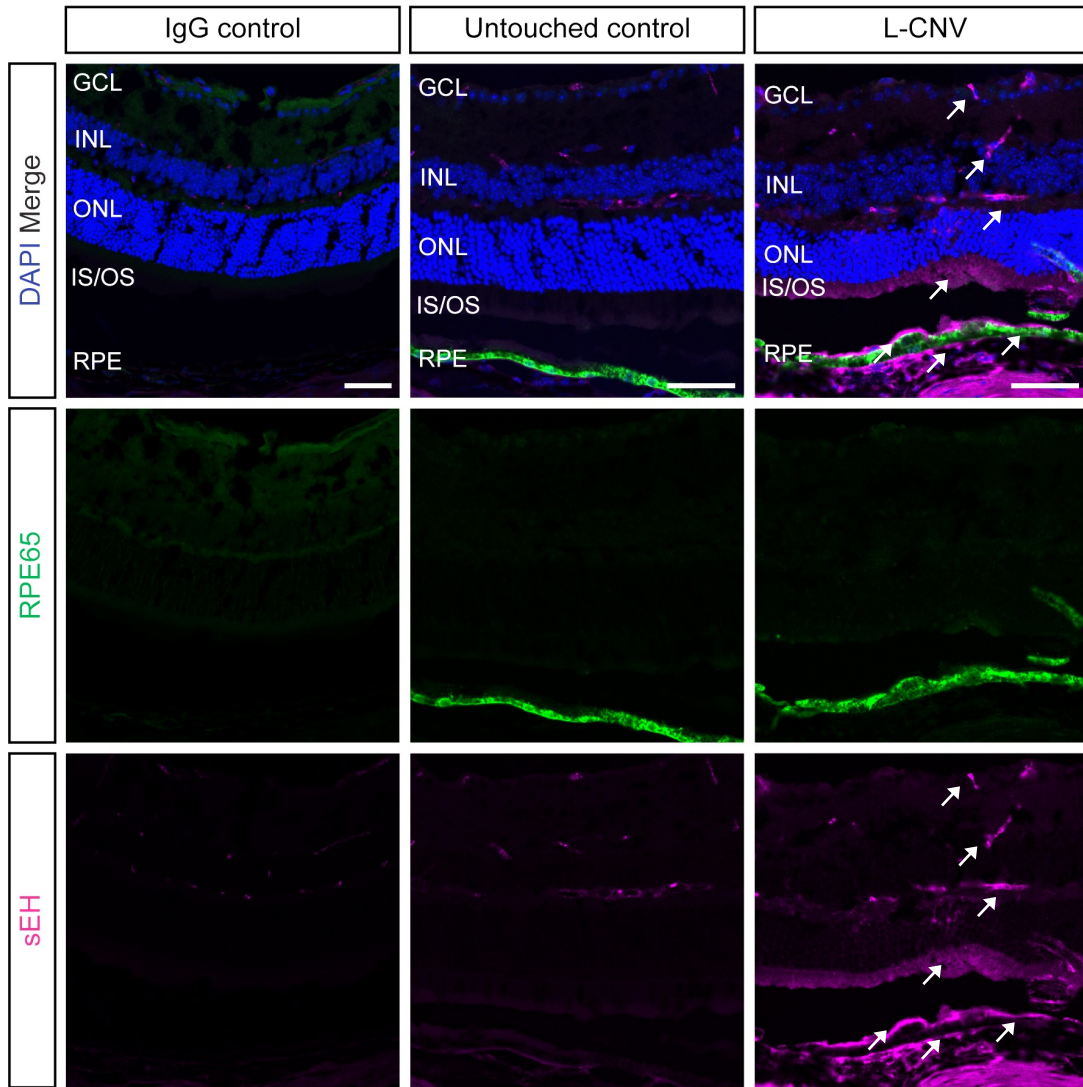


Figure 4.2: Colocalization of sEH with apical and basal surface of RPE cells in murine retinas undergoing choroidal neovascularization. Representative images of retinal sections from L-CNV (3 days post-laser-treatment) and control eyes stained with DAPI (blue), sEH (magenta), and RPE cell marker RPE65 (green). Scale bars = 50 μ m. IgG is a negative control with preimmune primary antibodies. GCL, ganglion cell layer; INL, inner nuclear layer; ONL, outer nuclear layer; IS/OS, photoreceptor inner/outer segments. Representative images from n = 3 untouched control eyes mice and n = 3 L-CNV eyes.

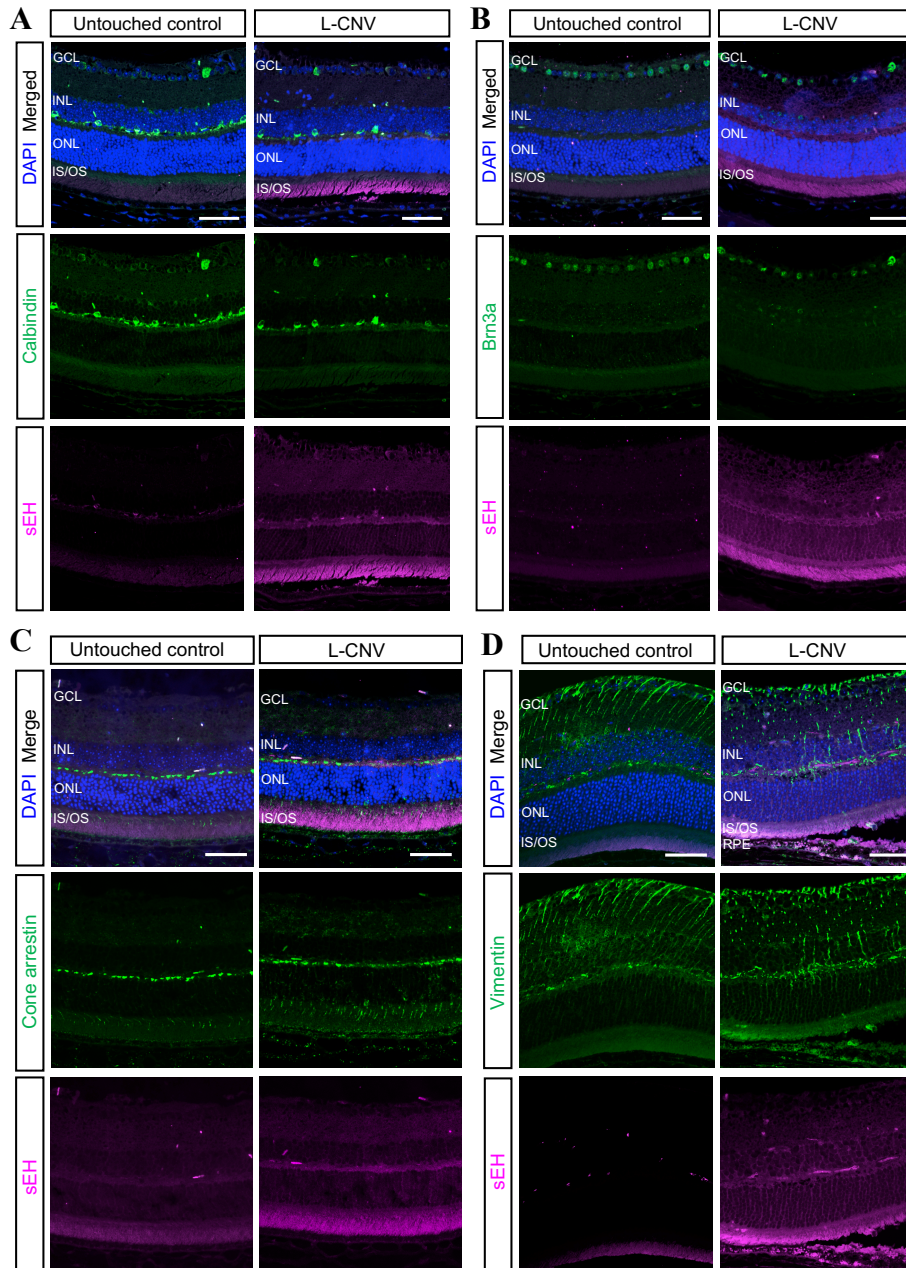


Figure 4.3: Immunolocalization of sEH with other retinal markers. Representative images of retinal sections from L-CNV (3 days post-laser treatment) and control eyes stained with DAPI (blue), sEH (magenta), and (A) horizontal cells (calbindin); (B) retinal ganglion cells (Brn3a); (C) cone photoreceptors (cone arrestin) and (D) Müller glia (vimentin). Cell type markers are green in all cases. Scale bars = 50 μ m. GCL, ganglion cell layer; INL, inner nuclear layer; ONL, outer nuclear layer; IS/OS, photoreceptor inner segments/outer segments; RPE, retinal pigment epithelium. Representative images from n = 3 untouched control eyes and n = 3 L-CNV eyes.

4.3.2 Immunolocalization of sEH in human retinas

Based on the findings that sEH is overexpressed in the outer retina involving photoreceptors and the RPE in murine L-CNV retinas, I aimed to examine sEH expression in the human disease state further. To determine where sEH is upregulated in human nvAMD retinas, I immunostained for sEH and other markers of retinal cell types: peanut agglutinin (PNA) for rod photoreceptor cells, wheat germ agglutinin (WGA) for cone photoreceptor cells and RPE65 for RPE cells in the human nvAMD and age-matched control retinas. PNA (green) distinctively identified cone matrix sheaths and WGA (yellow) labeled outer segments of rods (Figure 4.4A).

The expression of sEH (magenta) was observed throughout the retina but greater sEH expression was observed in photoreceptors and RPE cells that could be undergoing degenerative changes in nvAMD. sEH staining was associated with inner and outer segments of photoreceptor cells in nvAMD retinas (Figure 4.4A). Coimmunostaining of RPE65 (green) and sEH revealed that sEH overexpression in nvAMD colocalized with RPE65 positive RPE cells, particularly in the apical RPE (Figure 4.4B). This observation is recapitulated by further examples of sEH staining in human retinas (Figures 4.5, 4.6) While this expression pattern is reflected in my immunohistochemistry data of L-CNV murine retinas, the results are distinguished from other immunohistochemistry data in the literature in which sEH was predominantly expressed by murine Müller glial cells. The involvement of distinct cell types in various retinal diseases could be one of the explanations for such discrepancy in the target expression, because Müller glia closely interact with retinal vasculature (Coughlin, Feenstra et al. 2017), whereas the RPE is intimately associated with choroidal vasculature, and the RPE and choroid provide a

supporting system for photoreceptors (Nickla and Wallman 2010). Yet, the differential expression results indicated challenges in the validation of immunohistochemistry data due to potential physical limitations of antibodies including the lack of universally accepted standardization of antibody production, and lack of standardization in target specificity for antibodies can lead to discordant IHC/IF results between antibodies (Bordeaux, Welsh et al. 2010). Thus, this presented me a rationale to pursue the RNAscope in situ hybridization (ISH) method to provide complementary information regarding spatial and precise discrimination of the target expression in retina.

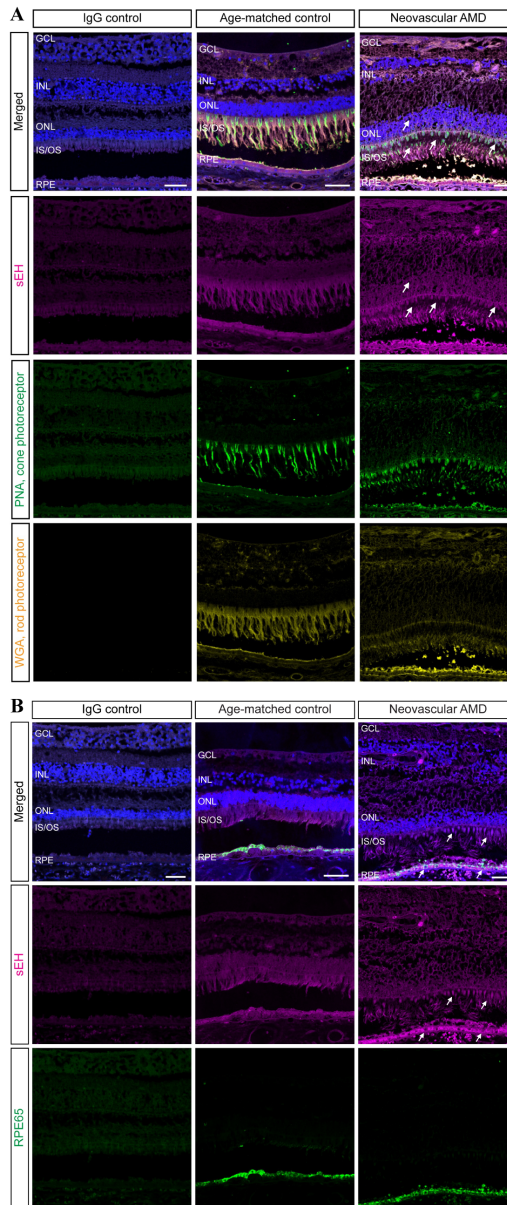


Figure 4.4: Colocalization of sEH with photoreceptors and RPE in human retinas from neovascular AMD patients. Representative images of retinal sections from nvAMD (81 y.o., male) and age-matched control eyes (82 y.o., male) stained with DAPI (blue), sEH (magenta), PNA (green), WGA (yellow) or RPE65 (green) (A) Labeling of retinal tissues with PNA and WGA for rods and cones showing colocalization of sEH in photoreceptors (circled). In nvAMD, sEH staining is strongly associated with the outer segments of cones and is enhanced compared to age-matched control (circled). (B) Immunohistochemistry using antibodies against sEH and RPE65 shows positive staining of sEH in RPE cells with more intense expression in neovascular AMD retinal tissue. Scale bars: 50 μ m. GCL, ganglion cell layer; INL, inner nuclear layer; ONL, outer nuclear layer; IS/OS, photoreceptor inner segments/outer segments; RPE, retinal pigment epithelium. Representative images from n = 2 control and n = 3 nvAMD subjects.

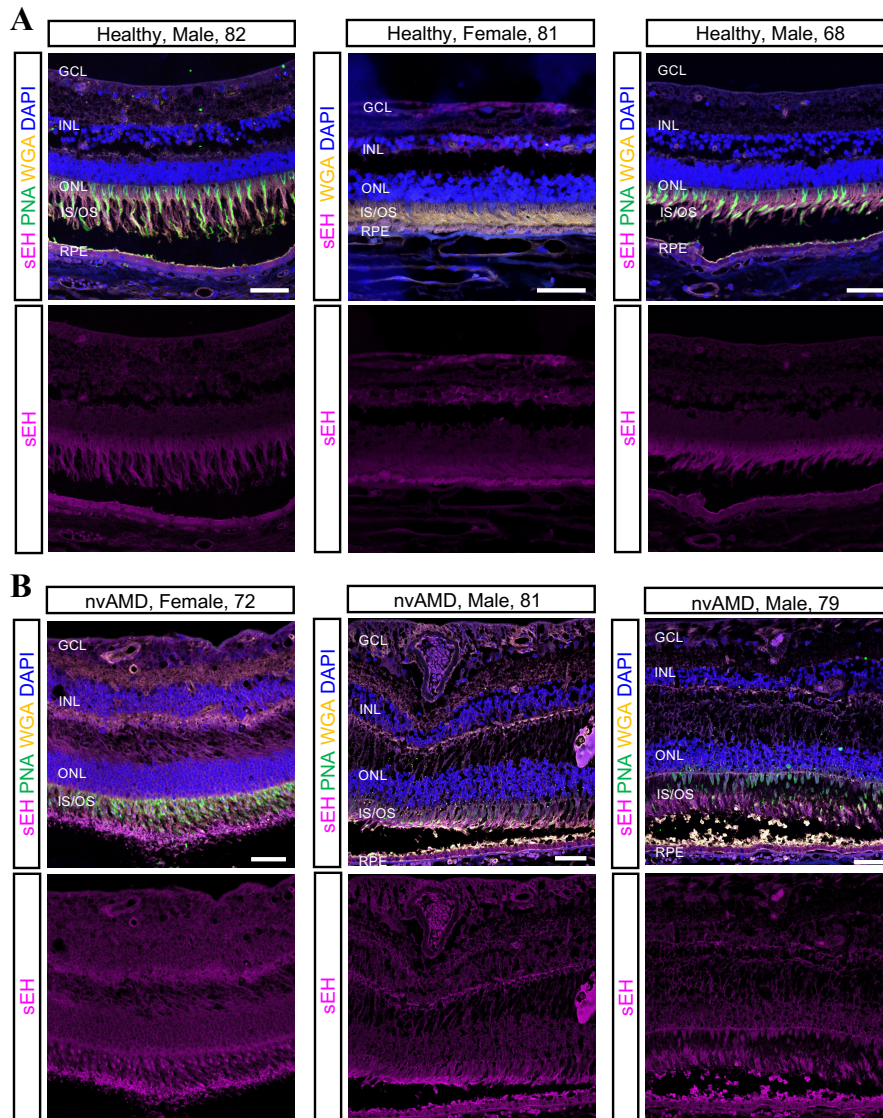


Figure 4.5: Colocalization of sEH with photoreceptors in human retinas from additional human subjects. Images of retinal sections stained with DAPI (blue), sEH (magenta), PNA (cone photoreceptors; green), WGA (rod photoreceptors; yellow). Labeling of retinal tissues with PNA and WGA for rods and cones showing colocalization of sEH in photoreceptors. Scale bars: 50 μ m. GCL, ganglion cell layer; INL, inner nuclear layer; ONL, outer nuclear layer; IS/OS, photoreceptor inner segments/outer segments; RPE, retinal pigment epithelium.

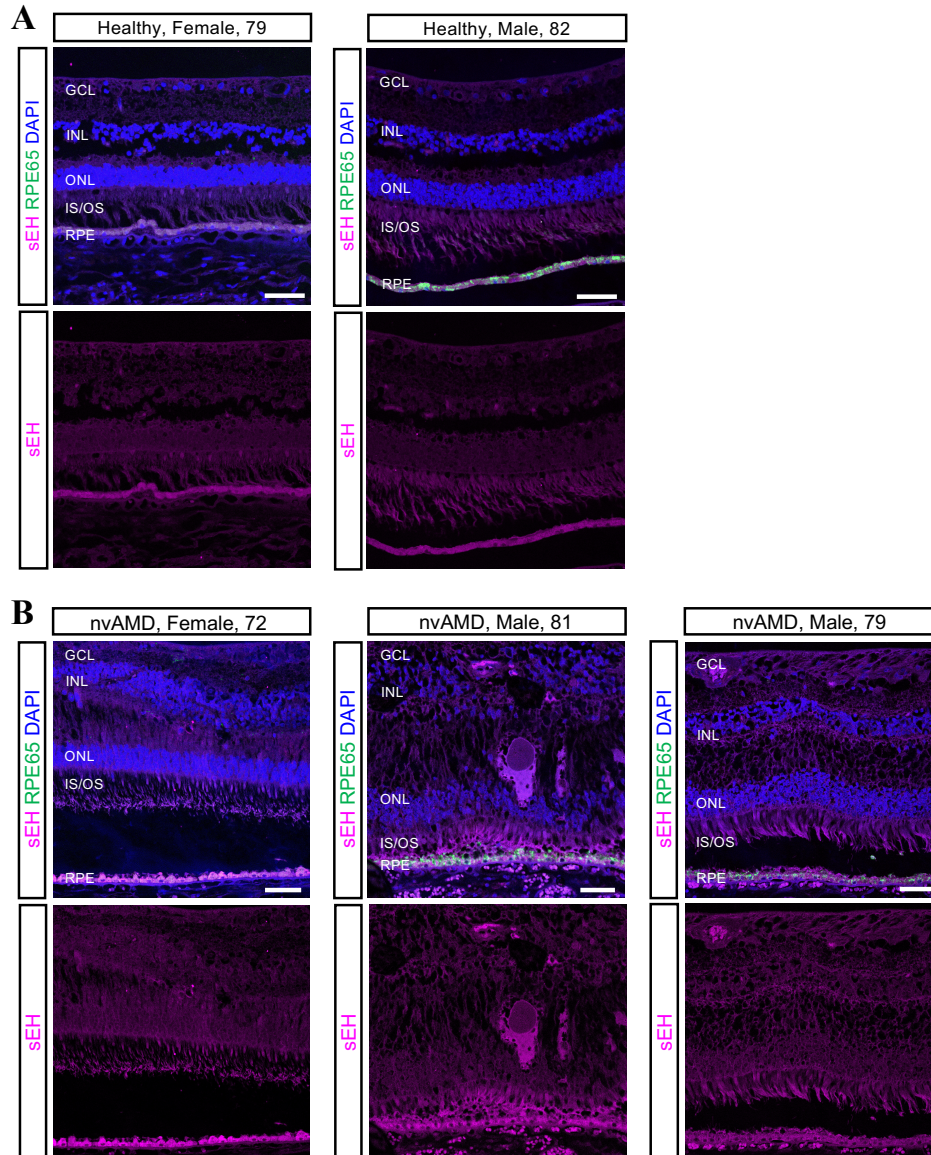


Figure 4.6: Colocalization of sEH with RPE in human retinas from additional human subjects. Images of retinal sections stained with DAPI (blue), sEH (magenta), RPE65 (RPE; green), WGA (rod photoreceptors; yellow). Labeling of retinal tissues with RPE65 for RPE cells showing colocalization of sEH in RPE layer. Scale bars: 50 μ m. GCL, ganglion cell layer; INL, inner nuclear layer; ONL, outer nuclear layer; IS/OS, photoreceptor inner segments/outer segments; RPE, retinal pigment epithelium.

4.3.3 RNAscope ISH evaluation of *EPHX2/Ephx2* mRNA expression

Fluorescent RNAscope ISH was performed to achieve single cell resolution for *EPHX2/Ephx2* mRNA detection in human nvAMD and murine L-CNV retinas. The human *EPHX2* mRNA expression pattern was consistent with what we observed at the protein level through immunohistochemistry. *EPHX2* was broadly expressed in vasculature and multiple cellular layers, but prominently in photoreceptor cell bodies and outer segments, and in RPE (Figure 4.7A-C). The *EPHX2* mRNA expression was markedly increased in nvAMD eyes, throughout the retina but most prominently in the RPE (Figure 4.6C).

Findings in murine retinas were similar, where *Ephx2* mRNA was expressed in photoreceptor cell bodies and outer segments, but also in the inner nuclear layer and at a low level in RPE of untouched eyes (Figure 4.8A). In L-CNV, there was a notable increase of *Ephx2* mRNA in the photoreceptors and elsewhere in the retina (Figure 4.8B-C), comparable to that seen in human nvAMD. However, the increase in *Ephx2* signals in RPE was more modest in the murine L-CNV model than in human nvAMD eyes.

Because sEH protein expression has previously been reported in Müller glia and the Müller glia dependent expression of sEH was implicated in retinal vasculature development and diabetic retinopathy (Hu, Popp et al. 2014, Hu, Dziumbala et al. 2017), I simultaneously detected *Ephx2* (magenta) and *ApoE* (green), as an mRNA marker for Müller glia cells. Apolipoprotein E (*ApoE*) is synthesized in the retina by Müller glial cells (Amaratunga, Abraham et al. 1996), therefore *ApoE* mRNA was previously used as a target in RNAscope assays to identify Müller glia (Menon, Mohammadi et al. 2019). I confirmed that *Ephx2* is expressed in Müller glia through co-localization with *ApoE*, but

that *Ephx2* overexpression is more prominent in photoreceptors and RPE in murine L-CNV than in Müller glia (Figure 4.8A).

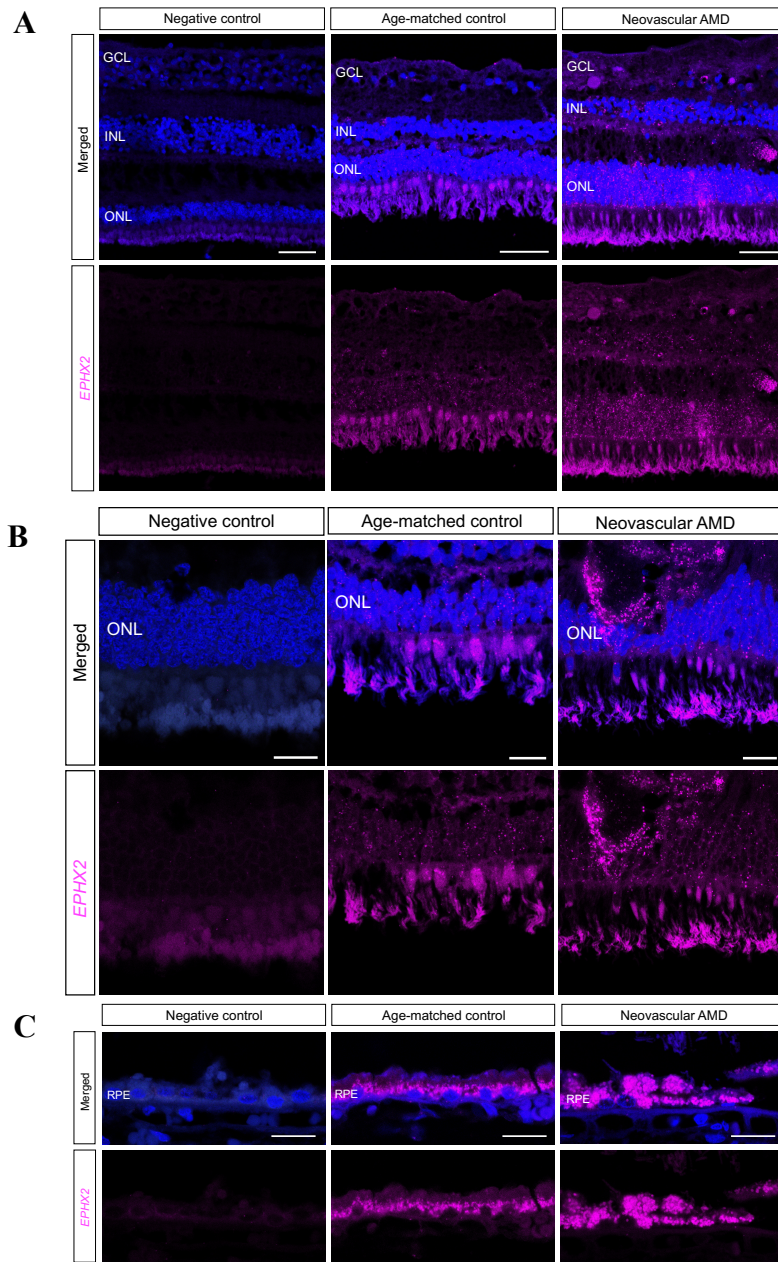


Figure 4.7: *EPHX2* mRNA is highly expressed in the retinal pigment epithelium (RPE) of AMD eyes. Representative Images of retinal sections from nvAMD (72 y.o., female) and age-matched control eyes (79 y.o., female). *EPHX2* encoding sEH is in magenta and nuclei (DAPI) are in blue. (A) *EPHX2* is detected across retina, including vasculature and photoreceptors. Scale bars = 50 μm. (B) 40X images of the same specimen. *EPHX2* mRNA is highly expressed in the photoreceptor cell bodies in outer nuclear layer (C) 40X images of the same specimen. *EPHX2* mRNA is highly expressed in RPE. Scale bars = 20 μm. In nvAMD, *EPHX2* mRNA signal is increased in INL, ONL and apical RPE. Bright fluorescent puncta represent positive mRNA signal. GCL, ganglion cell layer; INL, inner nuclear layer; ONL, outer nuclear layer. Representative images from n = 2 control and n = 3 nvAMD subjects.

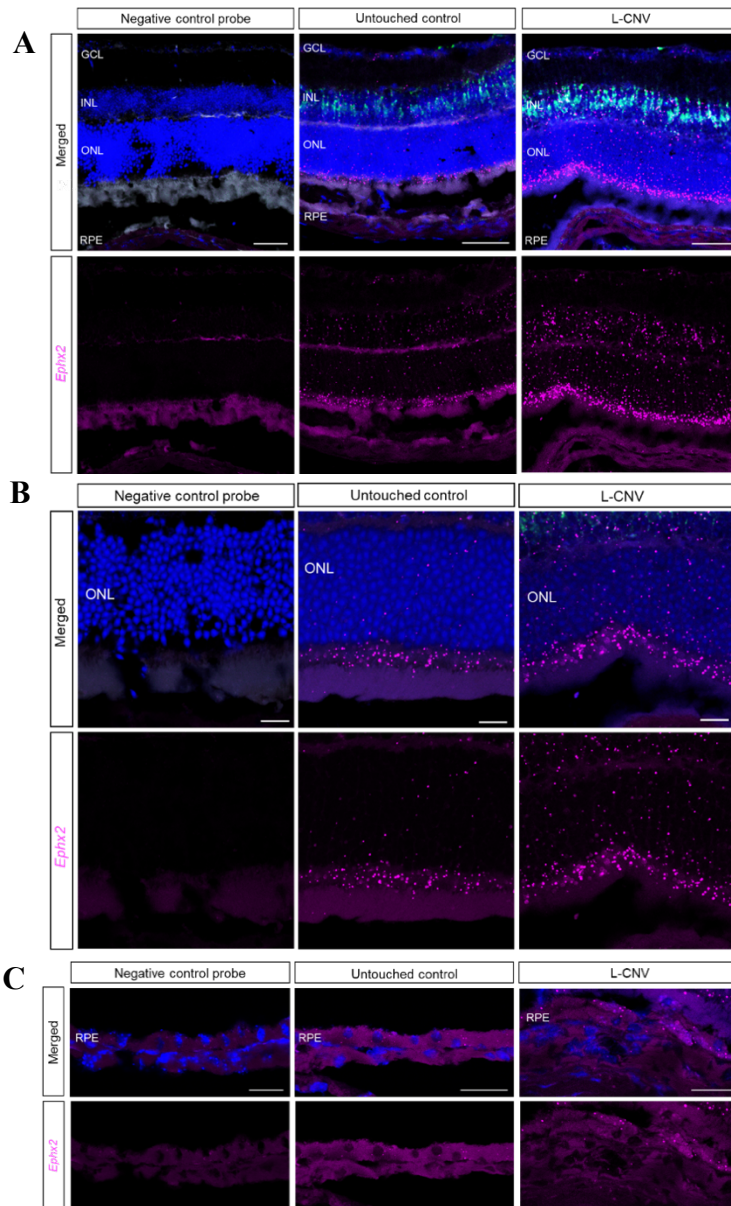


Figure 4.8: sEH mRNA expression is increased in the retinal pigment epithelium (RPE) of L-CNV eyes. Representative images of retinal sections from eyes of murine L-CNV and untouched control eyes. *Ephx2* mRNA encoding murine sEH is in magenta, *ApoE* mRNA (glial cell marker) is in green and DAPI is in blue. (A) *Ephx2* mRNA is detected throughout all cellular layers of the retina, but its signal is most prominently increased in INL and ONL of the photoreceptor cells in L-CNV. *Ephx2* detected in INL partially colocalizes with *ApoE*, indicating its expression in glial cells in addition to photoreceptor cells in L-CNV. Scale bars = 50 μ m. (B) *Ephx2* mRNA is highly expressed in the ONL and OS. (C) *Ephx2* mRNA is expressed at low levels in the RPE of the untouched control, whereas its expression is enhanced in the RPE of the L-CNV eyes. Scale bars = 20 μ m. Bright fluorescent puncta represent a positive RNA signal. GCL, ganglion cell layer; INL, inner nuclear layer; ONL, outer nuclear layer. Representative images from n = 2 control and n = 3 nvAMD subjects.

4.4 Discussion and Conclusions

CNV in nvAMD involves pathological changes within photoreceptors, RPE, Bruch's membrane and choroid, underlying visual impairment (van Lookeren Campagne, LeCouter et al. 2014). Therefore, knowing the localization of therapeutic target expression is critical for unraveling CNV pathology and developing optimal therapeutic strategies. Although we had previously demonstrated that sEH is upregulated in L-CNV, there was a knowledge gap in the precise retinal cellular expression of sEH (Sulaiman, Park et al. 2018).

In murine retinas, sEH was expressed at low levels in the normal untouched control murine retinas. The upregulated sEH in the L-CNV murine eyes showed prominent colocalization with rod photoreceptors and the apical and basal surface of the RPE. Intriguingly, coimmunostaining of sEH with cell type markers confirmed that sEH is overexpressed in photoreceptors and RPE cells in areas with degenerative changes in human nvAMD specimens, supporting the expression pattern observed in murine L-CNV retinas. Differences between the human and murine retinas were observed in the expression level in the non-disease state. In the murine control retinas, the baseline sEH expression level was minimal and limited to vasculature layers, and the expression was induced by CNV stimuli. Aged human eyes without pathological changes, in contrast, showed a broader pattern of expression. Overexpressed sEH in the murine retinas did not have substantial colocalization with cone photoreceptors in contrast to human retinal sEH expression, but this could also be a species difference: the rod-specific sEH expression was seen in response to CNV in the rod-dominant, nocturnal murine eye that does not have structural organization of the human macula.

However, others showed that sEH was primarily localized to Müller glia and astrocytes in the developing retina and in the oxygen-induced retinopathy model of retinal neovascularization (Hu, Popp et al. 2014). The discrepancies in sEH localization among studies suggested limitations of antibodies and immunohistochemistry approaches, including lack of universally accepted standardization of antibody production and antibodies having different specificity towards the target, and this may result in divergent IHC/IF results (Bordeaux, Welsh et al. 2010). Therefore, the sEH expression pattern warranted more detailed examination. My study demonstrated that RNAscope presents an ideal experimental tool to validate immunohistochemistry results. RNAscope is an ISH technique that detects each single RNA transcript which appears as a distinct dot that is visible using a fluorescence microscope. By RNAscope, I detected *EPHX2/Ephx2* mRNA throughout the retina, concentrated within the blood vessels, the ONL, and RPE. In nvAMD retinas compared to controls, *EPHX2* mRNA was highly expressed, with notable signals in the apical RPE. Intriguingly, scRNAseq data from the University of Iowa supports this finding, showing that *EPHX2* gene expression is more enriched in rod and RPE cells than other retinal cell types in human retina obtained from a mixed pool of donors that included healthy subjects, macular degeneration, and autoimmune retinopathy patients (Dataset: all_retina_rpe_chor; Singlecell-eye.org).

In murine retinas, *Ephx2* mRNA was observed mostly within the INL, photoreceptors, and moderately in RPE. Colocalization of *Ephx2* and *ApoE* in the inner nuclear layer supported other studies that previously reported sEH protein expression in Müller glial cells (Hu, Popp et al. 2014, Hu, Dziumbala et al. 2017). However, Müller glia do not appear to be the major producers of *Ephx2* in adult mice or in L-CNV. This could

have been due to disease model variations that may involve different stimuli leading to upregulation of sEH in different cell types. The expression increased in L-CNV retinas most notably in photoreceptors and RPE, which mirrors observations in human nvAMD retinas, though *EPHX2* signals were more prominent in human retinas.

These findings suggest the value of exploring the role of sEH in RPE dysfunction and also indicate the outsized role of RPE cells in human AMD pathology that is not fully recapitulated in the murine L-CNV model, which involves an acute laser injury to the photoreceptors, RPE and choroid to induce inflammation and angiogenesis (Nagai, Lundh von Leithner et al. 2014), whereas human AMD pathology involves sustained inflammatory and oxidative stress leading to damage of the RPE and photoreceptor cells combined with age-related changes (Pennington and DeAngelis 2016, Edwards and Luttly 2021, Fleckenstein, Keenan et al. 2021). As discussed in Chapter 1, RPE and photoreceptor pathology is not only a component of macular degeneration but also contributes to the development of choroidal neovascularization, which is an advanced form of macular degeneration. In the initiation stage of CNV, RPE and photoreceptor cells produce VEGF and other pro-angiogenic factors that incite angiogenesis (Kvanta, Algvere et al. 1996, Lopez, Sippy et al. 1996). The production of sEH by photoreceptors and the RPE could alter the balance between EpFAs and dihydroxy FAs, in the manner of depleting pro-resolving EpFAs. It is well known that growth factors and molecules produced by RPE promote angiogenesis. The future study may explore how altered lipid balance due to photoreceptor and RPE dependent overexpression of sEH have biological effects on not only photoreceptors and the RPE themselves, but also on the choroidal endothelial cells. In the present study, sEH was more strongly detected in the apical and

basal surface of the RPE. This distribution of sEH expression is also interesting because such a polarized distribution pattern is reflected by RPE-dependent production of important growth factors such as VEGF for which the basal secretion towards Bruch's membrane is greater than apical secretion (Blaauwgeers, Holtkamp et al. 1999). Altogether, overexpression of sEH at the protein and mRNA level in CNV and disease-relevant cell types indicate a functional role of sEH in AMD pathophysiology and provides a rationale to target these cell types for developing therapies, as detailed in the next chapter.

CHAPTER 5. EFFICACY OF AAV8-shRNA TARGETING *Ephx2* AGAINST MURINE CHOROIDAL NEOVASCULARIZATION

5.1 Overview

Major factors that contribute to clinical failure of drugs are issues with efficacy and safety. Therefore, once a drug target has been identified, comprehensive validation processes must be undertaken to build up a body of evidence supporting that the target modulation will lead to a therapeutic effect in a disease state. In **Chapter 5**, I hypothesized that sEH in the eye is required for CNV formation in vivo. I investigated the efficacy of adeno-associated virus (AAV) serotype 8 vector expressing shRNA against *Ephx2*, delivered intravitreally in the murine L-CNV model. Neovascular AMD patients and murine L-CNV retinas had overexpression of sEH in vasculature, photoreceptors, and retinal pigment epithelial cells as shown in **Chapter 4**. This provided a rationale to pursue AAV serotype 8 that has tropism towards these relevant cell types. The delivery of AAV8-*Ephx2* shRNA significantly reduced CNV. In addition, gene expression analysis showed reduced *Vegfc* and CNV-related inflammatory markers. Thus, depletion of sEH phenocopies the antiangiogenic effects seen with small molecule inhibitors, further demonstrating sEH as a promising therapeutic target in the treatment of CNV associated with nvAMD.

5.2 Background and Rationale

Drug discovery and development is a long and costly process. Most of the small molecule projects within the pharmaceutical industry fail at multiple stages and only 10% of them progress to candidate stage (Hughes, Rees et al. 2011). Therefore, early in-depth validation is crucial, to minimize the risk of drug failure in the clinic, and to increase confidence in the relationship between the druggable target and disease. This requires a body of evidence that demonstrates that a molecular target is directly implicated in a disease state, and that modulation of the target confers therapeutic effect, leading to increased likelihood of clinical success in future. There is a spectrum of target validation approaches to be undertaken, including utilizing lead pharmacological compounds and genetic confirmation (e.g., siRNA, shRNA, known mutations) (Figure 1.4).

Previously, we reported that chemical inhibition of sEH using small intravitreal molecules suppresses L-CNV (Sulaiman, Park et al. 2018). An inhibitory effect on ocular angiogenesis was also reported for other routes of administration of sEH inhibitors where oral administration of an sEH inhibitor TPPU reduced CNV lesions (Hasegawa, Inafuku et al. 2017). The economic sustainability of small molecules compared to biologics (Makurvet 2021) and formulation options for developing of small molecules present them as ideal candidate pharmacological compounds. In regard to drug delivery, small molecules are more permeable through blood retinal barriers than biologics; however, for the same reason, there is a barrier to using small molecules to treat retinal diseases because their half-life is short, and the intravitreal clearance of small molecules is much more rapid than that of biologics (del Amo, Rimpelä et al. 2017). The lack of target specificity is a potential limitation with small molecules, as they may have

uncharacterized targets beyond the protein of interest (Kawasumi and Nghiem 2007). As well, the propensity of small molecules to interact with sites other than the active site of a target (demonstrated by enzyme kinetics analysis in **Chapter 3** for both SH-11037 and compound 7 sEH inhibitors), put them at a disadvantage as a target validation tool (although their ability to interact with a wide range of targets compared to biologics presents exciting opportunities for ophthalmic drug therapy innovation, and polypharmacology can be employed as a therapeutic strategy). Thus, there is a rationale to pursue a genetic approach to evaluate whether depletion of the target can phenocopy the antiangiogenic effects observed with small molecule inhibitors to validate the target engagement in the disease progression (Cong, Cheung et al. 2012). The tissue-specific knockdown of sEH in the eye is more appealing than systemic knockout because: 1) sEH inhibition can have opposite effects on angiogenesis depending on tissue levels of PUFAs that are parent to epoxy lipids (Figure 1.3), and 2) Intraocular sEH knockdown will enable us to mimic the drug's effect more accurately than knocking out a gene constitutively. There have been studies showing delayed retinal angiogenesis in systemic sEH knockout mice and Müller cell specific sEH knockout mice (Hu, Popp et al. 2014), however intraocular sEH knockdown using a therapeutic gene approach in the context of CNV has never been studied before.

The unique physiological features of the retina have allowed substantial advances in gene therapy in retinal diseases. Though the retina is part of the central nervous system, its peripheral location provides clinical accessibility. The presence of tight blood-retinal barriers limits systemic side effects of the gene therapy by preventing exposure to other organs. The retina is also considered an immune privileged tissue. In addition to

physical barriers, the retina produces a number of molecules such as TGF- β that contribute to its immune suppressive microenvironment to protect tissue from external and internal insults that are inherent to retina due to its high metabolic activities (Chen, Luo et al. 2019, Dhurandhar, Sahoo et al. 2021). Therefore, gene therapy has enormous potential for clinical success in treating retinal diseases, amplified by the Luxturna market authorization (indicated for a rare form of inherited retinal disease, Leber congenital amaurosis), which is the first gene therapy to be approved by the FDA (Trapani, Tornabene et al. 2021).

The general mechanism of gene therapy viral vector-based gene therapy is carried out by in vivo delivery of specific genetic material by vectors based on lentiviruses, adenoviruses, or adeno-associated viruses (AAV). The advantage of lentivirus is in its persistent transduction in both dividing and nondividing cells, and its packing capacity of 8-9 kbp (Lukashev and Zamyatnin 2016). However, lentiviruses may integrate to the genome, trigger immunogenicity and have limited transduction in photoreceptor cells. Adenoviruses have broad tropism and can transduce both dividing and non-dividing cells, with a large packing capacity of 30-40 kbp (Appaiahgari and Vрати 2015). However, adenoviruses trigger substantial immunogenicity responses, which would be presented as an advantage in cases of vaccines and cancer therapy, but the risk of infecting off-target cells, severe infection and immune responses are major disadvantages of adenoviruses, therefore adenoviruses are not often used in retinal gene therapy (Wold and Toth 2013, Ginn, Amaya et al. 2018). Despite adeno-associated viruses (AAV) having a major setback in its packing capacity that is limited to 5 kbp, AAV is the most promising viral vector for retinal gene therapy because of low immunogenicity risk, ability to transduce

non-dividing cells, and stable transgene expression in retinal cell types (Dhurandhar, Sahoo et al. 2021, Sahu, Chug et al. 2021). The first clinical success with an FDA approval in gene therapy was with AAV (Luxturna), in treating inherited retinal disease, as briefly mentioned above (Bainbridge, Smith et al. 2008, Smalley 2017). The AAV vectors have been widely used in numerous preclinical proof-of-concept studies for gene delivery to the photoreceptors or RPE cells (Acland, Aguirre et al. 2001, Buck and Wijnholds 2020, Dhurandhar, Sahoo et al. 2021). The AAV virus capsid that determines the tropism was modified over the years, so that AAV serotypes can mediate transduction in diverse cell types in the retina. AAV8 is highly efficient in transducing photoreceptors and the RPE in both mice and humans (Day, Byrne et al. 2014, Dhurandhar, Sahoo et al. 2021). All together, these desirable properties of AAV provided a rationale to select AAV as a viral vector in my target validation study.

Here, I evaluated the efficacy of intravitreal delivery of adeno associated virus (AAV) serotype 8 mediated shRNA targeting *Ephx2* in the mouse L-CNV model. I examined CNV formation through ocular imaging over time in vivo and in subsequent immunohistochemical assessment. To determine sEH-modulated signaling pathways, gene expression analysis was performed on treated tissue samples.

5.3 Results

5.3.1 In vivo transduction of AAV8-*Ephx2* shRNA

Given the photoreceptor and RPE-localized overexpression of *Ephx2* in L-CNV (demonstrated in **Chapter 4**), I chose AAV8 vector to target the CNV and disease relevant cells for delivering shRNA against *Ephx2*, since AAV8 is well known to transduce photoreceptor and RPE cells (Lee, Kim et al. 2018). To determine the viral dose and experimental timeline for optimal transduction efficiency, AAV8 vectors encoding U6 promoter-driven *Ephx2* shRNA and CMV promoter-driven mCherry at low or high titer (4.9×10^6 GC or 1.9×10^7 GC) were administered intravitreally, then I evaluated dose and time-dependent in vivo transduction by detecting mCherry expression through fluorescence fundus imaging and cryosections (Figure 5.1A). Efficient transduction was evident in which mCherry expression was first detected by fluorescence funduscopy at 2 weeks after intravitreal injection, reached a maximum at week 3, and was stable through week 5. The corresponding OCT images of the representative fundus images show no substantial difference in anatomical structure of the retina cross sections at all viral doses tested. In addition to this time dependent increase in transduction, a dose-dependent increase in transduction efficiency was verified with greater transduction achieved at the higher titer, 4.9×10^6 GC (Figure 5.1B).

5.3.2 Localization of transduced cells

I next determined whether the AAV8-*Ephx2* shRNA viral vector efficiently and specifically targeted photoreceptor and RPE cells in vivo. At week 5, mouse eyes were enucleated for cryosectioning, and the sections underwent microscopic assessment and immunohistochemistry. Mouse eye cryosections showed mCherry expression localized

most strongly to the photoreceptor and RPE layers (Figure 5.1C). At the lower titer, mCherry expression was limited to the outer nuclear layer at a low level and absent in the RPE, whereas the higher titer resulted in more mCherry positive cells in both photoreceptor and RPE cell layers. These sections were then stained with antibodies for markers of rods, cones and RPE cells, verifying that these cell types were transduced by intravitreal injection of AAV8 (Figure 5.2A-C). Together these findings demonstrate in vivo transduction efficiency of the viral vector to the desired cells, photoreceptors and the RPE that predominantly overexpressed sEH in murine L-CNV and human nvAMD retinas (Chapter 4).

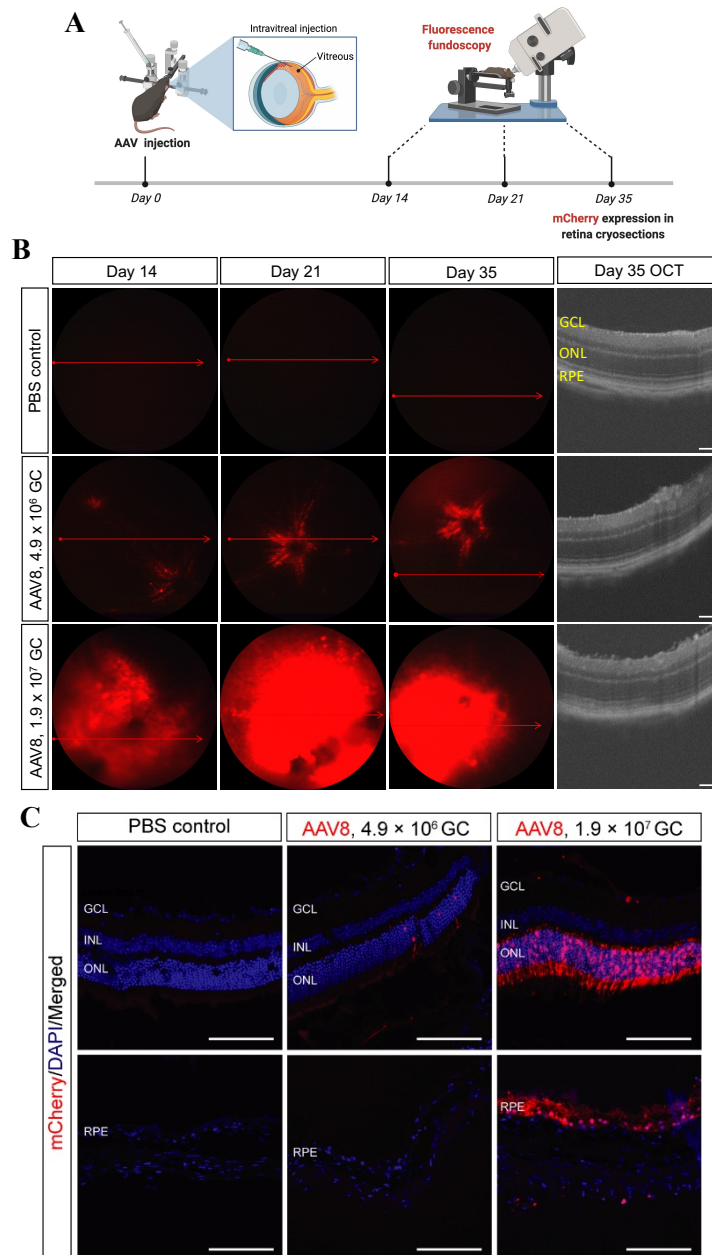


Figure 5.1: In vivo transduction of AAV8 in murine retina. (A) Study design and experimental timeline used to assess in vivo efficacy of AAV8-*Ephx2* shRNA. Noninvasive fluorescence funduscopy was used to assess mCherry expression in vivo on day 14, day 21, and day 35 post-injection, followed by cryosection imaging ex vivo. (B) Time-dependent and viral dose-dependent transduction efficiency. Fluorescence funduscopy showing in vivo mCherry expression in wide view image of retina (red lines indicating OCT scans) and corresponding OCT images on day 35 showing no substantial changes in retinal structure. (C) AAV transduction visualized in retinal sections five weeks after injection. Retinal sections showing mCherry positive cells in ONL and RPE. GCL, ganglion cell layer; INL, inner nuclear layer; ONL, outer nuclear layer; RPE, retinal pigment epithelium. Scale bars = 100 μ m

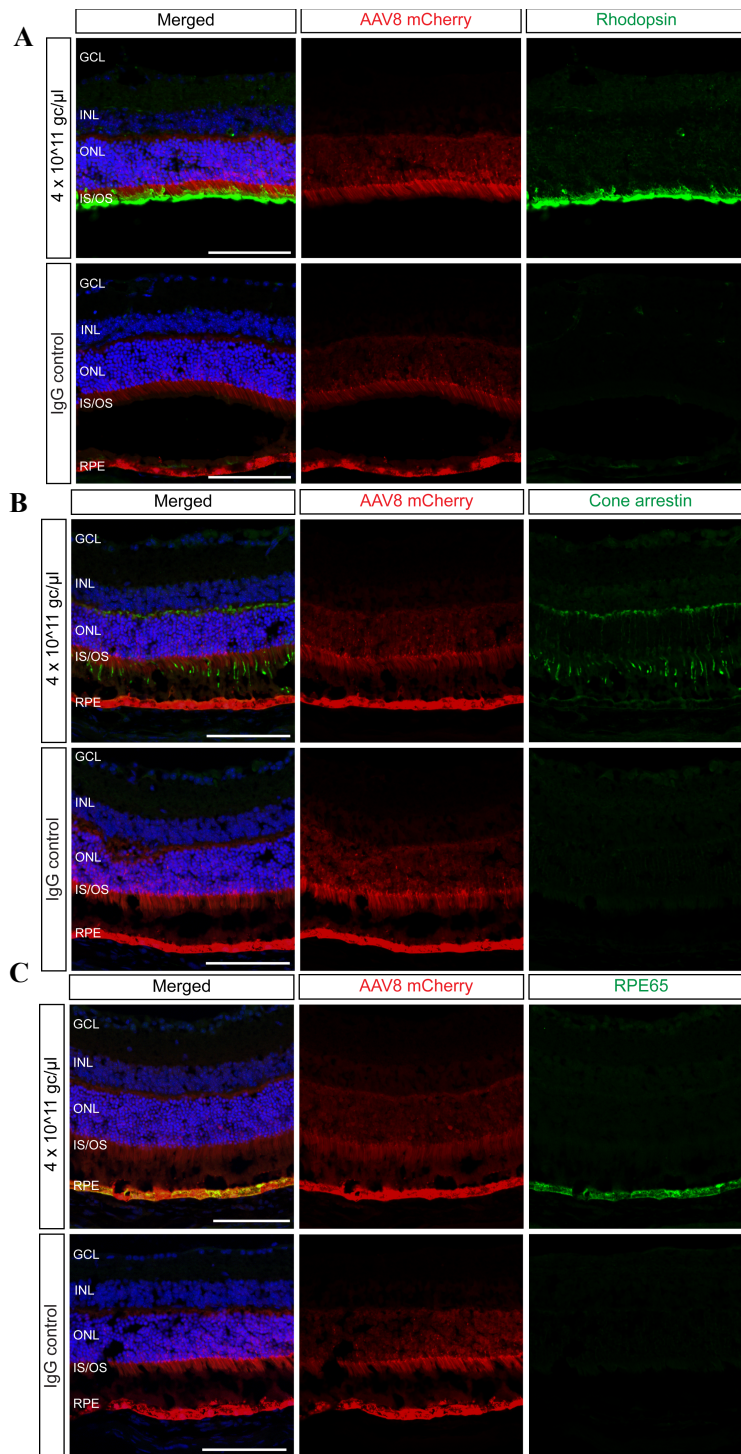


Figure 5.2: Immunolocalization of mCherry with cone arrestin, rhodopsin and RPE65 in AAV8 injected murine eyes. Five weeks after intravitreal injection, AAV8 transduction (mCherry; red) was observed in (A) rod photoreceptor cells (rhodopsin, which stains outer segments; green), (B) cone photoreceptor cells (cone arrestin; green) and RPE cells (RPE65; green). Nuclei (DAPI) are blue. GCL, ganglion cell layer; INL, inner nuclear layer; ONL, outer nuclear layer; IS/OS, photoreceptor inner/outer segments; RPE, retinal pigment epithelium. Scale bars = 100 μm

5.3.3 Suppression of L-CNV by AAV8-*Ephx2* shRNA

I evaluated whether intravitreal injection of AAV8-*Ephx2* shRNA would suppress the formation of CNV. Based on the *in vivo* transduction study of AAV8 (Figure 5.1), optimal viral dose and timeline were determined for the L-CNV experimental scheme (Figure 5.3). At day 0, mice received intravitreal injection of 1.9×10^7 GC of AAV8-*Ephx2* shRNA, AAV8-scrambled shRNA control or PBS control. At day 7, laser photocoagulation was performed to induce CNV where 3 laser burns were applied in each injected eye. At day 21 (day 14 post laser), fluorescence funduscopy was performed to assess transduction and *in vivo* optical coherence tomography (OCT) imaging and fluorescein angiography (FA) were performed to visualize L-CNV and consequent vascular leakage. Notably, AAV8-*Ephx2* shRNA reduced vascular leakage shown through FA imaging and CNV lesion volume which was assessed based on OCT images (Figure 5.3B and C). *Ex vivo* CNV volume measurements at day 21 (14 days post laser) likewise revealed a statistically significant attenuation in CNV in mice injected with AAV8-*Ephx2* shRNA compared to scrambled shRNA and PBS controls (Figure 5.3D and E).

To verify that the detected suppression in CNV volume coincided with the downregulation of sEH expression, immunoblot analysis was performed using total protein obtained from retina and RPE/choroid isolated from mice injected with 1.9×10^7 GC of AAV8-*Ephx2* shRNA, AAV8-scrambled shRNA control and PBS control. Compared to the PBS control and scrambled shRNA control, mice administered AAV8-*Ephx2* shRNA had markedly reduced retinal and RPE/choroidal sEH expression (Figure

5.4A, B). These findings support that AAV8 mediated delivery of shRNA targeting *Ephx2* can lead to depletion of target and suppress CNV progression.

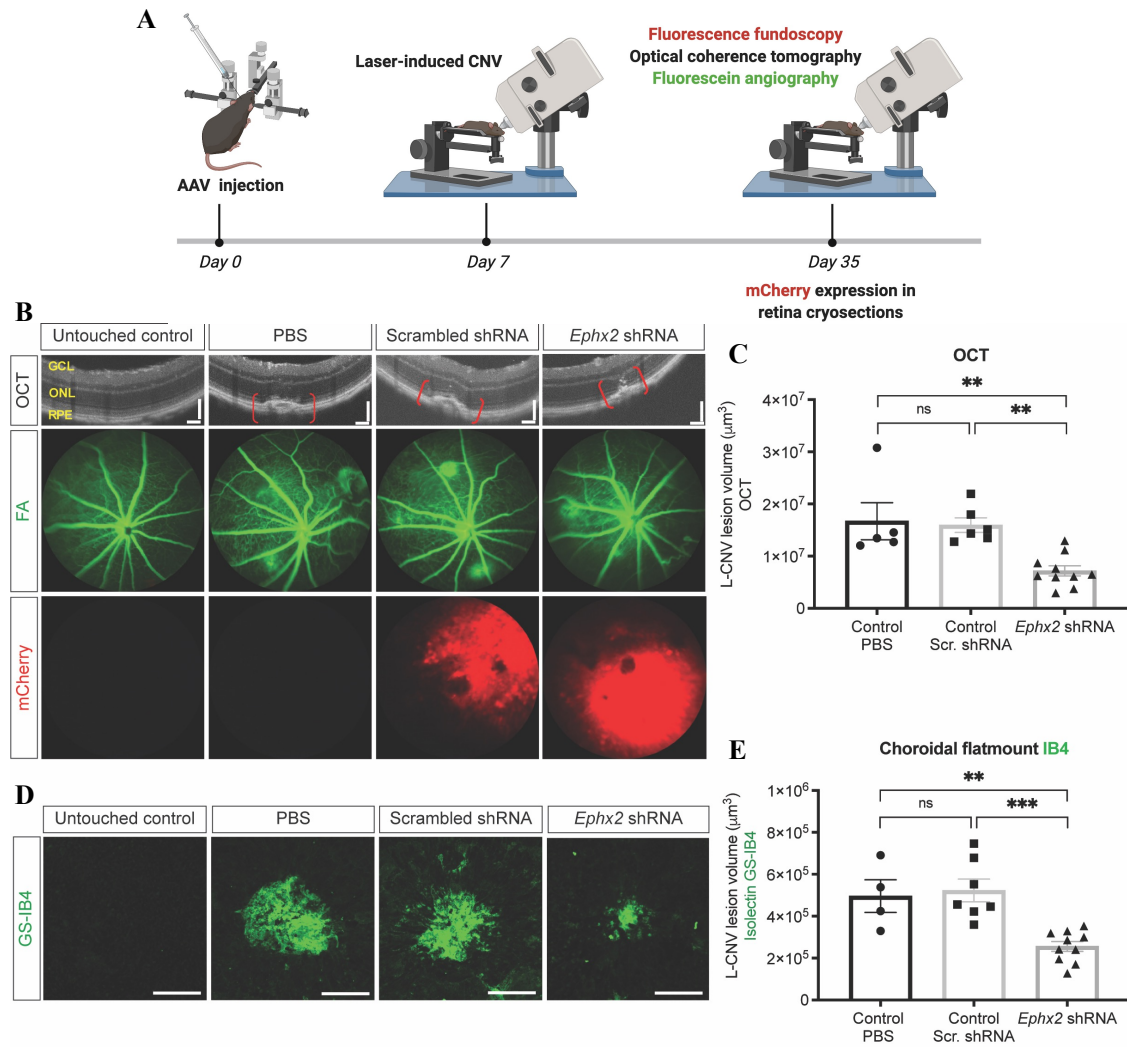


Figure 5.3: AAV8-delivery of shRNA against sEH suppresses L-CNV. (A) Study design and experimental timeline used to assess in vivo efficacy of AAV8-*Ephx2* shRNA. After seven days post intravitreal injection of viral vectors encoding *Ephx2* shRNA or scrambled shRNA or PBS vehicle; mice were treated with laser to induce CNV. Transduction level (mCherry fluorescence) and neovascular volume were assessed by weekly noninvasive ophthalmic imaging tools: funduscopy and optical coherence tomography (OCT) and fluorescein angiography (FA). On Day 14 post laser, retina and choroid tissue of each treatment group were harvested for choroidal flatmounts. (B) Representative OCT, FA (green) and AAV8 (mCherry; red) fluorescence fundus images on day 14. (C) CNV lesion volume was calculated as an ellipsoid from OCT images. (D) Representative images from confocal microscopy of *Griffonia simplicifolia* isolectin B4 (GS-IB4; green) stained CNV lesions 14 days post L-CNV. (E) CNV lesion volume from Z-stack confocal images, showing a reduction in CNV lesions with *Ephx2*-shRNA. Mean \pm SEM, N = 4-10, one-way ANOVA with Tukey's post hoc tests (ns, non-significant; **p<0.01; ***p<0.001). Scr: scrambled; GCL, ganglion cell layer; ONL, outer nuclear layer; RPE, retinal pigment epithelium.

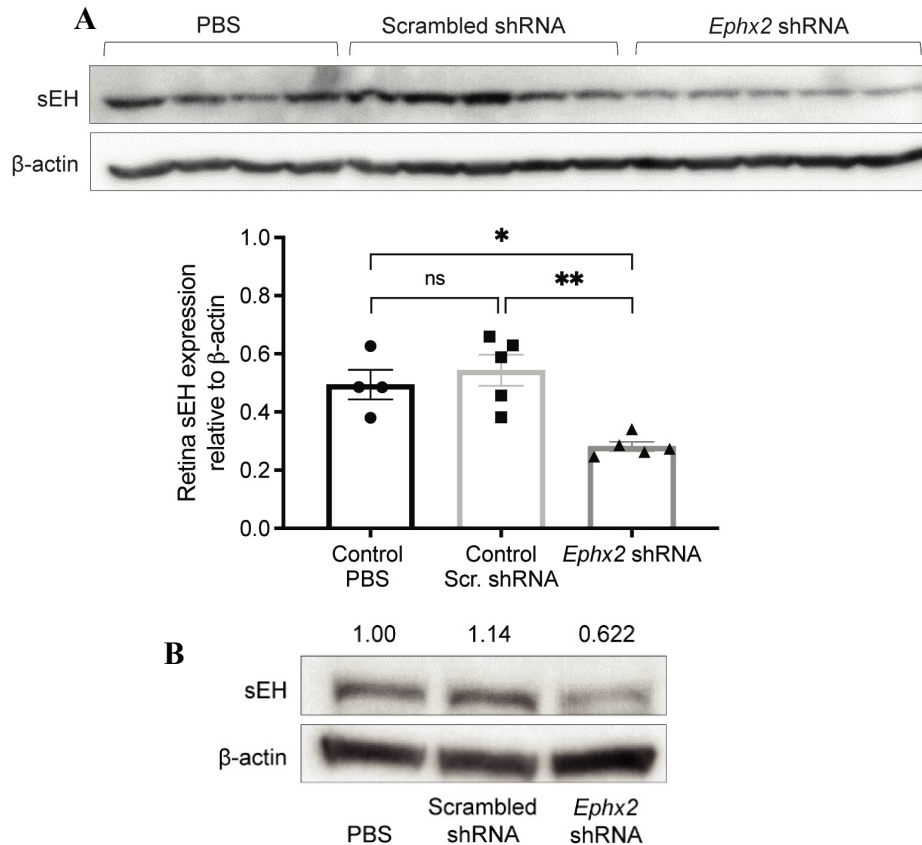


Figure 5.4: AAV8-*Ephx2* shRNA reduces sEH expression level. Inhibitory effect of AAV8-*Ephx2* shRNA on sEH expression was determined in tissues collected 3 weeks post intravitreal injection of 1.9×10^7 GC of AAV8-*Ephx2* shRNA, AAV8-scrambled shRNA control or PBS control. (A) sEH expression in retina. Each lane represents a single retina sample. Mean \pm SEM, N = 4-5 biological replicates, one-way ANOVA with Tukey's post-hoc tests (ns, non-significant; * $p < 0.05$; ** $p < 0.001$). (B) sEH expression in RPE/choroid. Each lane represents pooled tissue samples from 3-4 eyes. Intensity relative to PBS control, normalized to β -actin, is indicated.

5.3.4 Inhibition of CNV-related inflammatory gene expression by AAV8-*Ephx2* shRNA

To investigate the mechanisms by which *Ephx2* knockdown attenuates CNV formation, I isolated RNA from retina and RPE/choroid tissues of untouched eyes and eyes treated with either AAV8-scrambled shRNA control or AAV8-*Ephx2* shRNA in the L-CNV model. Through the stabilization of anti-inflammatory and pro-resolving EpFAs, inhibition of sEH has shown anti-inflammatory effects in various models of inflammation. The EpFA substrates of sEH, 11,12-EET or 19,20-EDP in combination with AUDA inhibit, whereas the dihydroxy fatty acids, 19,20-DHDP promotes, TNF- α -induced VCAM-1 and ICAM-1 expression in human retinal endothelial cells (Capozzi, Hammer et al. 2016). In a lipopolysaccharide (LPS) induced lung injury model, sEH inhibition had anti-inflammatory effects where pro-inflammatory cytokines levels (IL-1 β and TNF- α) and neutrophil infiltration to the lung were decreased (Askari, Thomson et al. 2014). The sEH inhibition and potentiating EpFAs are also being employed as a therapeutic strategy for treating neurodegenerative diseases, such as Parkinson's disease, that are strongly associated with neuroinflammation (Grinan-Ferre, Codony et al. 2020). In the context of CNV, sEH-regulated EpFAs suppressed CNV, and modulated leukocyte rolling velocity by changing the expression of adhesion molecules on the surfaces of leukocytes and in the CNV lesions (Hasegawa, Inafuku et al. 2017). Given this, the changes in mRNA expression levels of CNV relevant inflammatory molecules were analyzed by qPCR. Compared to scrambled shRNA control, I found that *Ephx2* shRNA-treated retinas had significantly lower mRNA levels of inflammatory cytokine genes, *Il1b*, *Il6*, and *Tnfa* (Figure 5.5A-C), and cell adhesion molecules, *Ccl2* and *Icam1* (Figure

5.5D, E). The inhibitory effect was also observed on the mRNA level of *Vegfc* in treated retinas (Figure 5.5F). In treated RPE/choroid, *Ephx2* shRNA likewise significantly reduced mRNA levels of *Il1b*, *Il6* and *Ccl2* (Figure 5.5G, H, J), whereas no significant differences were detected in *Tnfa*, *Icam1* and *Vegfc* (Figure 5.5I, K, L), which were also not significantly upregulated by L-CNV at 14 days post laser treatment in the RPE/choroid.

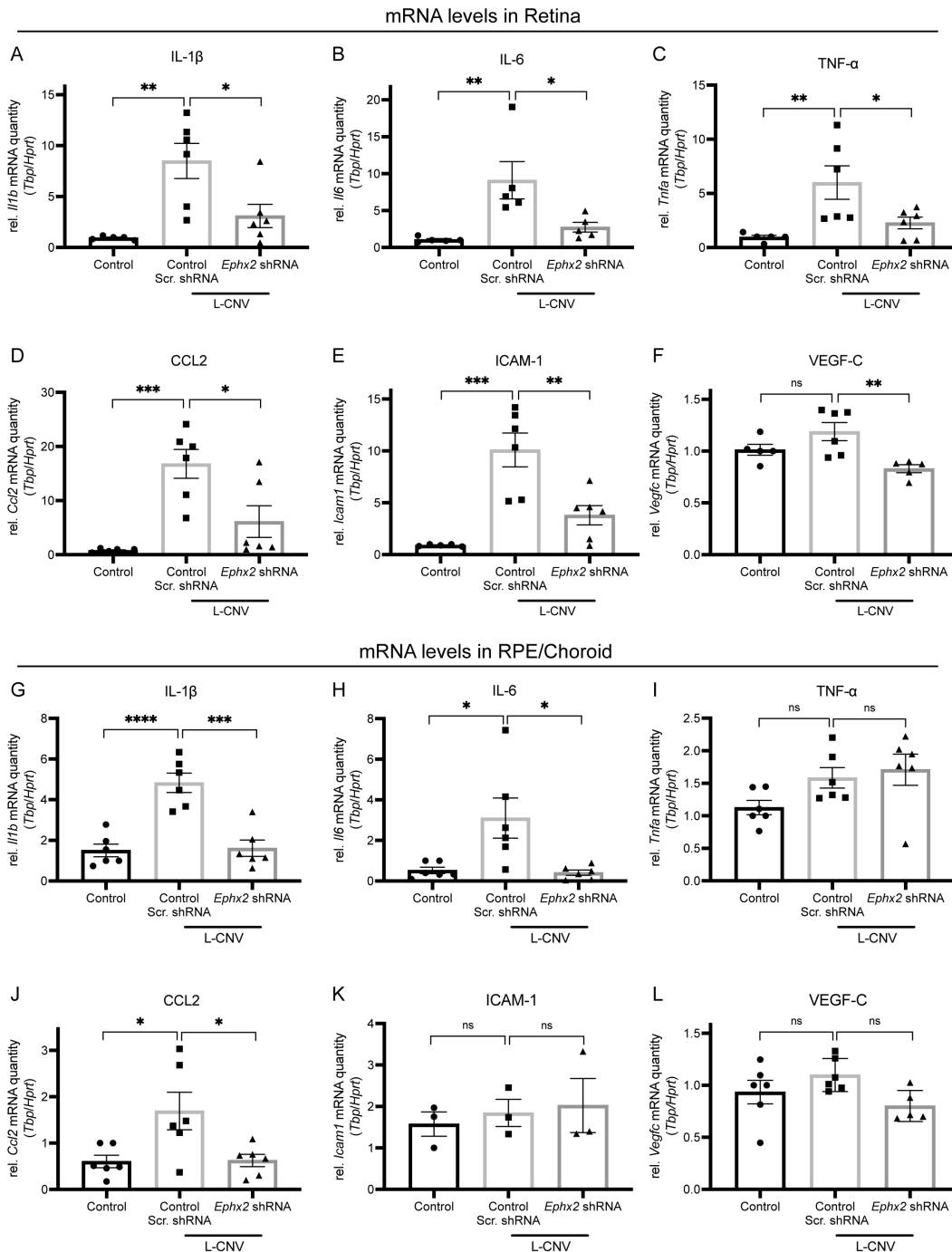


Figure 5.5: Inhibition of CNV-related inflammatory molecule expression by AAV-delivery of *Ephx2* shRNA. mRNA expression levels of inflammatory molecules (A, G) *Il1b*, (B, H) *Il6*, (C, I) *Tnfa*, (D, J) *Ccl2*, (E, K) *Icam1*, and (F, L) *Vegfc* in the retina (A-F) or RPE/choroid (G-L) of untreated control and L-CNV mice transduced with control scrambled shRNA or *Ephx2* shRNA. qPCR data for the indicated genes relative to *Tbp* and *Hprt* expression, normalized to control. Mean \pm SEM, N = 3-6 biological replicates (each data point represents pooled tissue sample from 2 biological replicates), one-way ANOVA with Tukey's post hoc tests (ns, non-significant; * $p < 0.05$; ** $p < 0.01$; *** $p < 0.001$; **** $p < 0.0001$) Scr: scrambled.

5.4 Discussion and Conclusions

I sought to pursue a genetic approach to test the hypothesis that sEH is required for CNV development and to evaluate whether depletion of sEH can phenocopy the antiangiogenic effects observed with small molecule inhibitors. In the systemic sEH knockout mice and Müller cell-specific sEH knockout mice, delayed retinal angiogenesis was observed when retinal vasculature development was compared to the wild-type mice (Hu, Popp et al. 2014). However, sEH knockdown within the eye and its effect on CNV have not been studied before. This would be critical in validating sEH as a therapeutic target to treat CNV because sEH inhibition can have varying effects on angiogenesis depending on tissue levels of PUFAs that are the parent to EpFAs as discussed in detail in the **Chapter 1** introduction. Intraocular sEH knockdown enables us to mimic an sEH-inhibiting drug's effect more accurately while sustaining the effect because of the long-term stable transduction ability of AAV in the relevant cell types.

I found that intravitreally administered AAV8-*Ephx2* shRNA efficiently transduced photoreceptors and RPE (key sEH-producing cell types), substantially reduced retinal and RPE/choroid sEH protein levels and suppressed the progression of CNV. It markedly reduced mRNA expression levels of CNV-relevant inflammatory molecules and VEGF-C. In treated retinas, AAV8-*Ephx2* shRNA normalized mRNA expression levels of pro-inflammatory cytokines – *Il1b*, *Il6*, *Tnfa*, and *Ccl*, and a cell adhesion molecule, *Icam1*. In treated RPE/choroid, AAV8-*Ephx2* shRNA normalized expression levels of *Il1b*, *Il6* and *Ccl2*. The production of interleukin-1 β (IL-1 β) is well established in the pathogenesis of both forms of AMD (Oh, Takagi et al. 1999, Zhao, Bai et al. 2015). IL-1 β is also known for activating IL-6 (McGeough, Pena et al. 2012), which

is a pro-inflammatory and pro-angiogenic cytokine that is involved in progression of nvAMD (Miao, Tao et al. 2012), and intraocular IL-6 was shown to be necessary for CNV in the murine L-CNV model (Droho, Cuda et al. 2021). Studies also demonstrated that inhibition of IL-1 β reduced the production of chemokines including *Ccl2* from both Müller glia and RPE cells (Natoli, Fernando et al. 2017). The sEH depletion having downstream effects in suppressing intraocular inflammatory molecules involved in CNV and AMD in the present study provides a potential mechanistic basis in understanding how sEH is implicated in choroidal angiogenesis.

There was a reduction in *Vegfc* mRNA expression level in AAV8 *Ephx2* shRNA treated retinas, but the relevance of *Vegfc* to day 14 CNV progression is not validated because *Vegfc* was not significantly upregulated by L-CNV. VEGF-C is primarily implicated in lymphangiogenesis by binding to VEGFR-3 but can also bind to VEGFR-2 and exert angiogenic potential. Intriguingly, another study using human umbilical vein endothelial cells (HUVECs) showed that a key EpFA substrate of sEH, 19,20-EDP, potently inhibited mRNA expression of VEGF-C and VEGF-induced phosphorylation of VEGFR-2 while having no effect on VEGF-A levels (Zhang, Panigrahy et al. 2013), indicating that sEH substrate EDP was antiangiogenic through modulating VEGF-C/VEGFR-2 signaling.

I also identified a number of inflammatory mediators that were reduced by AAV8-*Ephx2* shRNA in L-CNV. The mRNA expression levels of inflammatory cytokine genes *Il1b*, *Il6*, *Tnfa*, and *Ccl2*, and that of a cell adhesion molecule *Icam1* were significantly normalized by AAV8 *Ephx2* shRNA in treated L-CNV retinas compared to scrambled shRNA control. In treated RPE/choroid, AAV8-*Ephx2* shRNA had inhibitory

effects on the expression levels of *Il1b*, *Il6* and *Ccl2*, however, the treatment did not significantly alter the expression levels of *Tnfa*, *Icam1* and *Vegfc*. Thus, AAV8-*Ephx2* shRNA had inhibitory effects on inflammatory target molecules that were upregulated by L-CNV on day 14 post laser photocoagulation. The differential downregulation of target molecules between the treated retinas and RPE/choroid could be due to involvement of different signaling pathways in the microenvironment that are also dependent on CNV progression over time. Indeed, other researchers have found that signal transduction molecules, including cell adhesion molecules, are expressed differently between retina and choroid tissue at different timepoints of murine L-CNV progression (Jia, Qiu et al. 2021).

As discussed in **Chapter 1**, the initial stage of CNV is characterized by changes in the microenvironment due to RPE and photoreceptor cells producing growth factors that incite angiogenesis (Kvanta, Algvere et al. 1996, Lopez, Sippy et al. 1996). Inflammatory processes like microglia activation, leukocyte invasion, oxidative stress, lipid deposition, and NLRP3 inflammasome activation are all implicated in RPE dysfunction in AMD, leading to photoreceptor/RPE degeneration (Choudhary and Malek 2019). The production of inflammatory mediators resulting from inflammatory insults (e.g. oxidative stress, lipofuscin and drusen formation) can promote endothelium activation, resulting in increased adhesion molecules and vascular permeability and promote the production of angiogenic factors (Xu, Chen et al. 2009). Substantial work implicates sEH inhibition in inflammatory processes in the brain, cardiac system, and elsewhere in the body (Hasegawa, Inafuku et al. 2017, Darwesh, Keshavarz-Bahaghighat et al. 2019, Grinan-Ferre, Codony et al. 2020). sEH deficiency/inhibition has been linked

to attenuating neuroinflammation (Wu, Shyue et al. 2017) and retinal endothelial cell inflammation (Capozzi, Hammer et al. 2016) in addition to reducing reactive oxygen species (Liu, Qin et al. 2019). The present study supports that sEH is an important target involved in inflammatory processes in the eye. The study also highlights exciting potential in targeting sEH with an AAV mediated therapeutic gene approach that presents stable depletion of the therapeutic target in the disease relevant cell types, which may address shortcomings of other classes of pharmacological molecules, including biologics that have low efficiency in penetration and delivery to the ocular tissue due to their large molecular weight, and small molecules that have efficient penetration through the blood retinal barriers but have limitations due to fast clearance and off-target effects (del Amo, Rimpelä et al. 2017). Given the involvement of both angiogenesis and inflammation in the pathogenesis of CNV, stabilization of pro-resolving epoxy fatty acids through sEH inhibition with a therapeutic gene approach could be a promising therapeutic strategy for CNV underlying nvAMD.

CHAPTER 6. DISCUSSION AND CONCLUSIONS

6.1 Overview

The present **Chapter 6** will conclude the study by reviewing the background and summarizing the key research findings in relation to the research aims of my thesis. **Chapter 1** introduced the pathology of choroidal neovascularization in neovascular age-related macular degeneration, and the potential for targeting soluble epoxide hydrolase as a therapeutic strategy. In Chapter 2, I described the methodology used to address the research aims of my thesis project. In Chapter 3, I demonstrated that the lead pharmacological compound SH-11037 binds to and inhibits sEH, and I discovered the mode of inhibition of SH-11037 as a mixed-noncompetitive inhibition through mechanistic enzymology. In Chapter 4, I defined the cellular expression of the target enzyme, sEH, in photoreceptor and RPE cells of murine and human retinas under the disease states in an experimental model of choroidal neovascularization and human nvAMD. Lastly, in Chapter 5, I employed a gene therapeutic approach as a means of target validation. I demonstrated the efficacy of adeno-associated virus serotype 8 mediated delivery of shRNA targeting *Ephx2*, encoding sEH, in suppressing the progression of murine choroidal neovascularization while inhibiting gene expression levels of inflammatory molecules and VEGF-C. In conclusion, **Chapter 6** will discuss the value and contributions of the research findings, review the limitations of the study, and propose directions for future study.

6.2 Research Aims and Findings

6.2.1 Background Review

Ocular angiogenesis causes blindness in numerous eye diseases, including proliferative diabetic retinopathy, retinopathy of prematurity and neovascular age-related macular degeneration (nvAMD) (Das and McGuire 2003). nvAMD is the leading cause of blindness in adults over 60 years old and affects nearly 2 million people in the US (Fine, Berger et al. 2000, Rein, Wittenborn et al. 2009). nvAMD is characterized by aberrant blood vessel growth under the retina, choroidal neovascularization (CNV). This results in hemorrhage, retinal detachment, and irreversible loss of vision. In addition, nvAMD poses an economic burden causing yearly losses of \$5.4 billion to the GDP in the US (Brown, Brown et al. 2005). Today, the effort to treat nvAMD is hampered by resistance and refractory responses to the current standard of care, anti-vascular endothelial growth factor (VEGF) therapies (Lux, Llacer et al. 2007). Therefore, there is a critical need to elucidate cellular components involved in the pathophysiology and to develop novel therapeutic approaches.

The Corson lab used a forward chemical genetics approach to identify a novel target involved in ocular angiogenesis. The research outcomes included the total synthesis of an antiangiogenic natural homoisoflavonoid, cremastranone, for the first time (Lee, Basavarajappa et al. 2014). Then, a structure-activity relationship analysis of its derivatives was completed and a lead compound SH-11037 with greater potency and selectivity for endothelial cells was discovered (Basavarajappa, Lee et al. 2015, Sulaiman, Merrigan et al. 2016). Using SH-11037 based affinity reagents, we identified soluble epoxide hydrolase (sEH) as a cellular target of SH-11037 (Sulaiman, Park et al.

2018). Thus, the Corson lab has taken various approaches, including structure-based drug design, in vivo pharmacology, and toxicology, illustrated in Figure 6.1C. Interestingly, sEH, encoded by gene *EPHX2*, is a lipid-metabolizing enzyme that hydrolyzes epoxy fatty acids into corresponding diols, and sEH inhibitors have shown efficacy against numerous ocular diseases (Park and Corson 2019).

Our previous results showed increased expression of sEH in the laser-induced choroidal neovascularization (L-CNV) mouse model and human nvAMD eyes (Sulaiman, Park et al. 2018). Lipid profiles of eyes with L-CNV were also altered, with a pronounced shift in sEH substrate to product ratio of epoxy fatty acids to diols. This was indicative of enhanced sEH activity in disease and highlighted the importance of bioactive lipid metabolism in the eye. However, the mechanism by which SH-11037 interacts with its target sEH remained elusive, and the cellular role of sEH in CNV remained unclear. Therefore, the objectives of my thesis research were to elucidate drug-target interactions through enzyme kinetics, investigate sEH mediated mechanisms that regulate CNV, and preclinically validate sEH as a therapeutic target through expression profiling and genetic modulation of the target expression. I hypothesized that SH-11037 binds to the active site of sEH and inhibits its epoxide hydrolase activity. In relation to therapeutic target validation of sEH in CNV, I hypothesized that sEH is overexpressed by retinal cell types that are involved in CNV pathology. I also hypothesized that sEH expression is required for CNV progression and targeting the sEH overexpressing cell types would suppress CNV. The results of my thesis provided a novel understanding of SH-11037's mechanism of action against sEH, by demonstrating that SH-11037 is a mixed-noncompetitive inhibitor of sEH with binding affinities towards both the active site of the

enzyme, and the enzyme-substrate complex. My in-depth expression profiling study challenged the existing theory on retinal sEH expression distribution by providing key evidence that sEH is differentially overexpressed in outer retinal pathology like CNV. In addition, I showed that sEH is a critical mediator in CNV progression through demonstrating the efficacy of AAV8-*Ephx2*-shRNA in suppressing murine L-CNV. The long-term goal that I contributed to through my research is to advance the understanding of pathological choroidal neovascularization in nvAMD and develop a novel therapeutic strategy that can address the unmet shortcomings of existing therapy.

6.2.2 Inhibitory activity of SH-11037 against sEH

SH-11037 is an antiangiogenic homoisoflavonoid that the Corson lab previously discovered and identified sEH as its target in a pulldown assay. A lipidomic study indicated that SH-11037 is able to inhibit sEH dependent hydrolysis of epoxy fatty acids (EpFA) in vivo (Park and Corson 2019). In **Chapter 3**, I addressed the research aim of quantitatively and qualitatively evaluating the inhibitory activity of SH-11037 against sEH, thereby I provided the knowledge regarding potency and selectivity of SH-11037 against sEH and discovered the mode of action of enzyme inhibition as mixed noncompetitive inhibition by SH-11037 for the first time.

In the initial work of **Chapter 3**, I tested the inhibitory activity of SH-11037 on the cellular sEH activity in murine eye tissue lysates of L-CNV mice and the controls in a spectrophotometric assay, where sEH dependent hydrolysis of the substrate trans-stilbene oxide (t-SO) was measured as a change in absorbance at 230 nm. My study provided evidence that sEH activity is significantly enhanced in L-CNV eye lysates. This complemented previous Corson lab findings of sEH overexpression in L-CNV and

reduced ratio of sEH lipid substrate to product (DHA-derived 19,20-EDP: 19,20-DHDP) upon L-CNV induction, indicating increased sEH activity (Sulaiman, Park et al. 2018), therefore supporting that increased expression of sEH under the disease state is associated with increased enzymatic activity. The change in t-SO absorbance was significantly reduced by treatment with SH-11037 or a known sEH inhibitor, compound 7, suggesting inhibitory activities of these compounds on cellular sEH activity (Figure 3.1). This finding provided a rationale to determine quantitative metrics of inhibitory activity of SH-11037 that will provide information about the functional strength of SH-11037 as an sEH inhibitor.

In the following study in **Chapter 3**, I tested the hypothesis that SH-11037 binds to and inhibits epoxide hydrolase activity of a recombinant human enzyme. In this study, I used a fluorogenic substrate, PHOME (3-phenyl-cyano(6-methoxy-2-naphthalenyl)methyl ester-2-oxiraneacetic acid) (Cayman Chemical) in the enzyme activity assay, in which epoxide hydrolysis releases a fluorescent product, 6-methoxy-2-naphthaldehyde. In this assay, I included known sEH inhibitors as positive controls that are structurally distinct from SH-11037, which is a homoisoflavonoid. Trans-4-(4-[3-adamantan-1-yl-ureido]-cyclohexyloxy)-benzoic acid (t-AUCB) is a urea based specific sEH inhibitor while 7-(trifluoromethyl)-N-(4-(trifluoromethyl)phenyl) benzo[d]isoxazol-3-amine (compound 7), is an benzisoxazole sEH inhibitor (Hwang, Tsai et al. 2007, Shen, Ding et al. 2009, Park and Corson 2019). I also included an inactive analog of SH-11037, SH-11098 that previously showed no biological activity in vitro (Basavarajappa, Lee et al. 2015). I found that SH-11037 inhibits sEH activity with an IC_{50} value of 0.15 μ M, whereas other sEH inhibitors, compound 7 and t-AUCB showed greater functional

strengths with IC_{50} values of 9.5 nM (Figure 3.2; Table 3.1). This research output provided quantitative metrics of the relative functional strength of SH-11037 as an sEH inhibitor and presented a new kind of pharmacological compound for the inhibition of sEH. The results of a urea-based sEH inhibitor t-AUCB showing more favorable IC_{50} was coherent with enzymology and high content screening studies done, where substituted ureas including t-AUCB were discovered to be potent, selective, and competitive inhibitors of sEH with nanomolar K_i values based on the catalytic mechanism of sEH (Morisseau, Goodrow et al. 1999). However, for SH-11037, there was no comparative data about the underlying mechanism of action. Without a detailed enzymology study, there was no mechanistic basis to explain IC_{50} disparity of SH-11037 compared to other known sEH inhibitors while it showed favorable biological efficacy.

The half-maximal inhibitory concentration, IC_{50} , is defined as the concentration of inhibitor that confers a 50% decrease in rate under the specific assay conditions (Copeland, Pompliano et al. 2006). The key term in this definition is “specific assay conditions” because IC_{50} depends on enzyme concentration, and for competitive inhibition and mixed inhibition, IC_{50} will vary prominently depending on substrate concentration and its value will always be greater than K_i (Table 6.1) (Cha 1975). This means that the same inhibitor will have different IC_{50} under different assay conditions. In contrast to other specific sEH inhibitors like t-AUCB, high content mechanistic studies of drug-target interaction for SH-11037 were not investigated previously.

Quantitative metrics	Dependence on assay conditions		Example: competitive inhibitor
	[Substrate]	[Enzyme]	
Inhibition constant	No	No	K_i
Half-maximal inhibitory concentration	Yes	Yes	$IC_{50} = K_i (1 + [S]/K_M) + [E]/2$

Table 6.1: The difference between inhibition constant and half-maximal inhibitory concentration. The half-maximal inhibitory concentration, IC_{50} values obtained are highly dependent on assay conditions and the mode of inhibition. The inhibition constant, K_i is an intrinsic measure of potency.

6.2.3 Mechanistic basis of SH-11037 targeting sEH

Lastly, in **Chapter 3**, I reflected on the limitations of traditional quantitative metrics of IC_{50} alone and proposed to characterize the interaction of SH-11037 with its target with regards to modulating the enzymatic activity. Using recombinant human sEH and the fluorescent substrate PHOME, I conducted enzyme kinetics experiments and determined the rate of enzyme reaction with the range of inhibitor concentrations under different substrate concentrations. Based on enzyme kinetics parameters obtained from Michaelis-Menten and double-reciprocal (Lineweaver-Burk) plot, my enzyme kinetics analysis revealed that increasing concentrations of SH-11037 decreased V_{max} and increased K_M , with $K_i = 1.73 \pm 0.45 \mu\text{M}$ (Figure 3.3). This presented a special case of mixed-noncompetitive inhibition, which was confirmed by additional analysis through Dixon plot and secondary plots (Figure 3.5). Mixed-noncompetitive inhibition as shown by the mechanistic scheme in Figure 6.1 is distinct from competitive and uncompetitive inhibition, in which a competitive inhibitor binds to the enzyme and uncompetitive inhibitor binds only to the enzyme-substrate complex (Cha 1975). Mixed-inhibition may result in either an increase in K_M or decrease in K_M . With increasing concentrations of

SH-11037, K_M increased ($K_{Mapp} > K_M$), reiterated in Lineweaver-Burk plot in Figure 6.1B, indicating greater affinity of SH-11037 towards binding to the free enzyme and more closely representing competitive inhibition. To confirm the binding site and mode of action of SH-11037, our collaborator Dr. Meroueh in the Department of Biochemistry and Molecular Biology at Indiana University conducted molecular docking studies and showed that SH-11037 binds in the hydrolase catalytic pocket of sEH in energetically favorable binding modes.

My research findings in **Chapter 3** have relation to the real-world drug discovery and development process. There are six major categories of druggable targets - enzymes, cell surface receptors, nuclear hormone receptors, ion channels, transporters, and DNA (Robertson 2005). Among these, enzymes present unique opportunities that are not available to drug targets of other protein classes. Because of the dynamic nature of enzymes, a single enzyme represents multiple different targets as a result of a compound binding to substrates, intermediates, and products during the catalysis. By gaining knowledge of the chemical mechanism of the enzyme, its transition state can be structurally characterized, the nucleophilic, active site amino acid residues that form covalent adducts with electrophiles can be explored, or the substrate analogue can be synthesized to be developed as an inactivator. Thus, enzymes have such opportunities unlike any other targets because enzyme targeting drugs can be designed and optimized based on the chemical species and interactions that emerge during the catalytic cycle (Holdgate, Meek et al. 2018). For this reason, SH-11037 provides a good example as a mixed inhibitor that can bind to multiple targets in the enzyme's catalytic process. Therefore, the presence of SH-11037 does not completely prevent the substrate from

binding but slows down the rate at which the enzyme converts the substrate to product. Although most enzyme-targeting drugs are active site-binding competitive inhibitors, this does not undervalue the pharmacological potential of SH-11037 over other modes of enzyme inhibitors because there are marketed drugs of noncompetitive inhibitors that provided clinical success like neravirapine (nonnucleoside HIV-1 reverse transcriptase inhibitor) (Robertson 2005). The usefulness of noncompetitive inhibition in disease understanding and therapy is further presented by several examples: noncompetitive inhibition of hepatocellular carcinoma enzymes by disulfiram and inhibition of CYP450 enzymes by benzodiazepines (Heng, Harris et al. 2010, Goto, Kato et al. 2016). These examples also highlight the advantage of polypharmacology that is unique to small molecules.

As will be discussed further in future directions, enzymology is a powerful and established discipline that can provide important scientific insight in understanding drug-target interactions. By combining classical concepts of enzymology with new data analysis methods, my study provided knowledge of relative functional strength, inhibitory potency, and the mode of sEH inhibition by SH-11037 with a distinct pharmacophore.

Overall, my research outputs contributed to advancing the understanding of the drug-target relationship by quantitatively measuring the inhibitory activity of sEH inhibitors, including SH-11037 and defining the molecular mode of action of enzyme inhibition by SH-11037 for the first time. Characterization of half-maximal inhibitory concentration (IC_{50}) and inhibition constant (K_i) contributed to elucidating both the inhibitory activity and potency of SH-11037 against sEH. In addition, through the

inspection of kinetic parameters of sEH inhibition, I revealed SH-11037 as a mixed-noncompetitive inhibitor of sEH with binding affinity towards enzyme and enzyme-substrate complex as summarized in Figure 6.1.

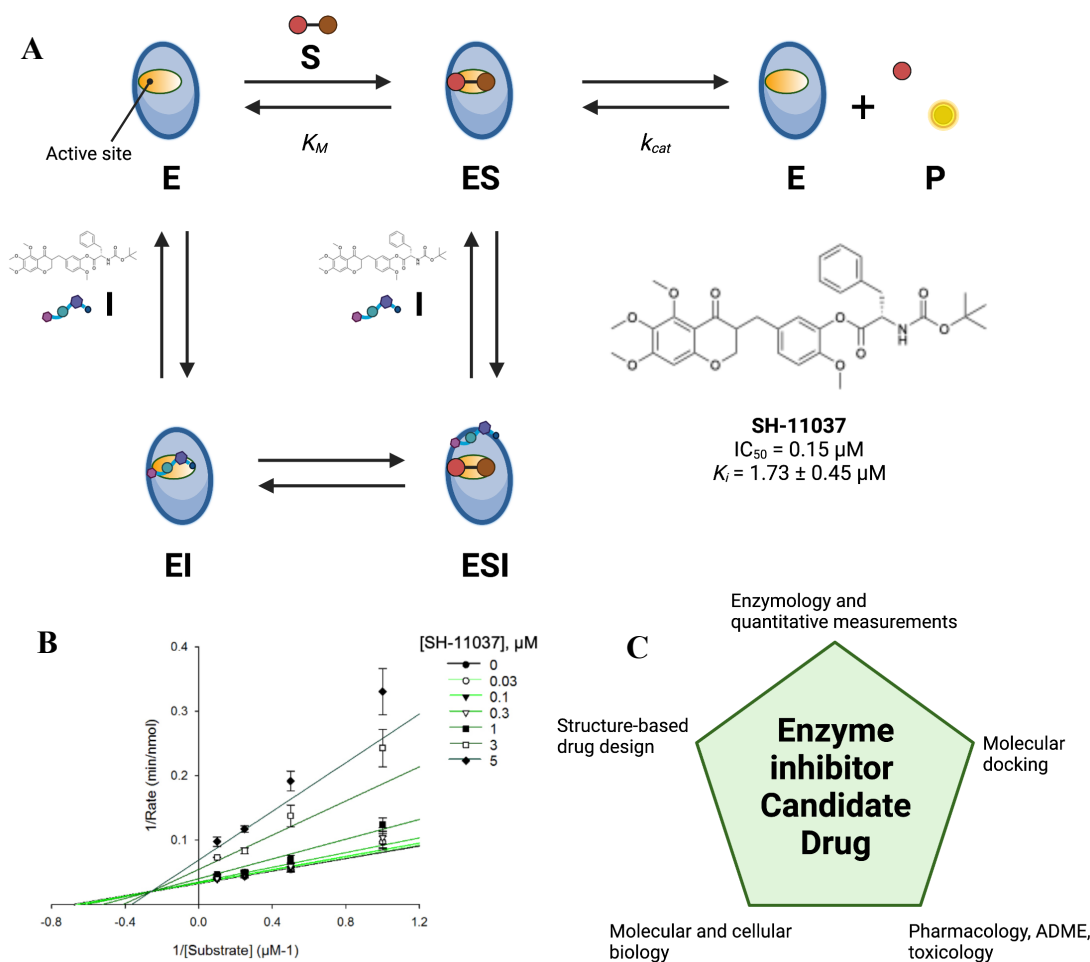


Figure 6.1: Schematic summary of Chapter 3 research discovery of mixed noncompetitive inhibition of sEH enzymatic activity upon binding of sEH with SH-11037. (A) SH-11037 is a mixed inhibitor with characteristics of both competitive and noncompetitive inhibitors, binding to E, enzyme, or ES, enzyme-substrate complex. Inhibitory activity of SH-11037 was determined by $IC_{50} = 0.15 \mu M$ and the potency of SH-11037 as an sEH inhibitor was determined by the inhibitory constant value, $K_i = 1.73 \pm 0.45 \mu M$. The chemical structure of I, inhibitor, SH-11037 is shown. S: substrate; ES: enzyme-substrate complex; EI: enzyme-inhibitor complex; EIS: enzyme-inhibitor-substrate complex; P: product. (B) Lineweaver-Burk plots of SH-11037 inhibition of sEH. (C) Various approaches to enzyme-targeted drug design.

6.2.4 Immunolocalization of sEH in RPE and photoreceptor cells in murine L-CNV and human nvAMD retinas

In the **Chapter 1** introduction, it was described in depth that the retina is a specialized neural tissue with a complex cellular composition where distinct cellular layers of neurons and supporting cells process visual information. The retinal pigment epithelium (RPE) and choroid constitute the support system for photoreceptor cells. The choroid is part of the systemic circulation, and it is composed of choriocapillaries in its innermost layer. The choroid is one of the most vascularized tissues in the body by weight, and it is the major blood supply in the eye because the choroid blood supply serves RPE and photoreceptor cells that have high metabolic demand. In nvAMD, abnormal new blood vessels from the choroid grow into the RPE and neuroretina, underlying visual impairment (Ehrlich, Harris et al. 2008, Bird 2010). Thus, pathological changes in nvAMD preferentially affect photoreceptors, RPE, and the choroid.

Given that retina is involved in cell type specific disorders, it is critical to gain knowledge of the localization of the therapeutic target expression in the eye. In **Chapter 4**, I tested the hypothesis that sEH is overexpressed by the cell types involved in CNV pathology in retina. This was to build on our previous discoveries that sEH is upregulated in tissue homogenates of L-CNV eyes and overexpressed in CNV lesion sites (Sulaiman, Park et al. 2018). My research aim was to conduct in-depth profiling of sEH expression to define cell types that overexpress sEH in human nvAMD eyes and murine L-CNV eyes, thereby addressing the knowledge gap about the cell type specificity and distribution of sEH expression under CNV in nvAMD.

The initial results in **Chapter 4** illustrated immunolocalization of sEH along with other retinal cell markers: RPE (RPE65), cone photoreceptor cells (cone arrestin), rod photoreceptor cells (rhodopsin), Müller glia (vimentin), horizontal cells (calbindin), and retinal ganglion cells (Brn3a) in retina cross sections of control and L-CNV mice. Under the normal condition, sEH at the protein level was expressed at low levels in adult murine retinas. The results in the retinas of mice that had undergone L-CNV were different. In response to laser-induced injury, a substantial level of sEH positive cells were observed in vasculature and the outer layer of the retina. The overexpressed sEH prominently colocalized with rod photoreceptor cells, and partially colocalized with basal and apical surfaces of RPE (Figure 4.1), while coexpression of sEH with other cell markers including vimentin for Müller glial cells was minimal, suggesting acute laser injury to Bruch's membrane, photoreceptors and the RPE induced expression of sEH (Figure 4.2).

To investigate the retinal expression of sEH in diseases state further in **Chapter 4**, I stained human nvAMD retinas with antibodies against sEH and RPE, and lectins with binding affinities towards human rod and cone photoreceptor cells. In murine retinas, sEH expression was not seen in other uninjured retinal cells in the normal control murine retinas. In contrast, sEH was more highly expressed throughout the normal age-matched control human retinas. Interestingly, a higher degree of colocalization of sEH with photoreceptor and RPE cell markers were observed in nvAMD human retinas (Figure 4.3) than in mice. This specific induction of sEH overexpression was detected in outer retina in human nvAMD, in areas that are likely undergoing degenerative changes. In contrast to murine retinas where colocalization of sEH and cone photoreceptor cells was not observed, sEH staining in human nvAMD retinas was substantially associated with

the outer segments of cones (Figure 4.3A). The immunofluorescence results also showed that sEH expression in human nvAMD is highly detected throughout RPE cells, not only limited to apical or basal surface, and colocalized with RPE65 (Figure 4.3B).

Immunolocalization of sEH in retinas of murine L-CNV and human nvAMD eyes addressed gaps in existing knowledge by providing evidence of the spatial expression pattern of sEH in photoreceptor and RPE cells in addition to the vasculature that are involved in the CNV pathology. However, these findings challenged relevant findings in the literature that identified Müller glial cells as a major cell type expressing sEH in developing mouse retinas and oxygen-induced retinopathy (Hu, Popp et al. 2014, Shao, Fu et al. 2014). Accordingly, the cross-interpretation of IHC/IF data among studies that used different antibodies against sEH was difficult, and highlighted potential limitations of the method where the lack of universally accepted standardization of antibody production, and potential variations in target specificity for antibodies can lead to discordant IHC/IF results (Bordeaux, Welsh et al. 2010).

6.2.5 Cellular expression and localization of *Ephx2* mRNA in murine L-CNV and human nvAMD retinas

For the precise discrimination of cellular expression of sEH, validation of IF results was critical. Thus, I sought out the RNAscope in situ hybridization (ISH) method to provide complementary information regarding spatial and precise discrimination of the target expression in retina. RNAscope is an ISH technology with a unique probe strategy that achieves simultaneous amplification of signal even from rare RNA, and suppression of nonspecific background to allow visualization of target RNA within intact cells and preserved tissue morphology (Kiyama and Mao 2020).

The retinal expression patterns of human *EPHX2* mRNA were consistent with prior IF data. The results illustrated broad expression of *EPHX2* mRNA in vasculature and multiple cellular layers, but substantially in photoreceptor cell bodies in the outer nuclear layer and outer segments and in RPE (Figure 4.6A-C). In terms of photoreceptor expression of sEH vs. *EPHX2* mRNA, sEH expression by IF was also substantial in the outer segments of photoreceptor, but *EPHX2* mRNA was more localized to photoreceptor cell bodies in the outer nuclear layer. This indicates a difference in where *EPHX2* mRNA is synthesized/produced and where the protein sEH is localized. The *EPHX2* mRNA expression was markedly increased in nvAMD eyes, throughout the retina but most prominently in the RPE (Figure 4.6C).

The retinal expression patterns of murine *Ephx2* mRNA were interesting. In addition to prominent *Ephx2* mRNA expression in the outer nuclear layer and moderate expression signals in the RPE, there were positive signals in the inner nuclear layer that colocalized with Apolipoprotein E mRNA (*ApoE*) which is synthesized in the retina by Müller glial cells. However, *Ephx2* mRNA in the inner nuclear layer was not upregulated following laser injury whereas *Ephx2* overexpression was prominently observed in photoreceptors and RPE in murine L-CNV (Figure 4.7A-C).

Chapter 4 effectively used RNAscope ISH to detect target mRNAs in formalin fixed paraffin embedded (FFPE) retinal sections prepared from human eyes, and in fixed frozen tissue prepared from murine eyes. Furthermore, through multicolor RNAscope ISH, simultaneous detection of *ApoE* and *Ephx2* mRNA bridged the gap in knowledge between differing IF data on where *Ephx2* mRNA was found in the inner retina, that could not be captured by our previous IF study. Nevertheless, the results

supported that major cell types responsible for the overexpression of sEH under CNV, reside in the photoreceptor and the RPE. Given the differences in structure and gene expression between human and mouse retinas, this research aim highlighted the importance of expression profiling study conducted in both human and mouse retinas.

6.2.6 Differential retinal distribution of sEH across species and disease

models

As described in the introduction, the retina is a host of cell type specific disorders. In nvAMD, the choroidal vasculature, RPE and photoreceptor cells of the outer retina are mostly involved in the pathological process, and in the mouse model of choroidal neovascularization, an injury is targeted towards those relevant cell types (Shah, Soetikno et al. 2015). In contrast, Müller glial cells that have intimate contact with retinal vasculature, play an outsized role upon retina injury that occurs in retinopathy (Coughlin, Feenstra et al. 2017), such as diabetic retinopathy and oxygen-induced retinopathy where cellular expression of sEH was more extensively profiled (Hu, Popp et al. 2014, Shao, Fu et al. 2014). Therefore, differential expression patterns of sEH across studies could be explained by biological differences among disease models and different cell types contributing to the distinct pathology. Indeed, differential target expression in the retina across disease models is ubiquitous. For instance, immunolocalization of phosphorylated mammalian target of rapamycin at S2448 (pmTOR at S2448) was strongly detected in outer and inner nuclear layers, and increased in the RPE, choroid and ganglion cell layers following the laser injury in the mouse L-CNV model (Yang, Madrakhimov et al. 2019).. Meanwhile, hyperglycemia induced pmTOR S2448 expression in streptozotocin (STZ)-

induced mouse model of diabetes murine retinas was immunolocalized to Müller glia in addition to ganglion cells in retinopathy (Madrakhimov, Yang et al. 2021)

My expression profiling study did not refute the previously reported Müller glia production of sEH, but it constructively challenged the existing studies by presenting evidence that showed that photoreceptors and the RPE are the major cell types responsible for the overexpression sEH in CNV. This highlighted a functional role of sEH in AMD pathophysiology (discussed further in **Chapter 6.4**) and provided a novel context to target these cell types in **Chapter 5** study employing a gene therapeutic approach.

6.2.7 Efficient and stable transduction of AAV serotype 8 mediated delivery of shRNA targeting *Ephx2* in photoreceptors and the RPE

Early in-depth target validation is critical in drug development to ensure that engagement of the target has a therapeutic benefit (Hughes, Rees et al. 2011). To test the hypothesis that sEH is required for CNV progression, I employed an adeno-associated virus (AAV) mediated gene therapeutic approach to disrupt target gene expression in the murine L-CNV model. With reference to **Chapter 5** background, AAV is one of the most widely used viral vectors in the eye, as highlighted by the first clinical success with AAV being in treating inherited retinal disease (Bainbridge, Smith et al. 2008, Smalley 2017). The favorable safety profile of AAV, low immunogenicity risk in the eye, and ability to stably transduce retinal cell types presented AAV as an ideal viral vector to deliver shRNA against *Ephx2* (Day, Byrne et al. 2014).

Upon intravitreal injections of two different viral doses of AAV8 vectors encoding U6 promoter-driven *Ephx2* shRNA and CMV promoter-driven mCherry (4.9 x

10^6 GC or 1.9×10^7 GC) or PBS vehicle as a control, I demonstrated in vivo transduction through evaluating mCherry expression. By fluorescence fundus imaging, I detected mCherry expression as early as 2 weeks post intravitreal injection of AAV (Figure 5.1A). Following imaging results showed a maximum level of fluorescence at week 3 and the persistent transduction was observed until week 5 with a higher transduction level achieved at 1.9×10^7 GC without causing substantial morphological changes to retina, which was assessed by OCT imaging (Figure 5.1B). Additionally, confocal microscopy imaging of transverse retinal sections allowed identification of transduction patterns of cell types by AAV8 vector. In AAV8 injected eyes, vector transduction in the outer nuclear layer, inner and outer segments of photoreceptors, and the RPE was evident at 1.9×10^7 GC. However, in the eyes injected with 4.9×10^6 GC of AAV8, only a minimal level of mCherry positive transduced cells were observed in the photoreceptor cells, and RPE transduction was not achieved (Figure 5.1C).

The study results of this initial work of **Chapter 5** aim to emphasize the importance of careful consideration of serotype, viral dose, timeline, and route of delivery when designing experiments using AAV as a viral vector for gene delivery. Different routes of intraocular injections may facilitate gene delivery to certain cell types. Intravitreal injections facilitate bringing AAV in contact with retinal cells in the inner retina, and the subretinal injections facilitate AAV access to the outer retinal cells (Garita-Hernandez, Routet et al. 2020). The mechanism of cell type specific AAV transduction is defined by the interaction between AAV capsid proteins and the cell surface molecules (Schultz and Chamberlain 2008, Haery, Deverman et al. 2019). Different primary and secondary receptors on the cell surface will allow AAV cell

attachment and entry through endocytosis, into the nucleus by different pathways. Thus, AAV transduction efficiency is based on protein composition of the capsid (the AAV serotype) and the cell surface molecules (distinct cell types) (Garita-Hernandez, Routet et al. 2020). The primary cellular receptors for most AAV serotypes, including AAV8, remain unknown, and the binding to the primary receptor alone is not sufficient for AAV cell entry, but interactions with secondary co-receptors on the cell surface are required for AAV vectors to be internalized. For AAV8, laminin receptor (LamR) had been identified as a co-receptor for AAV8 and other serotypes – AAV2, 3, and AAV9 (Akache, Grimm et al. 2006, Srivastava 2016). Studies have utilized retinal organoid and RPE cells derived from human induced pluripotent stem cells to verify retinal and RPE cell expression of LamR (Garita-Hernandez, Routet et al. 2020).

6.2.8 AAV serotype 8 mediated delivery of shRNA targeting *Ephx2* inhibited CNV progression

Following the determination of optimal viral dose and experimental timeline, the study presented in **Chapter 5** evaluated the efficacy of AAV8 expressing shRNA against *Ephx2*, delivered intravitreally in murine L-CNV. Mice received intravitreal injection of 1.9×10^7 GC of AAV8-*Ephx2* shRNA, AAV8-scrambled shRNA control or PBS control on day 0, and L-CNV was induced 7 days post AAV injection, and the CNV lesion progression along with in vivo transduction were kept under observation through weekly retinal imaging. The results demonstrated that 1.9×10^7 GC of AAV8-*Ephx2* shRNA significantly suppressed CNV lesion volume compared to AAV8-scrambled shRNA control or PBS control. The non-invasive retinal imaging showed stable mCherry expression, and immunoblotting analysis demonstrated downregulation of sEH

expression at the protein level in AAV8-*Ephx2* shRNA treated retinas and RPE/choroid tissue lysates. This verified that the suppression of CNV lesion progression concurred with downregulation of sEH expression and provided key evidence that sEH is implicated in a disease state. This provides a rationale for continuing a future study with a hypothesis that photoreceptor or RPE dependent expression of sEH causes choroidal neovascularization by promoting inflammation. If the hypothesis is true, sEH is present in photoreceptor and the RPE during choroidal neovascularization, which my study demonstrated in **Chapter 4**. Continuously, for the hypothesis to be true, choroidal neovascularization will be suppressed in the absence of sEH, which I demonstrated through Chapter 5 study that reduced sEH expression in photoreceptors and the RPE using a viral vector that has tropism towards those cells. Finally, for the causal to be true, a study must additionally demonstrate that sEH activity causes pro-inflammatory molecules to be activated in CNV of that inhibition of sEH and potentiation of EpFAs resolve inflammation. For most of the drug targets in lipid metabolism, such as cyclooxygenase (COX) and lipoxygenase (LOX), the pathway leads to the production of pro-inflammatory prostaglandins and leukotrienes. In contrast, sEH activity in the CYP pathway is involved in the production of anti-inflammatory, pro-resolving EpFAs (Wagner, McReynolds et al. 2017, Kodani and Morisseau 2019). In a conventional pharmacological therapeutic strategy, such as non-steroidal anti-inflammatory drugs (NSAIDs) with COX-inhibitor, the emphasis is on depletion of certain products by targeting the upstream protein, or enzyme. But in the sEH targeting strategy, rather than the production of pro-inflammatory products that are the case for COX or LOX, the therapeutic mechanism lies in the increased level of EpFAs that are anti-inflammatory, as

discussed in detail in **Chapter 1.8 sEH inhibition and EpFAs in Angiogenesis and Inflammation**. Therefore, in a future study, such resolving biological effects of EpFAs and sEH inhibition can be explored in specific cell types such as RPE, to strengthen the causal relationship between sEH and CNV.

Therapeutic efficacy of AAV8-*Ephx2* shRNA not only provided important knowledge in gaining confidence in the druggable target and disease, but also presents an exciting option of a therapeutic strategy in targeting sEH, that would address shortcomings of existing biologics or small molecule compounds that are efficacious but have limitations in absorption, distribution, and elimination. The molecular weight plays a key role in drug absorption and elimination. Small and lipophilic drugs can cross the blood-retinal barrier, but they are cleared in the posterior segment of the eye; therefore it is difficult to sustain a high level of small molecule drugs for the retinal diseases (Varela-Fernández, Díaz-Tomé et al. 2020, Sarkar, Junnuthula et al. 2021). Large molecular weight biologics are often administered via intravitreal injection, which is a highly targeted route of administration, overcoming systemic exposure and obtaining high bioavailability of the drugs in the vitreous chamber (Varela-Fernández, Díaz-Tomé et al. 2020). However, repeated intravitreal injections of anti-VEGFs are still required, contributing to intraocular complications (Cox, Elliott et al. 2021), and present a burden to patients and the healthcare system (Schmidt-Erfurth, Chong et al. 2014). Unlike anti-VEGF biologics that require frequent IVT injections, AAV gene therapy could offer stable delivery of therapeutic target manipulation that will persist (Sarkar, Junnuthula et al. 2021). Indeed, there are numerous completed and ongoing AAV based gene therapy clinical trials for nvAMD, such as a completed phase I clinical trial of intravitreal

injection of an AAV2 vector expressing the VEGF-neutralizing protein sFLT01 from Sanofi ([NCT01024998](#)). In addition to various advantages of AAV, it has shortcomings due to the restricted transgenic capacity, and there is a risk of rapid elimination in certain individuals who have previous exposure to viral vectors (Surace and Auricchio 2008).

6.2.9 AAV8 serotype 8 mediated delivery of shRNA targeting *Ephx2* suppressed expression levels of inflammatory molecules

A growing body of evidence has shown that sEH plays important roles in vascular abnormalities and inflammation (Capozzi, Hammer et al. 2016, Hasegawa, Inafuku et al. 2017, Wagner, McReynolds et al. 2017). Inflammation plays important roles in the pathogenesis of CNV where production of pro-inflammatory mediators induces endothelium activation, increased expression of adhesion molecules by the activated endothelium, migration of macrophages and increased vascular permeability, all together promoting choroidal neovascularization (Campa, Costagliola et al. 2010). Importantly, the current study presented in **Chapter 5** showed that downregulation of sEH expression with AAV8 mediated delivery of *Ephx2* shRNA decreased several major inflammatory molecules involved in CNV pathogenesis. The mRNA expression levels of inflammatory cytokine genes *Il1b*, *Il6*, *Tnfa*, and *Ccl2*, and that of a cell adhesion molecule *Icam1* were significantly reduced by *Ephx2* shRNA in treated retinas compared to scrambled shRNA control. Moreover, mRNA levels of *Il1b*, *Il6*, and *Ccl2* were significantly reduced in treated RPE/choroids compared to the scrambled shRNA control.

IL-1 β belongs to the IL-1 family of cytokines that are implicated in the initiation of acute inflammatory responses (Dinarello 2009). Furthermore, IL-1 β has potent chemotactic and angiogenic properties of IL-1 β in addition to initiating acute

inflammatory responses (Carmi, Voronov et al. 2009), and its implication in nvAMD pathogenesis is well established (Oh, Takagi et al. 1999, Zhao, Bai et al. 2015). In AMD, choroid vasculature and the RPE secrete IL-1 β (Oh, Takagi et al. 1999). IL-1 β was also shown to activate and enhance the production of IL-6 and *Ccl2* (McGeough, Pena et al. 2012) (Natoli, Fernando et al. 2017). Importantly, IL-6 has potent angiogenic properties and is involved in CNV development, along with numerous correlative observations in human nvAMD samples (Gopinathan, Milagre et al. 2015, Knickelbein, Chan et al. 2015, Droho, Cuda et al. 2021). Likewise, TNF- α has been implicated in human nvAMD and murine L-CNV (Wang, Han et al. 2016)(R. Klein et al., 2014). CCL2 is a member of the chemokine family that directs leukocyte migration (Raoul, Auvynet et al. 2010). CCL2 expression is very low in healthy retina and RPE (Chen, Liu et al. 2008), but significantly upregulated with acute inflammation, age, and oxidative stress in the RPE (Higgins, Wang et al. 2003, Nakazawa, Hisatomi et al. 2007). Several studies using CCL2 knockout mice strongly suggest that CCL2 mediated recruitment of monocytes and macrophages to the CNV lesion site contributes to creating a proangiogenic microenvironment (Raoul, Auvynet et al. 2010). Considering the role of CCL2 in leukocyte migration, the inhibitory effect on *Ccl2* expression by AAV8-*Ephx2* shRNA is intriguing and could corroborate other studies that reported sEH inhibition and the omega-3 EpFAs (lipid substrates of sEH) interfered with leukocyte invasion into the CNV lesion (Hasegawa, Inafuku et al. 2017).

The delivery of AAV8-*Ephx2* shRNA also significantly reduced *Vegfc* in the treated retinas. Interestingly, this study result is corroborated by a study which showed inhibition of VEGF-C mRNA expression by the EpFA substrate of sEH, 19,20-EDP

(Zhang, Panigrahy et al. 2013). In **Chapter 1** introduction, VEGF signaling in angiogenesis was discussed in depth (Figure 1.2). Unlike VEGF-A, which plays a dominant role in the regulation of angiogenesis, VEGF-C is primarily involved in lymphangiogenesis through VEGFR-3 signaling. However, it is yet premature to exclude the possibility of blood and lymphatic vessels regulating each other, as angiogenesis and lymphangiogenesis occur simultaneously (Nakao, Hafezi-Moghadam et al. 2012).

Overall, in relation to the current understanding of inflammatory contribution in CNV, the research outcome in **Chapter 5** showing the downregulation of pro-inflammatory molecules with potent angiogenic properties indicate that targeting sEH suppresses the inflammatory pathogenesis of CNV in vivo.

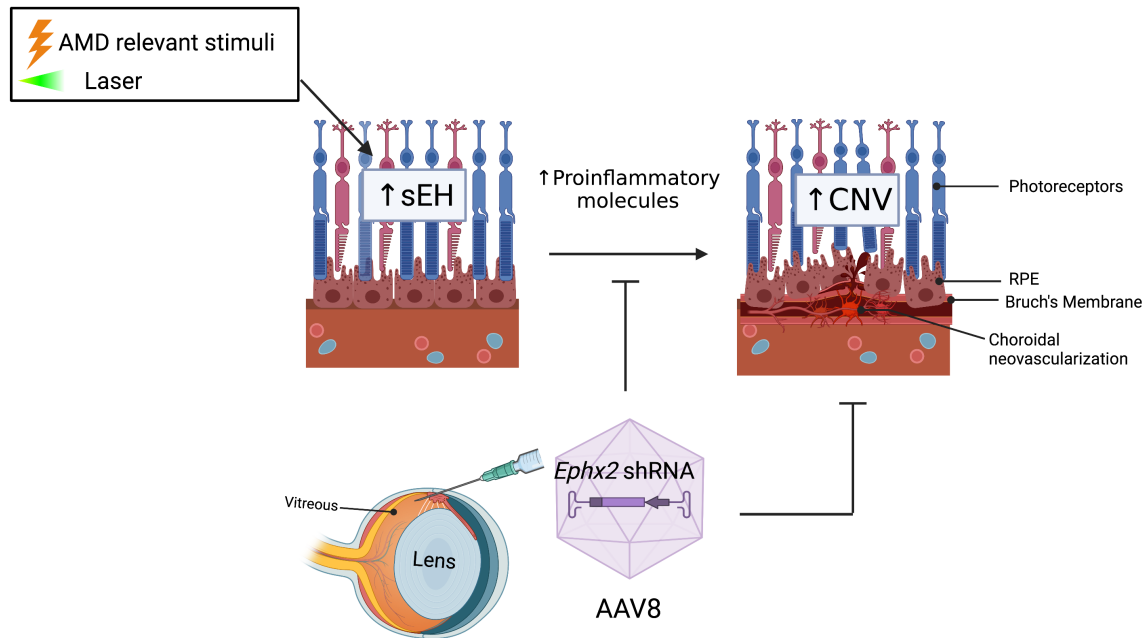


Figure 6.2: Schematic summary of Chapter 4 and 5 studies. Chapter 4 study of retinal spatial expression of sEH at both the protein and mRNA levels through immunohistochemistry and RNAscope concluded that photoreceptors and the RPE are the major cell types that overexpress sEH in the murine L-CNV and human nvAMD retinas. Chapter 5 study demonstrated the efficacy of targeting sEH expression in these cell types, with AAV8-*Ephx2* shRNA, which has tropism against RPE and photoreceptor cells. Intravitreal injection of AAV8-*Ephx2* shRNA significantly reduced CNV and normalized CNV-related inflammatory markers upon sEH knockdown. Thus, the present study revealed sEH overexpression in disease relevant retinal cell types, indicating a functional role of sEH in AMD pathophysiology, and providing a novel therapeutic strategy to target these cell types for developing pharmacotherapies.

6.3 Limitations

6.3.1 Use of synthetic substrate in sEH activity assay

The epoxide hydrolase activity of sEH catalyzes the addition of a water molecule to an epoxide into a corresponding diol (Harris and Hammock 2013). In **Chapter 3**, sEH activity assay was performed with different synthetic substrates, *trans*-stilbene oxide (t-SO) for the epoxide hydrolase activity assessment in the murine tissue lysates, and (3-phenyl-oxiranyl)-acetic acid cyano-(6-methoxynaphthalen-2-yl)-methyl ester (PHOME), for the recombinant human sEH activity assay (Figure 6.3).

Because t-SO is very sensitive to sEH epoxide hydrolase activity, it was useful in measuring sEH activity in the crude tissue lysates. However, t-SO is also a substrate for glutathione-S-transferases (GST) (Gill, Ota et al. 1983). To remove GSH from the tissue lysates, polarity extraction with two solvents would be required – firstly isooctane, a nonpolar solvent separates hydrophobic epoxide substrate from the water phase and retains the diol and glutathione conjugates in the buffer. Secondly, hexanol, a polar solvent extracts the epoxide and diol from the water phase; consequently, only the glutathione conjugates are left in the buffer phase (Morisseau and Hammock 2007). This extent of expertise in analytical chemistry was not established; therefore, the inherent activity of GSH in the tissue lysate could not be excluded.

The fluorogenic substrate PHOME was useful in measuring the inhibitory potency against sEH activity and it is an ideal substrate when working with the purified sEH (Morisseau and Hammock 2007). However, this substrate is structurally distinct from physiological endogenous lipid substrates of sEH (Figure 6.3). Measuring sEH activity using epoxy fatty acids would have provided additional information with more

physiological relevance, but these endogenous lipid substrates and products are neither absorbent, nor fluorogenic. Therefore, the only suitable method of detecting these lipids simultaneously would be to develop High Performance Liquid Chromatography with mass spectrometry HPLC-MS/MS. Besides this, another limitation of PHOME as a substrate is its epoxide being sensitive to extreme pH conditions, which was avoided by stabilizing the pH with reaction buffer in the assay.

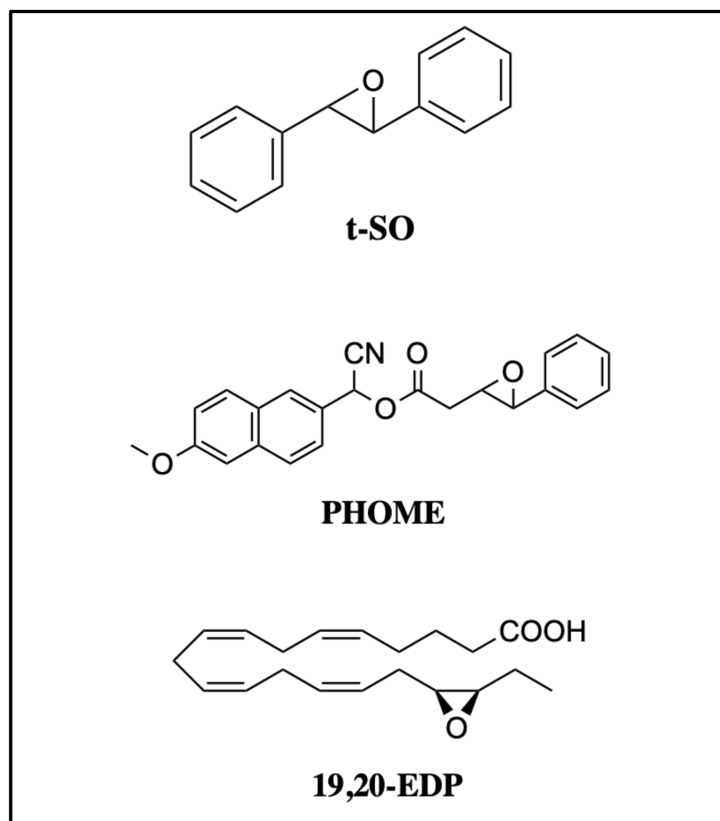


Figure 6.3: Synthetic and endogenous substrates of sEH hydrolase activity. Substrates used in the Chapter 3 study protocols to measure soluble epoxide hydrolase activity: t-SO, trans-stilbene oxide; PHOME, (3-phenyl-oxiranyl)-acetic acid cyano-(6-methoxynaphthalen-2-yl)-methyl ester, and a representative endogenous epoxy fatty acid substrate of sEH: 19,20-EDP, 19,20-epoxydocosapentaenoic acid.

6.3.2 Differences between human nvAMD etiology and murine L-CNV model

The mouse laser-induced choroidal neovascularization (L-CNV) model was used in the present studies. In **Chapter 3**, the epoxide hydrolase activity of sEH in L-CNV tissue lysates was examined. In Chapters 4 and 5, the L-CNV model was used to study the cellular expression of sEH and to determine the efficacy of AAV8-*Ephx2*-shRNA.

The mechanistic basis of L-CNV involves administration of photocoagulation, a targeted laser injury to the RPE and Bruch's membrane, inducing growth and invasion of new choroidal vessels into the subretinal space, thus recapitulating choroidal neovascularization of nvAMD (Gong, Li et al. 2015, Shah, Soetikno et al. 2015).

However, acute laser injury in the L-CNV model is not representative of the human AMD pathology, which is first initiated by multifactorial risk factors, including age-related changes, sustained inflammatory signaling, and oxidative stress (rather than acute inflammation) (Pennington and DeAngelis 2016, Fleckenstein, Keenan et al. 2021).

Another limitation of using the mouse model lies in the species difference between the organization of murine and human retinas. In human AMD pathology, there are certain features of the macula that makes it more susceptible to AMD. One that many researchers have focused on is the high photoreceptor density in the human macula leading to high phagocytic demand for the RPE and the thinness of Bruch's membrane compared to that of the peripheral retina (Chong, Keonin et al. 2005). Because murine retinas do not have a macula, therefore it would be challenging to ask questions using this model of what makes macula in the human retina more susceptible to AMD pathology. However, L-CNV is a powerful model when addressing questions about choroidal

neovascularization, and it is a validated method for testing the efficacy of novel therapy with anti-angiogenic and anti-inflammatory properties given that L-CNV presents angiogenesis under laser-induced inflammatory injury and mimics critical pathological features of nvAMD (Gong, Li et al. 2015).

6.3.3 Lack of longitudinal monitoring of L-CNV

Without longitudinal collection of tissue and analysis, a limitation of the **Chapter 5** study is that the data are only representative of changes in the chorioretinal microenvironment at day 14 post L-CNV. This may not fully capture the effects of *AAV8-Ephx2* shRNA on the molecular mechanisms implicated in temporal progression of CNV. In addition, the present study does not identify changes in sEH-dependent lipid metabolites. However, our previous lipid profiling study has demonstrated that the ratio of 19,20-EDP to 19,20-DHDP was significantly decreased in L-CNV chorioretina, indicative of increased sEH activity, and the pharmacological inhibition of sEH normalized this ratio, providing evidence that sEH inhibition potentiates 19,20-EDP in chorioretina microenvironment (Sulaiman, Park et al. 2018). This finding corroborates the antiangiogenic effects of dietary intake of ω -3 PUFAs and 19,20-EDP in animal models of ocular angiogenesis (Yanai, Mulki et al. 2014, Hasegawa, Inafuku et al. 2017).

6.4 Future Directions

6.4.1 Drug development of sEH inhibitors

In **Chapter 3**, my study excitingly demonstrated SH-11037 as a distinct chemotype of sEH inhibitor. Combined with previous *in vitro* and *in vivo* efficacy studies from the Corson lab, there is a rationale to explore routes of drug delivery other than intravitreal injection because small molecules could provide advantages over biologics as they might be administered through non-invasive routes such as eye drops. Unlike biologics with large molecular weight, small molecules have the advantage of being formulated as eye drops and administered topically, but most of the topically administered drugs are indicated for ocular diseases involving anterior segments (e.g., cornea, iris, or the conjunctiva). Historically, topical administration for treating posterior retinal diseases has been a challenging pharmacological strategy because sustaining therapeutic drug concentrations in the back of the eye is difficult due to weak drug penetration and rapid clearance (Varela-Fernández, Díaz-Tomé et al. 2020, Sarkar, Junnuthula et al. 2021). However, these challenges can be overcome if future research can combine small molecules with an innovative delivery technology.

Based on the mixed inhibition mode by SH-11037 in which SH-11037 had binding affinity towards entities other than the active site of the enzyme, target specificity of SH-11037 could be explored further to identify potential binding to other pharmacologically important proteins. The tendency of drugs to interact with multiple targets, known as polypharmacology, remains a major challenge because the off-target effects may cause unintended side effects. Polypharmacology, on the other hand, can also open new avenues to drug development and design (Reddy and Zhang 2013). It remains

unknown if SH-11037 has protein targets other than sEH. No other binding proteins were identified in our previous pulldown study using SH-11037 based affinity reagents,(Sulaiman, Park et al. 2018). To determine whether the nonspecific interaction could render beneficial therapeutic effects or have potential for unwanted adverse effects, it will be important to assess the overall risk and benefit ratio of SH-11037 in the eye related to its target specificity. However, no specificity induced adverse effects are likely with the intravitreal delivery of SH-11037, given the comprehensive safety profile and lack of intraocular toxicity that were previously demonstrated (Sulaiman, Merrigan et al. 2016).

As a means of target validation, nonspecificity of small molecule compound may present a disadvantage, but it is important to note that the ability of small molecule drugs to bind and interact with a wide range of therapeutic targets could be an advantage compared to biologics that only address extracellular targets. There are many examples of clinical success with polypharmacology of small molecules offering therapeutic benefits. For instance, it is the idea of polypharmacology that allows repurposing of drugs (Chopra and Samudrala 2016). Importantly, a COX-2/sEH dual inhibitor has been characterized as a potent agent against tumor angiogenesis and tumor growth (Wang, Zhang et al. 2018). Utilization of such dual inhibitors or combined treatment of sEH inhibitors with other anti-inflammatory agents could also provide therapeutic potential against neovascular and inflammatory eye diseases.

6.4.2 Functions of sEH in the RPE

Intriguing findings from **Chapters 4 and 5** studies include sEH overexpression in photoreceptors and the RPE of the murine CNV and human nvAMD retinas, and that intraocular knockdown of sEH suppressed inflammatory signaling molecules. Future research could pose a research question regarding the functional role of sEH in the RPE cells. It is important to note that the RPE cells and choroidal endothelial cells form the outer blood-retina barrier and regulate cellular migration and transport of molecules from the choroid (Campbell and Humphries 2012). Disruption of this barrier structure and function are major initiating factors in AMD pathogenesis and the transition from dry to nvAMD, as the RPE cells that make up the outer blood retina barrier get damaged, numerous growth factors and chemoattractants reach the choroid and activate choroidal endothelial cell transmigration into the sub-RPE space (Ambati, Atkinson et al. 2013). Therefore, dysregulation in either the RPE or choroid could result in stimulation of pathological CNV (McLeod, Grebe et al. 2009).

The future study may hypothesize that sEH inhibition and the resulting potentiation of pro-resolving EpFAs will restore RPE dysfunction that is caused by AMD-relevant inflammatory and oxidative stressors. For this, it would be critical to identify key sEH-dependent EpFAs in the RPE through lipidomic analysis. For instance, single cell lipidomic and comparative lipidomic analysis of the lipid profiles in the retinal sections are presented as promising methods of gaining knowledge of lipid composition of the retina (Voigt, Mulfaul et al. 2019, Pereiro, Fernández et al. 2020). Upon identifying specific sEH dependent EpFAs found in the RPE, photoreceptors and choroid,

further studies into these specific EpFAs and their protective roles against pathological changes may be explored.

Previously, I highlighted differences between human nvAMD etiology and the mouse model. Additionally, it is unknown whether the lipid changes seen in nvAMD are phenocopied in the retinas of mouse models. The plasma lipidomics of human and mouse showed similar lipid phenotypes, providing an overview of similarities in more than 100 lipid species (Kaabia, Poirier et al. 2018). To my knowledge, there is no published report of retina or ocular tissue specific comparative lipidomics between human and mouse. Therefore, translating lipidomics data from the mouse model in future should take potential differences into consideration, and utilize isolated cell culture system to dissect specific signaling roles of lipid species.

6.4.3 Sex differential mechanisms of sEH regulation

There is a growing awareness that sex is an important biological variable that needs to be more widely integrated into biomedical research. As discussed in **Chapter 1**, sex differences in the prevalence of AMD are apparent, where there is a greater number of female AMD patients, though the exact mechanistic basis remains to be elucidated. Regarding current anti-VEGF treatments for AMD, sex differential responses have been reported but results are conflicting. One study found that male sex reduced the therapeutic effect of anti-VEGF treatment on stabilizing the central retinal thickness in nvAMD patients (Bek and Klug 2018). This finding is supported by another study that identified male sex, in addition to age, as a factor that contributed to requiring re-treatment for recurrence during the first 12 months. In contrast, another study that evaluated the effects of cardiovascular risk factors (Kuroda, Yamashiro et al. 2015),

concluded that sex does not have a strong effects on therapeutic efficacy of anti-VEGF treatment for nvAMD (Ładkowska, Gawęcki et al. 2021). In retina, one study reported that estrogen replacement treatment in rats increased VEGF levels (Dundar, Ozcura et al. 2010) which may explain sex differential response to AMD treatment targeting VEGF. To complicate these findings even further, both female and male hormones regulate VEGF expression, however the results are conflicting depending on experimental conditions and tissues (Zhang, Wang et al. 2016, Xia, Xiao et al. 2021).

Overall, as we pursue sEH as a therapeutic target for AMD and move forward with sEH targeting drug development, potential sex differential regulation of sEH is to be elucidated. Interestingly, I discovered sex differences in ocular sEH expression for the first time, in which male mice exhibited greater sEH expression compared to female mice in a pilot study (Figure 6.4).

Interestingly, female specific downregulation of sEH expression was found in brain tissue (Zhang, Iliff et al. 2009). A recent publication revealed estrogen-dependent epigenetic regulation of sEH through the methylation of the *Ephx2* gene promoter, resulting in reduction of sEH expression (Yang, Sun et al. 2018). Together with my preliminary data that showed decreased sEH expression in female mice retinas, there is a strong rationale to dissect estrogen-dependent regulation of retinal sEH expression, and to explore whether males and females differ not only in their sEH expression, but also in their response to pharmacological intervention against sEH. Due to this observation of female specific downregulation of sEH, sex was identified as a confounding variable that had to be controlled, thus the **Chapter 5** study has a limitation for not having the comparison study results between male and female. Nevertheless, a future study

exploring this area would highlight the importance of sex and age (as estrogen level decreases with age (Horstman, Dillon et al. 2012)) in dosage optimization for sEH inhibition between male and females. As we pursue sEH as a therapeutic target for AMD and move forward with sEH targeting drug development, the female specific downregulation of sEH in the eye can provide insight into any potential role of estrogen in sEH-mediated ocular diseases and highlight the interesting future avenues for studying sex-differential responses to sEH inhibitors.

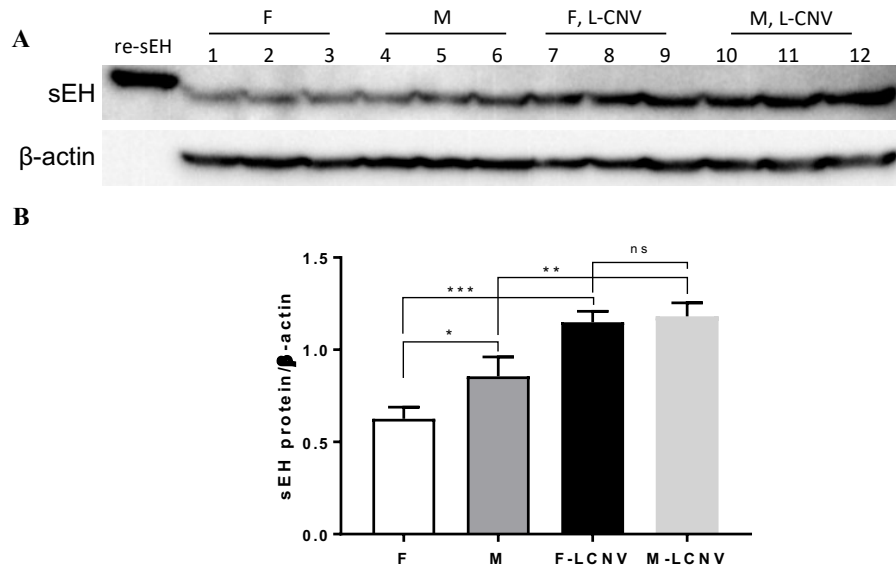


Figure 6.4: Sex differences in sEH protein expression in retina. A) Immunoblot of protein extract from retina of untouched/baseline (lanes 1-6) and L-CNV eyes (lanes 7-9) of female (F) or male (M) mice. Purified human recombinant sEH was used as a positive control for immunoblotting (re-sEH). Each lane is a single retina from an individual mouse. B) Immunoblot quantification showing lower sEH expression in female compared with male, higher sEH with L-CNV in both female and male, and no significant difference (ns) in female and male with L-CNV. Mean \pm SD, n = 3 biological replicates; *p<0.05, **p<0.01, ***p<0.001, ANOVA with Tukey's post hoc test.

6.5 Closing remarks

Ocular diseases cause visual impairment and blindness, imposing a devastating impact on quality of life and a substantial societal economic burden. Many such diseases, including neovascular AMD have unmet needs in pharmacotherapies. Therefore, understanding the mediators involved in their pathophysiology is necessary for the development of therapeutic strategies. To this end, the hydrolase activity of soluble epoxide hydrolase (sEH) has been explored in the context of several eye diseases, due to its implications in vascular diseases through metabolism of bioactive epoxy fatty acids. In the present thesis research, I discovered that SH-11037 is a mixed inhibitor of sEH through comprehensive mechanistic enzymology. I also identified photoreceptors and the RPE as major cell types that express sEH in murine and human retinas undergoing choroidal neovascularization and demonstrated the efficacy and molecular basis of AAV8-*Ephx2* shRNA targeting in the murine L-CNV model. Taken together, this work comprises important progress in our understanding of CNV pathogenesis and the potential development of novel therapeutic strategies targeting soluble epoxide hydrolase by various methods.

REFERENCES

- (2010). "Retina international disease database: retinal and macular dystrophies." from <http://www.retina-international.org/files/sci-news/remacdy.htm>
<http://www.retina-international.org/sci-news/databases/mutation-database>.
- Abramov, Y., S. Borik, C. Yahalom, M. Fatum, G. Avgil, A. Brzezinski and E. Banin (2004). "The effect of hormone therapy on the risk for age-related maculopathy in postmenopausal women." *Menopause* **11**(1): 62-68.
- Acland, G. M., G. D. Aguirre, J. Ray, Q. Zhang, T. S. Aleman, A. V. Cideciyan, S. E. Pearce-Kelling, V. Anand, Y. Zeng, A. M. Maguire, S. G. Jacobson, W. W. Hauswirth and J. Bennett (2001). "Gene therapy restores vision in a canine model of childhood blindness." *Nature Genetics* **28**(1): 92-95.
- Adams, R. H. and K. Alitalo (2007). "Molecular regulation of angiogenesis and lymphangiogenesis." *Nature Reviews Molecular Cell Biology* **8**(6): 464-478.
- Akache, B., D. Grimm, K. Pandey, S. R. Yant, H. Xu and M. A. Kay (2006). "The 37/67-kilodalton laminin receptor is a receptor for adeno-associated virus serotypes 8, 2, 3, and 9." *Journal of Virology* **80**(19): 9831-9836.
- Amaratunga, A., C. R. Abraham, R. B. Edwards, J. H. Sandell, B. M. Schreiber and R. E. Fine (1996). "Apolipoprotein E Is synthesized in the retina by muller glial cells, secreted into the vitreous, and rapidly transported into the optic nerve by retinal ganglion cells " *Journal of Biological Chemistry* **271**(10): 5628-5632.
- Ambati, J., J. P. Atkinson and B. D. Gelfand (2013). "Immunology of age-related macular degeneration." *Nature Review Immunology* **13**(6): 438-451.
- Ambati, J. and B. J. Fowler (2012). "Mechanisms of age-related macular degeneration." *Neuron* **75**(1): 26-39.
- Aninye, I. O., K. Digre, M. E. Hartnett, K. Baldonado, E. M. Shriver, L. M. Periman, J. Grutzmacher, J. A. Clayton and G. Society for Women's Health Research Women's Eye Health Working (2021). "The roles of sex and gender in women's eye health disparities in the United States." *Biology of Sex Differences* **12**(1): 57.
- Appaiahgari, M. B. and S. Vрати (2015). "Adenoviruses as gene/vaccine delivery vectors: promises and pitfalls." *Expert Opinion on Biological Therapy* **15**(3): 337-351.
- Apte, R. S., D. S. Chen and N. Ferrara (2019). "VEGF in signaling and disease: beyond discovery and development." *Cell* **176**(6): 1248-1264.
- Archelas, A., W. Zhao, B. Faure, G. Iacazio and M. Kotik (2016). "Epoxide hydrolase-catalyzed enantioselective conversion of trans-stilbene oxide: Insights into the reaction mechanism from steady-state and pre-steady-state enzyme kinetics." *Archives of Biochemistry and Biophysics* **591**: 66-75.
- Askari, A. A., S. Thomson, M. L. Edin, F. B. Lih, D. C. Zeldin and D. Bishop-Bailey (2014). "Basal and inducible anti-inflammatory epoxygenase activity in endothelial cells." *Biochemical and Biophysical Research Communications* **446**(2): 633-637.
- Bainbridge, J. W. B., A. J. Smith, S. S. Barker, S. Robbie, R. Henderson, K. Balaggan, A. Viswanathan, G. E. Holder, A. Stockman, N. Tyler, S. Petersen-Jones, S. S. Bhattacharya, A. J. Thrasher, F. W. Fitzke, B. J. Carter, G. S. Rubin, A. T. Moore and R. R. Ali (2008). "Effect of Gene Therapy on Visual Function in Leber's Congenital Amaurosis." *New England Journal of Medicine* **358**(21): 2231-2239.

- Barak, Y., W. J. Heroman and T. H. Tezel (2012). "The past, present, and future of exudative age-related macular degeneration treatment." Middle East African Journal of Ophthalmology **19**(1): 43-51.
- Basavarajappa, H. D., B. Lee, H. Lee, R. S. Sulaiman, H. An, C. Magana, M. Shadmand, A. Vayl, G. Rajashekhar, E. Y. Kim, Y. G. Suh, K. Lee, S. Y. Seo and T. W. Corson (2015). "Synthesis and biological evaluation of novel homoisoflavonoids for retinal neovascularization." Journal of Medicinal Chemistry **58**(12): 5015-5027.
- Bek, T. and S. E. Klug (2018). "Age, sex, and type of medication predict the effect of anti-VEGF treatment on central retinal thickness in wet age-related macular degeneration." Clinical ophthalmology (Auckland, N.Z.) **12**: 473-479.
- Bird, A. C. (2010). "Therapeutic targets in age-related macular disease." Journal of Clinical Investigation **120**(9): 3033-3041.
- Blaauwgeers, H. G., G. M. Holtkamp, H. Rutten, A. N. Witmer, P. Koolwijk, T. A. Partanen, K. Alitalo, M. E. Kroon, A. Kijlstra and V. W. van Hinsbergh (1999). "Polarized vascular endothelial growth factor secretion by human retinal pigment epithelium and localization of vascular endothelial growth factor receptors on the inner choriocapillaris: evidence for a trophic paracrine relation." The American journal of pathology **155**(2): 421-428.
- Bordeaux, J., A. Welsh, S. Agarwal, E. Killiam, M. Baquero, J. Hanna, V. Anagnostou and D. Rimm (2010). "Antibody validation." BioTechniques **48**(3): 197-209.
- Borhan, B., A. D. Jones, F. Pinot, D. F. Grant, M. J. Kurth and B. D. Hammock (1995). "Mechanism of soluble epoxide hydrolase. Formation of an alpha-hydroxy ester-enzyme intermediate through Asp-333." Journal of Biological Chemistry **270**(45): 26923-26930.
- Bourne, R., J. D. Steinmetz, S. Flaxman, P. S. Briant, H. R. Taylor, S. Resnikoff, R. J. Casson, A. Abdoli, E. Abu-Gharbieh, A. Afshin, H. Ahmadi, Y. Akalu, A. A. Alamneh, W. Alemayehu, A. S. Alfaar, V. Alipour, E. W. Anbesu, S. Androudi, J. Arabloo, A. Arditi, M. Asaad, E. Bagli, A. A. Baig, T. W. Bärnighausen, M. Battaglia Parodi, A. S. Bhagavathula, N. Bhardwaj, P. Bhardwaj, K. Bhattacharyya, A. Bijani, M. Bikbov, M. Bottone, T. Braithwaite, A. M. Bron, Z. A. Butt, C.-Y. Cheng, D.-T. Chu, M. V. Cicinelli, J. M. Coelho, B. Dagnew, X. Dai, R. Dana, L. Dandona, R. Dandona, M. A. Del Monte, J. P. Deva, D. Diaz, S. Djalalinia, L. E. Dreer, J. R. Ehrlich, L. B. Ellwein, M. H. Emamian, A. G. Fernandes, F. Fischer, D. S. Friedman, J. M. Furtado, A. M. Gaidhane, S. Gaidhane, G. Gazzard, B. Gebremichael, R. George, A. Ghashghaee, M. Golechha, S. Hamidi, B. R. Hammond, M. E. R. Hartnett, R. K. Hartono, S. I. Hay, G. Heidari, H. C. Ho, C. L. Hoang, M. Househ, S. E. Ibitoye, I. M. Ilic, M. D. Ilic, A. D. Ingram, S. S. N. Irvani, R. P. Jha, R. Kahloun, H. Kandel, A. S. Kasa, J. H. Kempen, M. Keramati, M. Khairallah, E. A. Khan, R. C. Khanna, M. N. Khatib, J. E. Kim, Y. J. Kim, S. Kisa, A. Kisa, A. Koyanagi, O. P. Kurmi, V. C. Lansingh, J. L. Leasher, N. Leveziel, H. Limburg, M. Majdan, N. Manafi, K. Mansouri, C. McAlinden, S. F. Mohammadi, A. Mohammadian-Hafshejani, R. Mohammadpourhodki, A. H. Mokdad, D. Moosavi, A. R. Morse, M. Naderi, K. S. Naidoo, V. Nangia, C. T. Nguyen, H. L. T. Nguyen, K. Ogundimu, A. T. Olagunju, S. M. Ostroff, S. Panda-Jonas, K. Pesudovs, T. Peto, Z. Quazi Syed, M.

- H. U. Rahman, P. Y. Ramulu, S. Rawaf, D. L. Rawaf, N. Reinig, A. L. Robin, L. Rossetti, S. Safi, A. Sahebkar, A. M. Samy, D. Saxena, J. B. Serle, M. A. Shaikh, T. T. Shen, K. Shibuya, J. I. Shin, J. C. Silva, A. Silvester, J. A. Singh, D. Singhal, R. S. Sitorus, E. Skiadaresi, V. Skirbekk, A. Soheili, R. A. R. C. Sousa, E. E. Spurlock, D. Stambolian, B. W. Taddele, E. G. Tadesse, N. Tahhan, M. I. Tareque, F. Topouzis, B. X. Tran, R. S. Travillian, M. K. Tsilimbaris, R. Varma, G. Virgili, Y. X. Wang, N. Wang, S. K. West, T. Y. Wong, Z. Zaidi, K. A. Zewdie, J. B. Jonas and T. Vos (2021). "Trends in prevalence of blindness and distance and near vision impairment over 30 years: an analysis for the Global Burden of Disease Study." The Lancet Global Health **9**(2): e130-e143.
- Bressler, S. B. (2009). "Introduction: Understanding the role of angiogenesis and antiangiogenic agents in age-related macular degeneration." Ophthalmology **116**(10, Supplement): S1-S7.
- Brown, G. C., M. M. Brown, S. Sharma, J. D. Stein, Z. Roth, J. Campanella and G. R. Beauchamp (2005). "The burden of age-related macular degeneration: a value-based medicine analysis." Transactions of the American Ophthalmological Society **103**: 173-184; discussion 184-176.
- Buck, T. M. and J. Wijnholds (2020). "Recombinant adeno-associated viral vectors (rAAV)-vector elements in ocular gene therapy clinical trials and transgene expression and bioactivity assays." International Journal of Molecular Sciences **21**(12).
- Bush, R. A., A. Malnoe, C. E. Reme and T. P. Williams (1994). "Dietary deficiency of N-3 fatty acids alters rhodopsin content and function in the rat retina." Investigative Ophthalmology & Visual Science **35**(1): 91-100.
- Cabral, T., L. G. M. Mello, L. H. Lima, J. Polido, C. V. Regatieri, R. Belfort and V. B. Mahajan (2017). "Retinal and choroidal angiogenesis: a review of new targets." International Journal of Retina and Vitreous **3**(1): 31.
- Campa, C., C. Costagliola, C. Incorvaia, C. Sheridan, F. Semeraro, K. De Nadai, A. Sebastiani and F. Parmeggiani (2010). "Inflammatory mediators and angiogenic factors in choroidal neovascularization: pathogenetic interactions and therapeutic implications." Mediators of inflammation **2010**: 546826.
- Campbell, J. P., M. Zhang, T. S. Hwang, S. T. Bailey, D. J. Wilson, Y. Jia and D. Huang (2017). "Detailed vascular anatomy of the human retina by projection-resolved optical coherence tomography angiography." Scientific Reports **7**: 42201-42201.
- Campbell, M. and P. Humphries (2012). "The blood-retina barrier: tight junctions and barrier modulation." Adv Exp Med Biol **763**: 70-84.
- Campochiaro, P. A., P. Soloway, S. J. Ryan and J. W. Miller (1999). "The pathogenesis of choroidal neovascularization in patients with age-related macular degeneration." Molecular Vision **5**: 34.
- Capozzi, M. E., S. S. Hammer, G. W. McCollum and J. S. Penn (2016). "Epoxygenated fatty acids inhibit retinal vascular inflammation." Scientific Reports **6**: 39211.
- Capozzi, M. E., G. W. McCollum and J. S. Penn (2014). "The role of cytochrome P450 epoxygenases in retinal angiogenesis." Investigative Ophthalmology & Visual Science **55**(7): 4253-4260.
- Carmi, Y., E. Voronov, S. Dotan, N. Lahat, M. A. Rahat, M. Fogel, M. Huszar, M. R. White, C. A. Dinarello and R. N. Apte (2009). "The role of macrophage-derived

- IL-1 in induction and maintenance of angiogenesis." Journal of Immunology **183**(7): 4705-4714.
- Cha, S. (1975). "Tight-binding inhibitors-I. Kinetic behavior." Biochemical Pharmacology **24**(23): 2177-2185.
- Chacos, N., J. Capdevila, J. R. Falck, S. Manna, C. Martin-Wixtrom, S. S. Gill, B. D. Hammock and R. W. Estabrook (1983). "The reaction of arachidonic acid epoxides (epoxyeicosatrienoic acids) with a cytosolic epoxide hydrolase." Archives of Biochemistry and Biophysics **223**(2): 639-648.
- Charles, R. L., J. R. Burgoyne, M. Mayr, S. M. Weldon, N. Hubner, H. Dong, C. Morisseau, B. D. Hammock, A. Landar and P. Eaton (2011). "Redox regulation of soluble epoxide hydrolase by 15-deoxy-delta-prostaglandin J2 controls coronary hypoxic vasodilation." Circulation Research **108**(3): 324-334.
- Chen, H., B. Liu, T. J. Lukas and A. H. Neufeld (2008). "The aged retinal pigment epithelium/choroid: a potential substratum for the pathogenesis of age-related macular degeneration." PloS one **3**(6): e2339-e2339.
- Chen, L., N. Miyamura, Y. Ninomiya and J. T. Handa (2003). "Distribution of the collagen IV isoforms in human Bruch's membrane." The British Journal of Ophthalmology **87**(2): 212-215.
- Chen, M., C. Luo, J. Zhao, G. Devarajan and H. Xu (2019). "Immune regulation in the aging retina." Progress in Retinal and Eye Research **69**: 159-172.
- Chiu, K., R. C.-C. Chang and K.-F. So (2007). "Intravitreal injection for establishing ocular diseases model." Journal of Visualized Experiments(8): 313-313.
- Chong, N. H., J. Keonin, P. J. Luthert, C. I. Frennesson, D. M. Weingeist, R. L. Wolf, R. F. Mullins and G. S. Hageman (2005). "Decreased thickness and integrity of the macular elastic layer of Bruch's membrane correspond to the distribution of lesions associated with age-related macular degeneration." The American Journal of Pathology **166**(1): 241-251.
- Chopra, G. and R. Samudrala (2016). "Exploring polypharmacology in drug discovery and repurposing using the CANDO Platform." Current pharmaceutical design **22**(21): 3109-3123.
- Choudhary, M. and G. Malek (2019). "A review of pathogenic drivers of age-related macular degeneration, beyond complement, with a focus on potential endpoints for testing therapeutic interventions in preclinical studies." Advances in Experimental Medicine and Biology **1185**: 9-13.
- Cong, F., A. K. Cheung and S.-M. A. Huang (2012). "Chemical genetics-based target identification in drug discovery." Annual Review of Pharmacology and Toxicology **52**(1): 57-78.
- Copeland, R. A., D. L. Pompliano and T. D. Meek (2006). "Drug-target residence time and its implications for lead optimization." Nature Reviews Drug Discovery **5**(9): 730-739.
- Coughlin, B. A., D. J. Feenstra and S. Mohr (2017). "Müller cells and diabetic retinopathy." Vision research **139**: 93-100.
- Cox, J. T., D. Elliott and L. Sobrin (2021). "Inflammatory Complications of Intravitreal Anti-VEGF Injections." Journal of Clinical Medicine **10**(5): 981.
- Darwesh, A. M., H. Keshavarz-Bahaghighat, K. L. Jamieson and J. M. Seubert (2019). "Genetic deletion or pharmacological inhibition of soluble epoxide hydrolase

- ameliorates cardiac ischemia/reperfusion injury by attenuating NLRP3 inflammasome activation." International Journal of Molecular Sciences **20**(14).
- Das, A. and P. G. McGuire (2003). "Retinal and choroidal angiogenesis: pathophysiology and strategies for inhibition." Progress in Retinal and Eye Research **22**(6): 721-748.
- Day, T. P., L. C. Byrne, D. V. Schaffer and J. G. Flannery (2014). "Advances in AAV vector development for gene therapy in the retina." Advances in Experimental Medicine and Biology **801**: 687-693.
- Defay, R., S. Pinchinat, S. Lumbroso, C. Sutan and C. Delcourt (2004). "Sex steroids and age-related macular degeneration in older French women: the POLA study." Annals of Epidemiology **14**(3): 202-208.
- del Amo, E. M., A.-K. Rimpelä, E. Heikkinen, O. K. Kari, E. Ramsay, T. Lajunen, M. Schmitt, L. Pelkonen, M. Bhattacharya, D. Richardson, A. Subrizi, T. Turunen, M. Reinisalo, J. Itkonen, E. Toropainen, M. Casteleijn, H. Kidron, M. Antopolsky, K.-S. Vellonen, M. Ruponen and A. Urtti (2017). "Pharmacokinetic aspects of retinal drug delivery." Progress in Retinal and Eye Research **57**: 134-185.
- Dhurandhar, D., N. K. Sahoo, I. Mariappan and R. Narayanan (2021). "Gene therapy in retinal diseases: A review." Indian Journal of Ophthalmology **69**(9).
- Dinarello, C. A. (2009). "Immunological and inflammatory functions of the interleukin-1 family." Annual Review of Immunology **27**: 519-550.
- Ding, Y. and V. C. Alfonso (2016). Chapter 1 - Overview of the Woodcock-Johnson IV: organization, content, and psychometric properties. WJ IV Clinical Use and Interpretation. D. P. Flanagan and V. C. Alfonso. San Diego, Academic Press: 1-30.
- Droho, S., C. M. Cuda, H. Perlman and J. A. Lavine (2021). "Macrophage-derived interleukin-6 is necessary and sufficient for choroidal angiogenesis." Scientific Reports **11**(1): 18084.
- Dundar, S. O., F. Ozcura, E. D. Cetin, N. Beder and M. Dundar (2010). "Effects of estrogen replacement therapy on vascular endothelial growth factor expression in choroidal and retinal vasculature." Bratislava Medical Journal **111**(9): 473-476.
- Edwards, M. and G. A. Luty (2021). "Bruch's membrane and the choroid in age-related macular degeneration." Advances in Experimental Medicine and Biology **1256**: 89-119.
- Ehrlich, R., A. Harris, N. S. Kheradiya, D. M. Winston, T. A. Ciulla and B. Wirostko (2008). "Age-related macular degeneration and the aging eye." Clinical Interventions in Aging **3**(3): 473-482.
- Eong, K.-G. A., S. Sanjay and S.-C. Lim (2006). "Treatment of age-related macular degeneration." The Lancet **368**(9543): 1235.
- Erke, M. G., G. Bertelsen, T. Peto, A. K. Sjølie, H. Lindekleiv and I. Njølstad (2014). "Cardiovascular risk factors associated with age-related macular degeneration: the Tromsø Study." Acta Ophthalmologica **92**(7): 662-669.
- Fine, S. L., J. W. Berger, M. G. Maguire and A. C. Ho (2000). "Age-related macular degeneration." The New England Journal of Medicine **342**(7): 483-492.

- Fleckenstein, M., T. D. L. Keenan, R. H. Guymer, U. Chakravarthy, S. Schmitz-Valckenberg, C. C. Klaver, W. T. Wong and E. Y. Chew (2021). "Age-related macular degeneration." Nature Reviews Disease Primers **7**(1): 31.
- Garita-Hernandez, M., F. Routet, L. Guibbal, H. Khabou, L. Toualbi, L. Riancho, S. Reichman, J. Duebel, J. A. Sahel, O. Goureau and D. Dalkara (2020). "AAV-Mediated Gene Delivery to 3D Retinal Organoids Derived from Human Induced Pluripotent Stem Cells." International Journal of Molecular Sciences **21**(3).
- Gill, S. S. and B. D. Hammock (1979). "Hydration of cis- and trans-epoxymethyl stearates by the cytosolic epoxide hydrase of mouse liver." Biochemical and Biophysical Research Communications **89**(3): 965-971.
- Gill, S. S., K. Ota and B. D. Hammock (1983). "Radiometric assays for mammalian epoxide hydrolases and glutathione S-transferase." Analytical Biochemistry **131**(1): 273-282.
- Ginn, S. L., A. K. Amaya, I. E. Alexander, M. Edelstein and M. R. Abedi (2018). "Gene therapy clinical trials worldwide to 2017: An update." Journal of Gene Medicine **20**(5): e3015.
- Gong, Y., Z. Fu, M. L. Edin, C.-H. Liu, Z. Wang, Z. Shao, T. W. Fredrick, N. J. Saba, P. C. Morss, S. B. Burnim, S. S. Meng, F. B. Lih, K. S. S. Lee, E. P. Moran, J. P. SanGiovanni, A. Hellström, B. D. Hammock, D. C. Zeldin and L. E. H. Smith (2016). "Cytochrome P450 oxidase 2C inhibition adds to ω -3 long-chain polyunsaturated fatty acids protection against retinal and choroidal neovascularization." Arteriosclerosis, thrombosis, and vascular biology **36**(9): 1919-1927.
- Gong, Y., J. Li, Y. Sun, Z. Fu, C.-H. Liu, L. Evans, K. Tian, N. Saba, T. Fredrick, P. Morss, J. Chen and L. E. H. Smith (2015). "Optimization of an image-guided laser-induced choroidal neovascularization model in mice." PloS one **10**(7): e0132643-e0132643.
- Gopinathan, G., C. Milagre, O. M. Pearce, L. E. Reynolds, K. Hodivala-Dilke, D. A. Leinster, H. Zhong, R. E. Hollingsworth, R. Thompson, J. R. Whiteford and F. Balkwill (2015). "Interleukin-6 Stimulates Defective Angiogenesis." Cancer Research **75**(15): 3098-3107.
- Goto, K., N. Kato and R. T. Chung (2016). "Anti-hepatocellular carcinoma properties of the anti-alcoholism drug disulfiram discovered to enzymatically inhibit the AMPK-related kinase SNARK in vitro." Oncotarget **7**(46): 74987-74999.
- Green, W. R. (1999). "Histopathology of age-related macular degeneration." Molecular Vision **5**: 27.
- Green, W. R. and D. J. Wilson (1986). "Choroidal neovascularization." Ophthalmology **93**(9): 1169-1176.
- Grinan-Ferre, C., S. Codony, E. Pujol, J. Yang, R. Leiva, C. Escolano, D. Puigoriol-Illamola, J. Companys-Aleman, R. Corpas, C. Sanfeliu, B. Perez, M. I. Loza, J. Brea, C. Morisseau, B. D. Hammock, S. Vazquez, M. Pallas and C. Galdeano (2020). "Pharmacological inhibition of soluble epoxide hydrolase as a new therapy for Alzheimer's Disease." Neurotherapeutics **17**(4): 1825-1835.
- Grossniklaus, H. E. and W. R. Green (2004). "Choroidal neovascularization." American Journal of Ophthalmology **137**(3): 496-503.

- Haery, L., B. E. Deverman, K. S. Matho, A. Cetin, K. Woodard, C. Cepko, K. I. Guerin, M. A. Rego, I. Ersing, S. M. Bachle, J. Kamens and M. Fan (2019). "Adeno-associated virus technologies and methods for targeted neuronal manipulation." Frontiers in Neuroanatomy **13**(93).
- Hageman, G. S., K. Gehrs, L. V. Johnson and D. Anderson (1995). Age-related macular degeneration (AMD). The Organization of the Retina and Visual System. H. Kolb, E. Fernandez and R. Nelson. Salt Lake City (UT): University of Utah Health Sciences Center, Webvision.
- Hammes, H.-P., J. Lin, O. Renner, M. Shani, A. Lundqvist, C. Betsholtz, M. Brownlee and U. Deutsch (2002). "Pericytes and the pathogenesis of diabetic retinopathy." Diabetes **51**(10): 3107-3112.
- Harris, T. R. and B. D. Hammock (2013). "Soluble epoxide hydrolase: gene structure, expression and deletion." Gene **526**(2): 61-74.
- Hasegawa, E., S. Inafuku, L. Mulki, Y. Okunuki, R. Yanai, K. E. Smith, C. B. Kim, G. Klokman, D. R. Bielenberg, N. Puli, J. R. Falck, D. Husain, J. W. Miller, M. L. Edin, D. C. Zeldin, K. S. S. Lee, B. D. Hammock, W. H. Schunck and K. M. Connor (2017). "Cytochrome P450 monooxygenase lipid metabolites are significant second messengers in the resolution of choroidal neovascularization." Proceedings of the National Academy of Sciences of the United States of America **114**(36): E7545-e7553.
- Hasegawa, L. S. and B. D. Hammock (1982). "Spectrophotometric assay for mammalian cytosolic epoxide hydrolase using trans-stilbene oxide as the substrate." Biochemical Pharmacology **31**(11): 1979-1984.
- Hayman, S. R., N. Leung, J. P. Grande and V. D. Garovic (2012). "VEGF inhibition, hypertension, and renal toxicity." Current Oncology Reports **14**(4): 285-294.
- Heesterbeek, T. J., L. Lorés-Motta, C. B. Hoyng, Y. T. E. Lechanteur and A. I. den Hollander (2020). "Risk factors for progression of age-related macular degeneration." Ophthalmic and Physiological Optics **40**(2): 140-170.
- Hellström, M., L.-K. Phng and H. Gerhardt (2007). "VEGF and notch signaling: the yin and yang of angiogenic sprouting." Cell Adhesion & Migration **1**(3): 133-136.
- Heng, S., K. M. Harris and E. R. Kantrowitz (2010). "Designing inhibitors against fructose 1,6-bisphosphatase: exploring natural products for novel inhibitor scaffolds." European Journal of Medicinal Chemistry **45**(4): 1478-1484.
- Higgins, G. T., J. H. Wang, P. Dockery, P. E. Cleary and H. P. Redmond (2003). "Induction of angiogenic cytokine expression in cultured RPE by ingestion of oxidized photoreceptor outer segments." Investigative Ophthalmology & Visual Science **44**(4): 1775-1782.
- Holdgate, G. A., T. D. Meek and R. L. Grimley (2018). "Mechanistic enzymology in drug discovery: a fresh perspective." Nature Reviews Drug Discovery **17**(2): 115-132.
- Horstman, A. M., E. L. Dillon, R. J. Urban and M. Sheffield-Moore (2012). "The role of androgens and estrogens on healthy aging and longevity." The journals of Gerontology. Series A, Biological Sciences and Medical Sciences **67**(11): 1140-1152.
- Hu, J., S. Dziumbila, J. Lin, S. I. Bibli, S. Zukunft, J. de Mos, K. Awwad, T. Fromel, A. Jungmann, K. Devraj, Z. Cheng, L. Wang, S. Fauser, C. G. Eberhart, A. Sodhi, B.

- D. Hammock, S. Liebner, O. J. Muller, C. Glaubitz, H. P. Hammes, R. Popp and I. Fleming (2017). "Inhibition of soluble epoxide hydrolase prevents diabetic retinopathy." Nature **552**(7684): 248-252.
- Hu, J., R. Popp, T. Fromel, M. Ehling, K. Awwad, R. H. Adams, H. P. Hammes and I. Fleming (2014). "Muller glia cells regulate notch signaling and retinal angiogenesis via the generation of 19,20-dihydroxydocosapentaenoic acid." Journal of Experimental Medicine **211**(2): 281-295.
- Hughes, J. P., S. Rees, S. B. Kalindjian and K. L. Philpott (2011). "Principles of early drug discovery." British Journal of Pharmacology **162**(6): 1239-1249.
- Hwang, S. H., H.-J. Tsai, J.-Y. Liu, C. Morisseau and B. D. Hammock (2007). "Orally bioavailable potent soluble epoxide hydrolase inhibitors." Journal of Medicinal Chemistry **50**(16): 3825-3840.
- Inceoglu, B., S. L. Jinks, A. Ulu, C. M. Hegedus, K. Georgi, K. R. Schmelzer, K. Wagner, P. D. Jones, C. Morisseau and B. D. Hammock (2008). "Soluble epoxide hydrolase and epoxyeicosatrienoic acids modulate two distinct analgesic pathways." Proceedings of the National Academy of Sciences **105**(48): 18901.
- Jacobs, B., N. Palmer, T. Shetty, H. Dimaras, A. Hajrasouliha, D. Jusufbegovic and T. W. Corson (2021). "Patient preferences in retinal drug delivery." Scientific Reports **11**(1): 18996-18996.
- Jensen, E. G., T. S. Jakobsen, S. Thiel, A. L. Askou and T. J. Corydon (2020). "Associations between the Complement System and Choroidal Neovascularization in Wet Age-Related Macular Degeneration." International Journal of Molecular Sciences **21**(24): 9752.
- Jia, J., D. Qiu, C. Lu, W. Wang, N. Li, Y. Han, P. Tong, X. Sun, M. Wu and J. Dai (2021). "Transcriptome Analysis of Choroid and Retina From Tree Shrew With Choroidal Neovascularization Reveals Key Signaling Moieties." Frontiers in Genetics **12**.
- Jian, L., Y. Panpan and X. Wen (2013). "Current Choroidal Neovascularization Treatment." Ophthalmologica **230**(2): 55-61.
- Kaabia, Z., J. Poirier, M. Moughaizel, A. Aguesse, S. Billon-Crossouard, F. Fall, M. Durand, E. Dagher, M. Krempf and M. Croyal (2018). "Plasma lipidomic analysis reveals strong similarities between lipid fingerprints in human, hamster and mouse compared to other animal species." Scientific Reports **8**(1): 15893.
- Kaji, Y. (2005). "Prevention of diabetic keratopathy." The British Journal of Ophthalmology **89**(3): 254-255.
- Kaplan, H. J. (2007). "Anatomy and function of the eye." Chemical Immunology and Allergy **92**: 4-10.
- Kawasumi, M. and P. Nghiem (2007). "Chemical genetics: elucidating biological systems with small-molecule compounds." Journal of Investigative Dermatology **127**(7): 1577-1584.
- Kefalov, V. J. (2012). "Rod and cone visual pigments and phototransduction through pharmacological, genetic, and physiological approaches." The Journal of Biological Chemistry **287**(3): 1635-1641.
- Kim, C. B., P. A. D'Amore and K. M. Connor (2016). "Revisiting the mouse model of oxygen-induced retinopathy." Eye and Brain **8**: 67-79.

- Kiyama, T. and C.-A. Mao (2020). Ultrasensitive RNAscope In Situ Hybridization System on Embryonic and Adult Mouse Retinas. Retinal Development: Methods and Protocols. C.-A. Mao. New York, NY, Springer US: 147-158.
- Klein, B. E., R. Klein and K. E. Lee (2000). "Reproductive exposures, incident age-related cataracts, and age-related maculopathy in women: the beaver dam eye study." American Journal of Ophthalmology **130**(3): 322-326.
- Knickelbein, J. E., C.-C. Chan, H. N. Sen, F. L. Ferris and R. B. Nussenblatt (2015). "Inflammatory Mechanisms of Age-related Macular Degeneration." International Ophthalmology Clinics **55**(3): 63-78.
- Kodani, S. D. and C. Morisseau (2019). "Role of epoxy-fatty acids and epoxide hydrolases in the pathology of neuro-inflammation." Biochimie **159**: 59-65.
- Kumar, S., H. Nakashizuka, A. Jones, A. Lambert, X. Zhao, M. Shen, M. Parker, S. Wang, Z. Berriochoa, A. Fnu, S. VanBeuge, P. Chévez-Barrios, M. Tso, J. Rainier and Y. Fu (2017). "Proteolytic degradation and inflammation play critical roles in polypoidal choroidal vasculopathy." The American Journal of Pathology **187**(12): 2841-2857.
- Kuroda, Y., K. Yamashiro, M. Miyake, M. Yoshikawa, H. Nakanishi, A. Oishi, H. Tamura, S. Ooto, A. Tsujikawa and N. Yoshimura (2015). "Factors associated with recurrence of age-related macular degeneration after anti-vascular endothelial growth factor treatment: A retrospective cohort study." Ophthalmology **122**(11): 2303-2310.
- Kvanta, A., P. Algvere, L. Berglin and S. Seregard (1996). "Subfoveal fibrovascular membranes in age-related macular degeneration express vascular endothelial growth factor." Investigative Ophthalmology and Visual Science **37**(9): 1929-1934.
- Ładkowska, J., M. Gawęcki and M. Szołkiewicz (2021). "Efficacy of Anti-Vascular Endothelial Growth Factor Treatment in Neovascular Age-Related Macular Degeneration and Systemic Cardiovascular Risk Factors." Journal of Clinical Medicine **10**(19): 4595.
- Lee, B., H. D. Basavarajappa, R. S. Sulaiman, X. Fei, S.-Y. Seo and T. W. Corson (2014). "The first synthesis of the antiangiogenic homoisoflavanone, cremastranone." Organic & Biomolecular Chemistry **12**(39): 7673-7677.
- Lee, S. H., Y. S. Kim, S. K. Nah, H. J. Kim, H. Y. Park, J. Y. Yang, K. Park and T. K. Park (2018). "Transduction Patterns of Adeno-associated Viral Vectors in a Laser-Induced Choroidal Neovascularization Mouse Model." Molecular Therapy. Methods & Clinical Development **9**: 90-98.
- Li, J. L. and A. L. Harris (2009). "Crosstalk of VEGF and notch pathways in tumour angiogenesis: therapeutic implications." Frontiers in Bioscience **14**: 3094-3110.
- Liu, X., Z. Qin, C. Liu, M. Song, X. Luo, H. Zhao, D. Qian, J. Chen and L. Huang (2019). "Nox4 and soluble epoxide hydrolase synergistically mediate homocysteine-induced inflammation in vascular smooth muscle cells." Vascular Pharmacology: 106544.
- Lopez, P. F., B. D. Sippy, H. M. Lambert, A. B. Thach and D. R. Hinton (1996). "Transdifferentiated retinal pigment epithelial cells are immunoreactive for vascular endothelial growth factor in surgically excised age-related macular

- degeneration-related choroidal neovascular membranes." Investigative Ophthalmology & Visual Science **37**(5): 855-868.
- Lukashev, A. N. and A. A. Zamyatnin, Jr. (2016). "Viral Vectors for Gene Therapy: Current State and Clinical Perspectives." Biochemistry (Mosc) **81**(7): 700-708.
- Lux, A., H. Llacer, F. M. Heussen and A. M. Jousseaume (2007). "Non-responders to bevacizumab (Avastin) therapy of choroidal neovascular lesions." British Journal of Ophthalmology **91**(10): 1318-1322.
- Madrakhimov, S. B., J. Y. Yang, J. H. Kim, J. W. Han and T. K. Park (2021). "mTOR-dependent dysregulation of autophagy contributes to the retinal ganglion cell loss in streptozotocin-induced diabetic retinopathy." Cell Communication and Signaling **19**(1): 29.
- Makurvet, F. D. (2021). "Biologics vs. small molecules: Drug costs and patient access." Medicine in Drug Discovery **9**: 100075.
- Malamas, A., A. Chranioti, C. Tsakalidis, S. A. Dimitrakos and A. Mataftsi (2017). "The omega-3 and retinopathy of prematurity relationship." International Journal of Ophthalmology **10**(2): 300-305.
- Mannu, G. S. (2014). "Retinal phototransduction." Neurosciences (Riyadh, Saudi Arabia) **19**(4): 275-280.
- May, A., F. Su, B. Dinh, R. Ehlen, C. Tran, H. Adivikolanu and P. X. Shaw (2021). "Ongoing controversies and recent insights of the ARMS2-HTRA1 locus in age-related macular degeneration." Experimental Eye Research **210**: 108605.
- McGeough, M. D., C. A. Pena, J. L. Mueller, D. A. Pociask, L. Broderick, H. M. Hoffman and S. D. Brydges (2012). "Cutting edge: IL-6 is a marker of inflammation with no direct role in inflammasome-mediated mouse models." Journal of Immunology **189**(6): 2707-2711.
- McLellan, G. J., Z. Aktas, E. Hennes-Beean, A. W. Kolb, I. V. Larsen, E. J. Schmitz, H. R. Clausius, J. Yang, S. H. Hwang, C. Morisseau, B. Inceoglu, B. D. Hammock and C. R. Brandt (2016). "Effect of a soluble epoxide hydrolase inhibitor, UC1728, on LPS-induced uveitis in the rabbit." Journal of Ocular Biology **4**(1).
- McLeod, D. S., R. Grebe, I. Bhutto, C. Merges, T. Baba and G. A. Luty (2009). "Relationship between RPE and choriocapillaris in age-related macular degeneration." Investigative Ophthalmology & Visual Science **50**(10): 4982-4991.
- Menon, M., S. Mohammadi, J. Davila-Velderrain, B. A. Goods, T. D. Cadwell, Y. Xing, A. Stemmer-Rachamimov, A. K. Shalek, J. C. Love, M. Kellis and B. P. Hafler (2019). "Single-cell transcriptomic atlas of the human retina identifies cell types associated with age-related macular degeneration." Nature Communications **10**(1): 4902.
- Miao, H., Y. Tao and X. X. Li (2012). "Inflammatory cytokines in aqueous humor of patients with choroidal neovascularization." Molecular Vision **18**: 574-580.
- Michaelis, U. R., N. Xia, E. Barbosa-Sicard, J. R. Falck and I. Fleming (2008). "Role of cytochrome P450 2C epoxygenases in hypoxia-induced cell migration and angiogenesis in retinal endothelial cells." Investigative Ophthalmology & Visual Science **49**(3): 1242-1247.

- Miller, J. W., L. L. D'Anieri, D. Husain, J. B. Miller and D. G. Vavvas (2021). "Age-Related Macular Degeneration (AMD): A View to the Future." Journal of Clinical Medicine **10**(5): 1124.
- Minaz, N., R. Razdan, B. D. Hammock and S. K. Goswami (2018). "An inhibitor of soluble epoxide hydrolase ameliorates diabetes-induced learning and memory impairment in rats." Prostaglandins & Other Lipid Mediators **136**: 84-89.
- Morisseau, C., M. H. Goodrow, D. Dowdy, J. Zheng, J. F. Greene, J. R. Sanborn and B. D. Hammock (1999). "Potent urea and carbamate inhibitors of soluble epoxide hydrolases." Proceedings of the National Academy of Sciences of the United States of America **96**(16): 8849-8854.
- Morisseau, C. and B. D. Hammock (2007). "Measurement of soluble epoxide hydrolase (sEH) activity." Current Protocols in Toxicology **Chapter 4**: Unit 4.23.
- Morisseau, C., B. Inceoglu, K. Schmelzer, H. J. Tsai, S. L. Jinks, C. M. Hegedus and B. D. Hammock (2010). "Naturally occurring monoepoxides of eicosapentaenoic acid and docosahexaenoic acid are bioactive antihyperalgesic lipids." Journal of Lipid Research **51**(12): 3481-3490.
- Morris, B., F. Imrie, A. M. Armbrrecht and B. Dhillon (2007). "Age-related macular degeneration and recent developments: new hope for old eyes?" Postgraduate Medical Journal **83**(979): 301-307.
- Nagai, N., P. Lundh von Leithner, K. Izumi-Nagai, B. Hosking, B. Chang, R. Hurd, P. Adamson, A. P. Adamis, R. H. Foxton, Y. S. Ng and D. T. Shima (2014). "Spontaneous CNV in a novel mutant mouse is associated with early VEGF-A-driven angiogenesis and late-stage focal edema, neural cell loss, and dysfunction." Investigative ophthalmology & visual science **55**(6): 3709-3719.
- Nakao, S., A. Hafezi-Moghadam and T. Ishibashi (2012). "Lymphatics and Lymphangiogenesis in the Eye." Journal of Ophthalmology **2012**: 783163.
- Nakazawa, T., T. Hisatomi, C. Nakazawa, K. Noda, K. Maruyama, H. She, A. Matsubara, S. Miyahara, S. Nakao, Y. Yin, L. Benowitz, A. Hafezi-Moghadam and J. W. Miller (2007). "Monocyte chemoattractant protein 1 mediates retinal detachment-induced photoreceptor apoptosis." Proceedings of the National Academy of Sciences of the United States of America **104**(7): 2425-2430.
- Natoli, R., N. Fernando, M. Madigan, J. A. Chu-Tan, K. Valter, J. Provis and M. Rutar (2017). "Microglia-derived IL-1 β promotes chemokine expression by Müller cells and RPE in focal retinal degeneration." Molecular Neurodegeneration **12**(1): 31.
- Newman, A. M., N. B. Gallo, L. S. Hancox, N. J. Miller, C. M. Radeke, M. A. Maloney, J. B. Cooper, G. S. Hageman, D. H. Anderson, L. V. Johnson and M. J. Radeke (2012). "Systems-level analysis of age-related macular degeneration reveals global biomarkers and phenotype-specific functional networks." Genome Medicine **4**(2): 16.
- Nickla, D. L. and J. Wallman (2010). "THE MULTIFUNCTIONAL CHOROID." Progress in retinal and eye research **29**(2): 144-168.
- Norwood, S., J. Liao, B. D. Hammock and G. Y. Yang (2010). "Epoxyeicosatrienoic acids and soluble epoxide hydrolase: potential therapeutic targets for inflammation and its induced carcinogenesis." American Journal of Translational Research **2**(4): 447-457.

- Oh, H., H. Takagi, C. Takagi, K. Suzuma, A. Otani, K. Ishida, M. Matsumura, Y. Ogura and Y. Honda (1999). "The potential angiogenic role of macrophages in the formation of choroidal neovascular membranes." Investigative Ophthalmology & Visual Science **40**(9): 1891-1898.
- Oltman, C. L., N. L. Weintraub, M. VanRollins and K. C. Dellsperger (1998). "Epoxyeicosatrienoic acids and dihydroxyeicosatrienoic acids are potent vasodilators in the canine coronary microcirculation." Circulation Research **83**(9): 932-939.
- Paduch, R. (2016). "The role of lymphangiogenesis and angiogenesis in tumor metastasis." Cellular oncology (Dordrecht) **39**(5): 397-410.
- Park, B. and T. W. Corson (2019). "Soluble epoxide hydrolase inhibition for ocular diseases: vision for the future." Frontiers in Pharmacology **10**: 95-95.
- Parson, S. H. (2009). "Clinically Oriented Anatomy, 6th edn." Journal of Anatomy **215**(4): 474-474.
- Pascolini, D. and S. P. Mariotti (2012). "Global estimates of visual impairment: 2010." British Journal of Ophthalmology **96**(5): 614-618.
- Pennington, K. L. and M. M. DeAngelis (2016). "Epidemiology of age-related macular degeneration (AMD): associations with cardiovascular disease phenotypes and lipid factors." Eye and vision (London, England) **3**: 34-34.
- Pereiro, X., R. Fernández, G. Barreda-Gómez, N. Ruzafa, A. Acera, J. Araiz, E. Astigarraga and E. Vecino (2020). "Comparative lipidomic analysis of mammalian retinal ganglion cells and Müller glia in situ and in vitro using High-Resolution Imaging Mass Spectrometry." Scientific Reports **10**(1): 20053.
- Podolin, P. L., B. J. Bolognese, J. F. Foley, E. Long, 3rd, B. Peck, S. Umbrecht, X. Zhang, P. Zhu, B. Schwartz, W. Xie, C. Quinn, H. Qi, S. Sweitzer, S. Chen, M. Galop, Y. Ding, S. L. Belyanskaya, D. I. Israel, B. A. Morgan, D. J. Behm, J. P. Marino, Jr., E. Kurali, M. S. Barnette, R. J. Mayer, C. L. Booth-Genthe and J. F. Callahan (2013). "In vitro and in vivo characterization of a novel soluble epoxide hydrolase inhibitor." Prostaglandins Other Lipid Mediat **104-105**: 25-31.
- Pozzi, A., I. Macias-Perez, T. Abair, S. Wei, Y. Su, R. Zent, J. R. Falck and J. H. Capdevila (2005). "Characterization of 5,6- and 8,9-epoxyeicosatrienoic acids (5,6- and 8,9-EET) as potent in vivo angiogenic lipids." Journal of Biological Chemistry **280**(29): 27138-27146.
- Querques, G., R. Forte and E. H. Souied (2011). "Retina and omega-3." Journal of Nutrition and Metabolism **2011**: 748361.
- Raoul, W., C. Auvynet, S. Camelo, X. Guillonneau, C. Feumi, C. Combadière and F. Sennlaub (2010). "CCL2/CCR2 and CX3CL1/CX3CR1 chemokine axes and their possible involvement in age-related macular degeneration." Journal of Neuroinflammation **7**(1): 87.
- Reichenbach, A. and A. Bringmann (2013). "New functions of muller cells." Glia **61**(5): 651-678.
- Rein, D. B., J. S. Wittenborn, X. Zhang, A. A. Honeycutt, S. B. Lesesne, J. Saaddine and G. Vision Health Cost-Effectiveness Study (2009). "Forecasting age-related macular degeneration through the year 2050: The potential impact of new treatments." JAMA Ophthalmology **127**(4): 533-540.

- Robertson, J. G. (2005). "Mechanistic Basis of Enzyme-Targeted Drugs." Biochemistry **44**(15): 5561-5571.
- Rose, T. E., C. Morisseau, J. Y. Liu, B. Inceoglu, P. D. Jones, J. R. Sanborn and B. D. Hammock (2010). "1-Aryl-3-(1-acylpiperidin-4-yl)urea inhibitors of human and murine soluble epoxide hydrolase: structure-activity relationships, pharmacokinetics, and reduction of inflammatory pain." Journal of Medicinal Chemistry **53**(19): 7067-7075.
- Rufer, A. C. (2021). "Drug discovery for enzymes." Drug Discovery Today **26**(4): 875-886.
- Sahu, B., I. Chug and H. Khanna (2021). "The Ocular Gene Delivery Landscape." Biomolecules **11**(8): 1135.
- Sameshima, M., F. Uehara and N. Ohba (1987). "Specialization of the interphotoreceptor matrices around cone and rod photoreceptor cells in the monkey retina, as revealed by lectin cytochemistry." Experimental Eye Research **45**(6): 845-863.
- Sarkar, A., V. Junnuthula and S. Dyawanapelly (2021). "Ocular Therapeutics and Molecular Delivery Strategies for Neovascular Age-Related Macular Degeneration (nAMD)." International Journal of Molecular Sciences **22**(19).
- Schaal, S., H. J. Kaplan and T. H. Tezel (2008). "Is there tachyphylaxis to intravitreal anti-vascular endothelial growth factor pharmacotherapy in age-related macular degeneration?" Ophthalmology **115**(12): 2199-2205.
- Schmidt-Erfurth, U., V. Chong, A. Loewenstein, M. Larsen, E. Souied, R. Schlingemann, B. Eldem, J. Monés, G. Richard and F. Bandello (2014). "Guidelines for the management of neovascular age-related macular degeneration by the European Society of Retina Specialists (EURETINA)." British Journal of Ophthalmology **98**(9): 1144-1167.
- Schraermeyer, U. and K. Heimann (1999). "Current understanding on the role of retinal pigment epithelium and its pigmentation." Pigment Cell Research **12**(4): 219-236.
- Schultz, B. R. and J. S. Chamberlain (2008). "Recombinant Adeno-associated Virus Transduction and Integration." Molecular Therapy **16**(7): 1189-1199.
- Scott, A. and M. Fruttiger (2009). "Oxygen-induced retinopathy: a model for vascular pathology in the retina." Eye **24**: 416.
- Sergejeva, O., R. Botov, R. Liutkevičienė and L. Kriauciūnienė (2016). "Genetic factors associated with the development of age-related macular degeneration." Medicina **52**(2): 79-88.
- Shah, R. S., B. T. Soetikno, M. Lajko and A. A. Fawzi (2015). "A Mouse Model for Laser-induced Choroidal Neovascularization." Journal of visualized experiments : JoVE(106): e53502-e53502.
- Shao, Z., Z. Fu, A. Stahl, J.-S. Joyal, C. Hatton, A. Juan, C. Hurst, L. Evans, Z. Cui, D. Pei, Y. Gong, D. Xu, K. Tian, H. Bogardus, M. L. Edin, F. Lih, P. Sapieha, J. Chen, D. Panigrahy, A. Hellstrom, D. C. Zeldin and L. E. H. Smith (2014). "Cytochrome P450 2C8 ω3-long-chain polyunsaturated fatty acid metabolites increase mouse retinal pathologic neovascularization—brief report." Arteriosclerosis, thrombosis, and vascular biology **34**(3): 581-586.
- Shen, H. C., F.-X. Ding, Q. Deng, S. Xu, X. Tong, X. Zhang, Y. Chen, G. Zhou, L.-Y. Pai, M. Alonso-Galicia, S. Roy, B. Zhang, J. R. Tata, J. P. Berger and S. L. Colletti (2009). "A strategy of employing aminoheterocycles as amide mimics to

- identify novel, potent and bioavailable soluble epoxide hydrolase inhibitors." Bioorganic & Medicinal Chemistry Letters **19**(19): 5716-5721.
- Shen, H. C. and B. D. Hammock (2012). "Discovery of inhibitors of soluble epoxide hydrolase: a target with multiple potential therapeutic indications." Journal of Medicinal Chemistry **55**(5): 1789-1808.
- Smalley, E. (2017). "First AAV gene therapy poised for landmark approval." Nature Biotechnology **35**(11): 998-999.
- Snow, K. K., J. Cote, W. Yang, N. J. Davis and J. M. Seddon (2002). "Association between reproductive and hormonal factors and age-related maculopathy in postmenopausal women." American Journal of Ophthalmology **134**(6): 842-848.
- Spaide, R. F., G. J. Jaffe, D. Sarraf, K. B. Freund, S. R. Sadda, G. Staurenghi, N. K. Waheed, U. Chakravarthy, P. J. Rosenfeld, F. G. Holz, E. H. Souied, S. Y. Cohen, G. Querques, K. Ohno-Matsui, D. Boyer, A. Gaudric, B. Blodi, C. R. Baumal, X. Li, G. J. Coscas, A. Brucker, L. Singerman, P. Luthert, S. Schmitz-Valckenberg, U. Schmidt-Erfurth, H. E. Grossniklaus, D. J. Wilson, R. Guymer, L. A. Yannuzzi, E. Y. Chew, K. Csaky, J. M. Monés, D. Pauleikhoff, R. Tadayoni and J. Fujimoto (2020). "Consensus Nomenclature for Reporting Neovascular Age-Related Macular Degeneration Data: Consensus on Neovascular Age-Related Macular Degeneration Nomenclature Study Group." Ophthalmology **127**(5): 616-636.
- Srivastava, A. (2016). "In vivo tissue-tropism of adeno-associated viral vectors." Current Opinion in Virology **21**: 75-80.
- Steen, B., S. Sejersen, L. Berglin, S. Seregard and A. Kvanta (1998). "Matrix metalloproteinases and metalloproteinase inhibitors in choroidal neovascular membranes." Investigative ophthalmology & visual science **39**(11): 2194-2200.
- Steinmetz, J. D., R. R. A. Bourne, P. S. Briant, S. R. Flaxman, H. R. B. Taylor, J. B. Jonas, A. A. Abdoli, W. A. Abrha, A. Abualhasan, E. G. Abu-Gharbieh, T. G. Adal, A. Afshin, H. Ahmadiéh, W. Alemayehu, S. A. S. Alemzadeh, A. S. Alfaar, V. Alipour, S. Androudi, J. Arabloo, A. B. Arditi, B. B. Aregawi, A. Arrigo, C. Ashbaugh, E. D. Ashrafi, D. D. Atnafu, E. A. Bagli, A. A. W. Baig, T. W. Bärnighausen, M. Battaglia Parodi, M. S. Beheshti, A. S. Bhagavathula, N. Bhardwaj, P. Bhardwaj, K. Bhattacharyya, A. Bijani, M. Bikbov, M. Bottone, T. M. Braithwaite, A. M. Bron, S. A. Burugina Nagaraja, Z. A. Butt, F. L. L. Caetano dos Santos, V. L. J. Carneiro, R. J. Casson, C.-Y. J. Cheng, J.-Y. J. Choi, D.-T. Chu, M. V. M. Cicinelli, J. M. G. Coelho, N. G. A. Congdon, R. A. A. Couto, E. A. M. Cromwell, S. M. Dahlawi, X. Dai, R. Dana, L. Dandona, R. A. Dandona, M. A. Del Monte, M. Derbew Molla, N. A. Derveniz, A. A. P. Desta, J. P. Deva, D. Diaz, S. E. Djalalinia, J. R. Ehrlich, R. R. Elayedath, H. R. B. Elhabashy, L. B. Ellwein, M. H. Emamian, S. Eskandarieh, F. G. Farzadfar, A. G. Fernandes, F. S. Fischer, D. S. M. Friedman, J. M. Furtado, S. Gaidhane, G. Gazzard, B. Gebremichael, R. George, A. Ghashghaee, S. A. Gilani, M. Golechha, S. R. Hamidi, B. R. R. Hammond, M. E. R. K. Hartnett, R. K. Hartono, A. I. Hashi, S. I. Hay, K. Hayat, G. Heidari, H. C. Ho, R. Holla, M. J. Househ, J. J. E. Huang, S. E. M. Ibitoye, I. M. D. Ilic, M. D. D. Ilic, A. D. N. Ingram, S. S. N. Irvani, S. M. S. Islam, R. Itumalla, S. P. Jayaram, R. P. Jha, R. Kahloun, R. Kalhor, H. Kandel, A. S. Kasa, T. A. Kavetsky, G. A. H. Kayode, J. H. Kempen,

- M. Khairallah, R. A. Khalilov, E. A. C. Khan, R. C. Khanna, M. N. A. Khatib, T. A. E. Khoja, J. E. Kim, Y. J. Kim, G. R. Kim, S. Kisa, A. Kisa, S. Kosen, A. Koyanagi, B. Kucuk Bicer, V. P. Kulkarni, O. P. Kurmi, I. C. Landires, V. C. L. Lansingh, J. L. E. Leasher, K. E. LeGrand, N. Leveziel, H. Limburg, X. Liu, S. Madhava Kunjathur, S. Maleki, N. Manafi, K. Mansouri, C. G. McAlinden, G. G. M. Meles, A. M. Mersha, I. M. R. Michalek, T. R. Miller, S. Misra, Y. Mohammad, S. F. A. Mohammadi, J. A. H. Mohammed, A. H. Mokdad, M. A. A. Moni, A. A. R. Montasir, A. R. F. Morse, G. F. C. Mulaw, M. Naderi, H. S. Naderifar, K. S. Naidoo, M. D. Naimzada, V. Nangia, S. M. Narasimha Swamy, D. M. Naveed, H. L. Negash, H. L. Nguyen, V. A. Nunez-Samudio, F. A. Ogbo, K. T. Ogundimu, A. T. E. Olagunju, O. E. Onwujekwe, N. O. Otstavnov, M. O. Owolabi, K. Pakshir, S. Panda-Jonas, U. Parekh, E.-C. Park, M. Pasovic, S. Pawar, K. Pesudovs, T. Q. Peto, H. Q. Pham, M. Pinheiro, V. Podder, V. Rahimi-Movaghar, M. H. U. Y. Rahman, P. Y. Ramulu, P. Rathi, S. L. Rawaf, D. L. Rawaf, L. Rawal, N. M. Reinig, A. M. Renzaho, A. L. Rezapour, A. L. Robin, L. Rossetti, S. Sabour, S. Safi, A. Sahebkar, M. A. M. Sahraian, A. M. Samy, B. Sathian, G. K. Saya, M. A. Saylan, A. A. A. Shaheen, M. A. T. Shaikh, T. T. Shen, K. S. Shibuya, W. S. Shiferaw, M. Shigematsu, J. I. Shin, J. C. Silva, A. A. Silvester, J. A. Singh, D. S. Singhal, R. S. Sitorus, E. Y. Skiadaresi, V. Y. A. Skryabin, A. A. Skryabina, A. B. Soheili, M. B. A. R. C. Sorrie, R. A. R. C. T. Sousa, C. T. Sreeramareddy, D. G. Stambolian, E. G. Tadesse, N. I. Tahhan, M. I. Tareque, F. X. Topouzis, B. X. Tran, G. K. Tsegaye, M. K. Tsilimbaris, R. Varma, G. Virgili, A. T. Vongpradith, G. T. Vu, Y. X. Wang, N. H. Wang, A. H. K. Weldemariam, S. K. G. West, T. G. Y. Wondmeneh, T. Y. Wong, M. Yaseri, N. Yonemoto, C. S. Yu, M. S. Zastrozhin, Z.-J. R. Zhang, S. R. Zimsen, S. Resnikoff and T. Vos (2021). "Causes of blindness and vision impairment in 2020 and trends over 30 years, and prevalence of avoidable blindness in relation to VISION 2020: the Right to Sight: an analysis for the Global Burden of Disease Study." *The Lancet Global Health* **9**(2): e144-e160.
- Stillwell, W. and S. R. Wassall (2003). "Docosahexaenoic acid: membrane properties of a unique fatty acid." *Chemistry and Physics of Lipids* **126**(1): 1-27.
- Stinson, A. M., R. D. Wiegand and R. E. Anderson (1991). "Recycling of docosahexaenoic acid in rat retinas during n-3 fatty acid deficiency." *Journal of Lipid Research* **32**(12): 2009-2017.
- Sulaiman, R. S., S. Merrigan, J. Quigley, X. Qi, B. Lee, M. E. Boulton, B. Kennedy, S.-Y. Seo and T. W. Corson (2016). "A novel small molecule ameliorates ocular neovascularisation and synergises with anti-VEGF therapy." *Scientific Reports* **6**(1): 25509.
- Sulaiman, R. S., S. Merrigan, J. Quigley, X. Qi, B. Lee, M. E. Boulton, B. Kennedy, S.-Y. Seo and T. W. Corson (2016). "A novel small molecule ameliorates ocular neovascularisation and synergises with anti-VEGF therapy." *Scientific Reports* **6**: 25509.
- Sulaiman, R. S., B. Park, S. P. Sheik Pran Babu, Y. Si, R. Kharwadkar, S. K. Mitter, B. Lee, W. Sun, X. Qi, M. E. Boulton, S. O. Meroueh, X. Fei, S. Y. Seo and T. W. Corson (2018). "Chemical proteomics reveals soluble epoxide hydrolase as a

- therapeutic target for ocular neovascularization." ACS Chemical Biology **13**(1): 45-52.
- Sulaiman, R. S., J. Quigley, X. Qi, M. N. O'Hare, M. B. Grant, M. E. Boulton and T. W. Corson (2015). "A simple optical coherence tomography quantification method for choroidal neovascularization." Journal of Ocular Pharmacology and Therapeutics **31**(8): 447-454.
- Sun, H., P. Lee, C. Yan, N. Gao, J. Wang, X. Fan and F.-S. Yu (2018). "Inhibition of soluble epoxide hydrolase 2 ameliorates diabetic keratopathy and impaired wound healing in mouse corneas." Diabetes.
- Sura, P., R. Sura, A. E. Enayetallah and D. F. Grant (2008). "Distribution and expression of soluble epoxide hydrolase in human brain." The Journal of Histochemistry and Cytochemistry **56**(6): 551-559.
- Surace, E. M. and A. Auricchio (2008). "Versatility of AAV vectors for retinal gene transfer." Vision Research **48**(3): 353-359.
- Tadayoni, R., L. Sararols, G. Weissgerber, R. Verma, A. Clemens and F. G. Holz (2021). "Brolicizumab: A Newly Developed Anti-VEGF Molecule for the Treatment of Neovascular Age-Related Macular Degeneration." Ophthalmologica **244**(2): 93-101.
- Tien, L., M. E. Rayborn and J. G. Hollyfield (1992). "Characterization of the interphotoreceptor matrix surrounding rod photoreceptors in the human retina." Experimental Eye Research **55**(2): 297-306.
- Tomi, A. and I. Marin (2014). "Angiofluorographic aspects in age-related macular degeneration." Journal of Medicine and Life **7**(Spec Iss 4): 4-17.
- Trapani, I., P. Tornabene and A. Auricchio (2021). "Large gene delivery to the retina with AAV vectors: are we there yet?" Gene Therapy **28**(5): 220-222.
- van Lookeren Campagne, M., J. LeCouter, B. L. Yaspan and W. Ye (2014). "Mechanisms of age-related macular degeneration and therapeutic opportunities." The Journal of Pathology **232**(2): 151-164.
- Varela-Fernández, R., V. Díaz-Tomé, A. Luaces-Rodríguez, A. Conde-Penedo, X. García-Otero, A. Luzardo-Álvarez, A. Fernández-Ferreiro and F. J. Otero-Espinar (2020). "Drug Delivery to the Posterior Segment of the Eye: Biopharmaceutic and Pharmacokinetic Considerations." Pharmaceutics **12**(3).
- Veleri, S., C. H. Lazar, B. Chang, P. A. Sieving, E. Banin and A. Swaroop (2015). "Biology and therapy of inherited retinal degenerative disease: insights from mouse models." Disease Models and Mechanisms **8**(2): 109-129.
- Velilla, S., J. J. García-Medina, A. García-Layana, R. Dolz-Marco, S. Pons-Vázquez, M. D. Pinazo-Durán, F. Gómez-Ulla, J. F. Arévalo, M. Díaz-Llopis and R. Gallego-Pinazo (2013). "Smoking and Age-Related Macular Degeneration: Review and Update." Journal of Ophthalmology **2013**: 895147.
- Virgili, G. and A. Bini (2007). "Laser photocoagulation for neovascular age-related macular degeneration." Cochrane Database of Systematic Reviews(3).
- Voigt, A. P., K. Mulfaul, N. K. Mullin, M. J. Flamme-Wiese, J. C. Giacalone, E. M. Stone, B. A. Tucker, T. E. Scheetz and R. F. Mullins (2019). "Single-cell transcriptomics of the human retinal pigment epithelium and choroid in health and macular degeneration." Proceedings of the National Academy of Sciences **116**(48): 24100.

- Wagner, K., S. Vito, B. Inceoglu and B. D. Hammock (2014). "The role of long chain fatty acids and their epoxide metabolites in nociceptive signaling." Prostaglandins & other lipid mediators **0**: 2-12.
- Wagner, K. M., C. B. McReynolds, W. K. Schmidt and B. D. Hammock (2017). "Soluble epoxide hydrolase as a therapeutic target for pain, inflammatory and neurodegenerative diseases." Pharmacology & therapeutics **180**: 62-76.
- Wang, F., H. Zhang, A. H. Ma, W. Yu, M. Zimmermann, J. Yang, S. H. Hwang, D. Zhu, T. Y. Lin, M. Malfatti, K. W. Turteltaub, P. T. Henderson, S. Airhart, B. D. Hammock, J. Yuan, R. W. de Vere White and C. X. Pan (2018). "COX-2/sEH dual inhibitor PTUPB potentiates the antitumor efficacy of cisplatin." Molecular Cancer Therapy **17**(2): 474-483.
- Wang, H., X. Han, E. S. Wittchen and M. E. Hartnett (2016). "TNF- α mediates choroidal neovascularization by upregulating VEGF expression in RPE through ROS-dependent β -catenin activation." Molecular vision **22**: 116-128.
- Wenzel, A. A., M. N. O'Hare, M. Shadmand and T. W. Corson (2015). "Optical coherence tomography enables imaging of tumor initiation in the TAg-RB mouse model of retinoblastoma." Molecular vision **21**: 515-522.
- Williams, M. A., D. Craig, P. Passmore and G. Silvestri (2009). "Retinal drusen: harbingers of age, safe havens for trouble." Age Ageing **38**(6): 648-654.
- Wold, W. S. and K. Toth (2013). "Adenovirus vectors for gene therapy, vaccination and cancer gene therapy." Current Gene Therapy **13**(6): 421-433.
- Wolf, G. (2004). "The visual cycle of the cone photoreceptors of the retina." Nutrition Reviews **62**(7 Pt 1): 283-286.
- Wolf, N. M., C. Morisseau, P. D. Jones, B. Hock and B. D. Hammock (2006). "Development of a high-throughput screen for soluble epoxide hydrolase inhibition." Analytical biochemistry **355**(1): 71-80.
- Wong, W. L., X. Su, X. Li, C. M. Cheung, R. Klein, C. Y. Cheng and T. Y. Wong (2014). "Global prevalence of age-related macular degeneration and disease burden projection for 2020 and 2040: a systematic review and meta-analysis." Lancet Glob Health **2**(2): e106-116.
- Wright, A. F., C. F. Chakarova, M. M. Abd El-Aziz and S. S. Bhattacharya (2010). "Photoreceptor degeneration: genetic and mechanistic dissection of a complex trait." Nature Reviews Genetics **11**: 273.
- Wu, C.-H., S.-K. Shyue, T.-H. Hung, S. Wen, C.-C. Lin, C.-F. Chang and S.-F. Chen (2017). "Genetic deletion or pharmacological inhibition of soluble epoxide hydrolase reduces brain damage and attenuates neuroinflammation after intracerebral hemorrhage." Journal of Neuroinflammation **14**(1): 230.
- Xia, Z., J. Xiao and Q. Chen (2021). "Solving the Puzzle: What Is the Role of Progesterone in Neovascularization?" Biomolecules **11**(11): 1686.
- Xu, D. Y., B. B. Davis, Z. H. Wang, S. P. Zhao, B. Wasti, Z. L. Liu, N. Li, C. Morisseau, N. Chiamvimonvat and B. D. Hammock (2013). "A potent soluble epoxide hydrolase inhibitor, t-AUCB, acts through PPAR γ to modulate the function of endothelial progenitor cells from patients with acute myocardial infarction." International Journal of Cardiology **167**(4): 1298-1304.
- Xu, H., M. Chen and J. V. Forrester (2009). "Para-inflammation in the aging retina." Progress in Retinal and Eye Research **28**(5): 348-368.

- Yanai, R., L. Mulki, E. Hasegawa, K. Takeuchi, H. Sweigard, J. Suzuki, P. Gaissert, D. G. Vavvas, K.-H. Sonoda, M. Rothe, W.-H. Schunck, J. W. Miller and K. M. Connor (2014). "Cytochrome P450-generated metabolites derived from ω -3 fatty acids attenuate neovascularization." Proceedings of the National Academy of Sciences of the United States of America **111**(26): 9603-9608.
- Yang, J. Y., S. B. Madрахimov, D. H. Ahn, H. S. Chang, S. J. Jung, S. K. Nah, H. Y. Park and T. K. Park (2019). "mTORC1 and mTORC2 are differentially engaged in the development of laser-induced CNV." Cell Communication and Signaling **17**(1): 64.
- Yang, S., J. Zhao and X. Sun (2016). "Resistance to anti-VEGF therapy in neovascular age-related macular degeneration: a comprehensive review." Drug Design, Development and Therapy **10**: 1857-1867.
- Yang, Y.-M., D. Sun, S. Kandhi, G. Froogh, J. Zhuge, W. Huang, B. D. Hammock and A. Huang (2018). "Estrogen-dependent epigenetic regulation of soluble epoxide hydrolase via DNA methylation." Proceedings of the National Academy of Sciences of the United States of America **115**(3): 613.
- Ye, D., D. Zhang, C. Oltman, K. Dellsperger, H. C. Lee and M. VanRollins (2002). "Cytochrome p-450 epoxygenase metabolites of docosahexaenoate potently dilate coronary arterioles by activating large-conductance calcium-activated potassium channels." Journal of Pharmacology and Experimental Therapeutics **303**(2): 768-776.
- Yonekawa, Y., J. W. Miller and I. K. Kim (2015). "Age-Related Macular Degeneration: Advances in Management and Diagnosis." Journal of Clinical Medicine **4**(2): 343-359.
- Zetterberg, M. (2016). "Age-related eye disease and gender." Maturitas **83**: 19-26.
- Zhang, G., S. Kodani and B. D. Hammock (2014). "Stabilized epoxygenated fatty acids regulate inflammation, pain, angiogenesis and cancer." Progress in lipid research **53**: 108-123.
- Zhang, G., D. Panigrahy, L. M. Mahakian, J. Yang, J.-Y. Liu, K. S. Stephen Lee, H. I. Wettersten, A. Ulu, X. Hu, S. Tam, S. H. Hwang, E. S. Ingham, M. W. Kieran, R. H. Weiss, K. W. Ferrara and B. D. Hammock (2013). "Epoxy metabolites of docosahexaenoic acid (DHA) inhibit angiogenesis, tumor growth, and metastasis." Proceedings of the National Academy of Sciences **110**(16): 6530-6535.
- Zhang, G., D. Panigrahy, L. M. Mahakian, J. Yang, J. Y. Liu, K. S. Stephen Lee, H. I. Wettersten, A. Ulu, X. Hu, S. Tam, S. H. Hwang, E. S. Ingham, M. W. Kieran, R. H. Weiss, K. W. Ferrara and B. D. Hammock (2013). "Epoxy metabolites of docosahexaenoic acid (DHA) inhibit angiogenesis, tumor growth, and metastasis." Proceedings of the National Academy of Sciences **110**(16): 6530-6535.
- Zhang, W., J. J. Iliff, C. J. Campbell, R. K. Wang, P. D. Hurn and N. J. Alkayed (2009). "Role of soluble epoxide hydrolase in the sex-specific vascular response to cerebral ischemia." Journal of Cerebral Blood Flow & Metabolism **29**(8): 1475-1481.
- Zhang, Y., C. L. Oltman, T. Lu, H. C. Lee, K. C. Dellsperger and M. VanRollins (2001). "EET homologs potently dilate coronary microvessels and activate BK(Ca)

- channels." American Journal of Physiology-Heart and Circulatory Physiology **280**(6): H2430-2440.
- Zhang, Y., S.-F. Wang, J.-D. Zheng, C.-B. Zhao, Y.-N. Zhang, L.-L. Liu and J.-H. Huang (2016). "Effects of testosterone on the expression levels of AMH, VEGF and HIF-1 α in mouse granulosa cells." Experimental and therapeutic medicine **12**(2): 883-888.
- Zhao, M., Y. Bai, W. Xie, X. Shi, F. Li, F. Yang, Y. Sun, L. Huang and X. Li (2015). "Interleukin-1 β Level Is Increased in Vitreous of Patients with Neovascular Age-Related Macular Degeneration (nAMD) and Polypoidal Choroidal Vasculopathy (PCV)." PloS one **10**(5): e0125150-e0125150.
- Zhou, P., S. Zheng, E. Wang, P. Men and S. Zhai (2021). "Conbercept for Treatment of Neovascular Age-Related Macular Degeneration and Visual Impairment due to Diabetic Macular Edema or Pathologic Myopia Choroidal Neovascularization: A Systematic Review and Meta-Analysis." Frontiers in Pharmacology **12**(2211).

CURRICULUM VITAE

Bomina Park

Education

Ph.D. in Pharmacology

2016 – 2022

Indiana University

B.S. in Biochemistry

2012 – 2016

Idaho State University

Research Experience

PhD Graduate Research Assistant

August 2016 – May 2022

Department of Pharmacology and Toxicology, Indiana University School of Medicine

Advisor: Tim Corson, PhD

- Extensively trained in drug discovery and evaluation research
- Identified a therapeutic target to treat pathological angiogenesis involved in retinal neurodegenerative disease, and performed in vivo target validation through expression profiling and delivering a gene therapeutic approach
- Evaluated safety and efficacy of novel anti-angiogenic pharmacotherapy
- Characterized small molecule inhibitors using enzyme assays and enzyme inhibition kinetics

- Designed, planned, and performed experiments for research collaborations to characterize novel anti-angiogenic small molecules with Dr. Mark Kelley at Indiana University, to investigate the role of vitamin D in ocular angiogenesis with Dr. Breandan Kennedy at University College Dublin, and translated eye drop formulation methods document from Korean and English for a project with Dr. Seo at Chungnam University.
- Conducted collaborative research with a medical student and developed an innovative noninvasive smartphone based retinal imaging system
- Used expertise in technical analyses and scientific knowledge to provide advice to internal and external stakeholders including scientists, clinicians, industry representatives, and research staff
- Trained research students on general research practices and scientific writing

Undergraduate Research Assistant

2014 – 2016

Department of Chemistry and Biochemistry, Idaho State University

Advisors: Robert Holman, PhD and Kenneth Rodnick, PhD

Mechanistic investigation of nonenzymatic glycation: Studied kinetics of glucose mutarotation using NMR spectroscopy, and assessed glucose binding to HbA via computational modeling such as MOE and AutoDock

Professional Experience

U.S. Food and Drug Administration, Summer ORISE Fellow

June - August 2021

Office of Clinical Pharmacology/Center of Drug Evaluation and Research

Mentors: Kimberly Maxfield, PhD and Yow-Ming Wang, PhD

- Systematically reviewed labels and immunogenicity clinical studies to evaluate potential factors that may contribute to immunogenicity risk of single administered biologics approved by the FDA
- Compiled the PK similarity study results of FDA-approved biosimilar BLAs to build on the developing database of clinical pharmacology studies for biosimilar 351(k) applications
- Developed skills in the regulatory review of clinical assessments that are crucial in evaluating the safety of therapeutic products and learned how that can be translated into labeling language
- Attended and participated in regular meetings of Guidance and Policy and Biologic Therapeutic Products teams

Awards

- 2021 K.K. Chen Award, Department of Pharmacology and Toxicology, Indiana University, \$1,500 honorarium
- 2021 Paradise Travel Award, Department of Pharmacology and Toxicology, Indiana University

- 2021 Association for Research in Vision and Ophthalmology (ARVO) Travel Grant
- 2021 BrightFocus Foundation Outstanding Paper Award at Association for Ocular Pharmacology and Therapeutics (AOPT)
- 2020 American College of Clinical Pharmacology (ACCP) Student Abstract Award, \$1,000 honorarium. Awarded as the best student abstract. 8 students were awarded nationwide.
- 2020 Pharmaceutical Research and Manufacturers of America (PhRMA) Foundation Predoctoral Fellowship in Pharmacology/Toxicology, \$25,000. 12/2020-11/2021, Stipend support for doctoral research in pharmacology/toxicology.
- 2020 Eli Lilly-Stark Neurosciences Predoctoral Research Fellowship in Neurodegeneration, \$40,756. 01/2020-11/2020, A predoctoral fellowship in translational age-related neurodegenerative disease research.
- 2018-2019 Graduate and Professional Educational Grant (GPEG), Indiana University-Purdue University, Indianapolis, IN, \$1,000
- 2019 Bright Focus Travel Award, \$1,279. Awarded to attend AOPT meeting in New Orleans, LA
- 2018 Graduate Student Travel Award, Indiana University School of Medicine, Indianapolis, IN, \$500.
- 2018 NIH/NIEHS Travel Grant Award, ASPET Epoxide Hydrolase Session, San Diego, CA, \$1,000.

- 2015-2016 Chemistry Alumni Scholarships, Idaho State University, Pocatello, ID, \$2,000.
- 2014 Associated Students of Idaho State University (ASISU) Scholarships, Pocatello, ID, \$1,000.
- 2012-2016 Tuition Waiver Scholarship, Idaho State University, Pocatello, ID, \$10,000 per year.

Publications

1. Park, B., S. Sardar Pasha, K. Sishtla, X. Qi, M. E. Boulton and T.W. Corson (2022). "AAV8 mediated expression of shRNA targeting soluble epoxide hydrolase suppresses murine choroidal neovascularization." Manuscript submitted.
2. Sishtla, K., N. Lambert-Cheatham, B. Lee, D. H. Han, J. Park, S. Sardar Pasha, S. Lee, S. Kwon, A. Muniyandi, B. Park, N. Odell, S. Waller, I. Y. Park, S. J. Lee, S. Y. Seo & T. W. Corson (2022). "Small-molecule inhibitors of ferrochelatase are antiangiogenic agents." *Cell Chemical Biology*, S2451-9456(22)00001-0. Advance online publication. <https://doi.org/10.1016/j.chembiol.2022.01.001>
3. Swallow, E.A. and B. Park (2021). "Peer Wellness Coaches as Agents of Cultural Change in Academic Medicinal Research." *Academic Medicine*. Epub ahead of print. doi: 10.1097/ACM.0000000000004403.
4. Shetty, T., B. Park and T.W. Corson (2021). "Measurement of Mitochondrial Respiration in Murine Retina using Seahorse Extracellular Flux Analyzer." *STAR Protocols*, 2(2):100533.

5. Peng, M., B. Park, H. Harikrishnan, S. Jahan, J. Dai, N. P. Rayana, C. K. Sugali, T. P. Sharma, S. Imanishi, Y. Imanishi, T. W. Corson and W. Mao (2021). "A smartphone based method for mouse fundus imaging." *Experimental Eye Research*, 206:108530.
6. Barry, Z., B. Park and T. W. Corson (2020). "Pharmacological Potential of Small Molecules for Treating Corneal Neovascularization." *Molecules*, 25(15), 3468.
7. Shetty T, K. Sishtla, B. Park, M. J. Repass and T. W. Corson (2020). "Heme Synthesis Inhibition Blocks Angiogenesis via Mitochondrial Dysfunction." *iScience*, 23(8):101391.
8. Merrigan, S., B. Park, Z. Ali, Lassee. J, T. W. Corson and B. Kennedy (2020). "Calcitriol and Non-Calcemic Vitamin D Analogue, 22-Oxacalcitriol, Attenuate Developmental and Pathological Choroidal Vasculature Angiogenesis Ex Vivo and In Vivo." *Oncotarget*, 11(5), 493–509.
9. Park, B. and T. W. Corson (2019). "Soluble Epoxide Hydrolase Inhibition for Ocular Diseases: Vision for the Future." *Frontiers in Pharmacology* 10: 95-95.
10. Sardar Pasha, S. P. B., K. Sishtla, R. S. Sulaiman, B. Park, T. Shetty, F. Shah, M. L. Fishel, J. H. Wikel, M. R. Kelley and T. W. Corson (2018). "Ref-1/APE1 Inhibition with Novel Small Molecules Blocks Ocular Neovascularization." *Journal of Pharmacology and Experimental Therapeutics* 367(1): 108.
11. Sulaiman, R. S., B. Park, S. P. Sheik Pran Babu, Y. Si, R. Kharwadkar, S. K. Mitter, B. Lee, W. Sun, X. Qi, M. E. Boulton, S. O. Meroueh, X. Fei, S. Y. Seo and T. W. Corson (2018). "Chemical Proteomics Reveals Soluble Epoxide

- Hydrolase as a Therapeutic Target for Ocular Neovascularization." ACS Chem Biol 13(1): 45-52.
12. Smith, B. A., C. R. Mottishaw, A. J. Hendricks, J. Mitchell, S. Becker, P. S. Ropski, B. Park, M. Finkbeiner-Caufield, B. Garay-Nontol, R. W. Holman and K. J. Rodnick (2018). "Potential roles of inorganic phosphate on the progression of initially bound glucopyranose toward the nonenzymatic glycation of human hemoglobin: Mechanistic diversity and impacts on site selectivity." Cogent Biology 4(1): 1425196.
 13. Park, B., R. W. Holman, T. Slade, M. Murdock, K. J. Rodnick and A. L. M. Swislocki (2016). "A Biochemistry Question-Guided Derivation of a Potential Mechanism for HbA1c Formation in Diabetes Mellitus Leading to a Data-Driven Clinical Diagnosis." Journal of Chemical Education 93(4): 795-797.

Conference Presentations

1. Park, B., X. Qi, M.E. Boulton and T. W. Corson (2021). "Cell type specific expression of soluble epoxide hydrolase protein and mRNA in human AMD and murine eyes with choroidal neovascularization." Paper presentation at Association for Research in Vision and Ophthalmology (ARVO)
2. Park, B., S. P. Sheik Pran Babu, K. Sishtla and T. W. Corson (2020). "AAV8 mediated expression of shRNA targeting soluble epoxide hydrolase suppresses choroidal Neovascularization." Oral presentation at American College of Clinical Pharmacology (ACCP)

3. Park, B., S. P. Sheik Pran Babu, K. Sishtla and T. W. Corson (2020). "AAV8 mediated expression of shRNA targeting soluble epoxide hydrolase suppresses choroidal Neovascularization." Oral Presentation at Association for Research in Vision and Ophthalmology (ARVO) (virtual due to COVID-19).
4. Park, B., S. P. Sheik Pran Babu, SY. Seo and T. W. Corson (2019). "Assessment of soluble epoxide hydrolase and role of lipid mediators in choroidal neovascularization." Poster at Association for Ocular Pharmacology and Therapeutics (AOPT) meeting in New Orleans, LA.
5. Park, B., S. P. Sheik Pran Babu, S. Yubing, S. Meroueh, SY Seo and T. W. Corson (2018). "Characterization of a novel inhibitor of soluble epoxide hydrolase and role in ocular neovascularization." Poster at American Society for Pharmacology and Experimental Therapeutics (ASPET) meeting in San Diego, CA.
6. Park, B., Ropski, P., Hintze, T., Finkbeiner, M., Cundick, B., Titus, G., ... and Holman, R. (2016). "Towards an understanding of nonenzymatic glycation: The role of phosphate-catalyzed glucose degradation products in non-covalent protein binding." Poster at ACS meeting in San Diego, CA.
7. Holman, RW., S. Clark, M. Murdock, B. Garay-Nontol, B. Park, A. Hoisington, H. Roy and K. Rodnick (2014). "A comparison of the initial noncovalent binding of D-glucose and D-fructose with hemoglobin and albumin in nonenzymatic glycation." Poster at American Chemical Society (ACS) meeting in San Francisco, CA.